Use of Cell Cycle Analysis in Early State Estimation and Process Control

Peyman Pezeshki

A Thesis Submitted to the School of Chemical Engineering of the University of Birmingham for the Degree of
MASTER OF PHILOSOPHY

The School of Chemical Engineering
The University of Birmingham
Birmingham, UK
B15 2TT
August 2002

Abstract

The purpose of this project was to develop mathematical models which could predict the behaviour of Chinese Hamster Ovary cells (CHO320) many hours ahead by using their cell cycle profile. Experiments were carried out to study the growth kinetics of CHO320 cells. The initial concentration of glucose in the medium did not appear to have any effect on growth and cell cycle profile of CHO320. However, variation of the initial concentration of glutamine led to decreases in total cell number at concentration of 1 and 0.5 mmol in comparison to the standard medium concentration of 2 mmol. Glucose uptake rates were also found to be lower in batches with 1 and 0.5 mmol concentrations of glutamine. Batch culture studies of CHO320 cells having different cell cycle populations at the start of the culture were also made. Variations in viable, non-viable, substrate consumption and mean relative size and mass in these cultures were observed, but they were found to be largely accountable by reference to their corresponding cell cycle profiles. Variations and similarities in the patterns of cell cycle progression in these cultures were found mainly to be due to the presence or absence of specific period(s) e.g. lag period. Short and long term dynamic mathematical models were constructed. The best performing estimator of short term data was found to be that of models where transition between the phases of cell cycles is based on a predator-prey type of relationship and those with oscillatory rate coefficients. Physiological models based on molecular mechanism of cell cycle transition for prediction of short or long term data were found to be inadequate. As far as the longer term models were concerned, those with substrate dependent G1-S transition and death terms were found to be the most plausible option.

ACKNOWLEDGEMENTS

I am grateful to Mr A. N. Emery, my supervisor, for his guidance and support throughout the time I spent in Birmingham. I would like to thank Dr M. Al-Rubeai and Dr C.A. Kent for their advice. Special thanks to all the people in the animal cell culture technology group who helped me, in particular Mr D. R. Lloyd who provided and maintained the cell-line for me. I would also like to thank Dr M. T. Syddall for his advice and guidance with the use of Matlab. Finally I gratefully acknowledge the financial support of BBSRC during my MPhil studentship.

TABLE OF CONTENTS

LIST OF FIGURES

LIST OF TABLES

LIST OF ABBREVIATIONS

A	Indeterminate Phase of Cell Cycle Model of Variable Duration	(-)
A*	Arrested Phase in Cazzador's Cell Cycle Model	(-)
a	Cell Age	(hr^{-1})
a	Rate Constant for the Rate of Increase in the Prey Chemical in the Predator-Prey Cell Cycle Model	(hr^{-1})
B	Determinate Phase of Cell Cycle Model of Fixed Duration	(-)
B	Birth of New Cells	(-)
B_Q,C_Q	Constants in the Expression Describing the Return of Cells from the Arrested Phase in the Model of Cazzador	(s^{-1})
B_1	Post-Mitotic Phase	(-)
B_2	Pre-Mitotic Phase	(-)
b	Rate Constant for Degeneration of Predator Chemical	(hr^{-1})
C_2	Rate Constant for the Dephosphorylation of PRb	(hr^{-1})
C_c	Critical Concentration of Cyclins in Nielsen Model	(c)
cdk_i	Cyclin Dependent Kinases	(-)
c_2	Rate Constant for the Formation of PRb	(hr^{-1})
D	Dilution Rate in Linardos and Cazzador Models	(s^{-1})
D	Death of Cells in the Overall Population Balance	(-)
E	Emigration of Cells in the Overall Population Balance	(-)
E2f	A Family of Transcription Factors involved in Cell Cycle Transition of Cells	(-)
f	Frequency of Oscillation of Cell Cycle Transition Rates	(hr^{-1})
f_i	Fraction of Arrested Cells in Stage *i* of Cell Cycle in Suzuki's Model	(-)
G_1	Number of Cells in G_1 Phase of the Cell Cycle	($Cells.ml^{-1}$)
G_2M	Number of Cells in G_2 and Mitosis phases of the Cell Cycle	($Cells.ml^{-1}$)
g	Predation Rate Constant for the Predator-Prey Cell Cycle Model	(hr^{-1})
I	Immigration of Cells in the Overall Population Balance	(-)

J_i	Saturation Constant for the Phosphorylation and Dephosphorylation of Chemical Species *i* in the Physiological Model Value of Specific	(c)
K	Growth Rate at Which Probability of Cell arrest is 0.5	(d^{-1})
K_1	Rate Constant for the Formation of the RbE2f Complex	(hr^{-1})
K_2	Overall Rate Constant for the Dephosphorylation of PRb to Rb	(hr^{-1})
K_3	Rate Constant for the Formation of PRb	(hr^{-1})
K_4	Rate Constant for the Inhibition of RbE2f Complex	(hr^{-1})
K_c	Death Rate Constant for Cyclin Cells in Linardos Model	(d^{-1})
K_d	Death Rate Constant in the Age Based Models	(hr^{-1})
K_d	Death Rate in Nielsen Model	($Cells.hr^{-1}$)
K_{d0}	Maximum Death Rate at Zero Substrate Concentration	($Cells.hr^{-1}$)
K_{Di}	Death Rate Constant for the Cell Cycle Sub-Population *i*	(hr^{-1})
K_D	Death Saturation Constant	(mmol)
K_{ij}	Rate Coefficient for the Migration of Cells from Phase *i* to Phase *j*	(hr^{-1})
K_V	Maturity Saturation Constant in Chau Model	(d^{-1})
m_i	Biomass in Stage *i*	(μg)
me	Maintenance Coefficient	($\mu g.cell^{-1}.hr^{-1}$)
n	Relative Degree of Smoothness of the Curve of the Probability of Cell Arrest	(-)
N_D	Population of Cells at $t < 0$	($cells.ml^{-1}$)
N_V	Total Viable Cell Number	($cells.ml^{-1}$)
n_i	Cell Age Density in the State *i* of the Cell Cycle	($cells.hr^{-1}.ml^{-1}$)
O	Apoptotic State in Martens Model	(-)
P	Probability of Cell Arrest	(-)
Pd	Concentration of Predator Chemical	(c)
Pr	Concentration of Prey Chemical	(c)
PRb	Phosphorylated Retinoblastoma Protein	(c)
Rb	Retinobalstoma Protein	(c)
r	Specific Growth Rate in Cazzador Model	(s^{-1})

S	Number of Cells in the S Phase of the Cell Cycle	(Cells.ml^{-1})
s	Substrate	(mmol)
t	Time	(hr)
t_a	Duration of the State A of Cell Cycle	(hr)
t_b	Duration of the State B of Cell Cycle	(hr)
t_c	Duration of Cell Cycle	(hr)
V_i	Maturity Velocity of Stage *i*	(age.d^{-1})
V_{max}	Maximum Maturity Velocity	(hr^{-1})
V_2	Rate Constant for the Rate of Dephosphorylation of PRb to Rb Based on E2f Concentration	(hr^{-1})
Z	A Constant Replaced for the Expression 1/T.dT/dt in the Age Based Model	(-)

Greek Symbols

α	Amplitude of Oscillation	(hr^{-1})
Γ	Substrate in Substrate Dependent G1-S Transition Model	(mmol)
$\gamma_{N\Gamma}$	Yield of Cell Number on Substrate	(Cells.mmol^{-1})
ε	The Probability of a Cell Returning to the Cell Cycle in Cazzador Model	(-)
Θ_i	Oscillatory Rate Coefficient of Stage *i*	(hr^{-1})
Θ	Loss Factor in the Age-Based Population Balance Model of Foerster	(-)
λ	Rate of Cycling Cells Exiting the Cycle	(Cells.hr^{-1})
μ	Specific Growth Rate	(hr^{-1})
ν	Rate of Mass Accumulation	(Cells.hr^{-1})
τ	Lag Period Between Cell Mass and Cell Number Dynamics	(hr^{-1})
φ	Saturation Constant for the Substrate Dependent G1-S Transition Model	(mmol)
ϑ_{max}	Maximum G1-S Transition Rate	(Cells.hr^{-1})
Ψ	Average Cell Division Time	(hr)
ω	Angular Frequency of Oscillatory Rate Cofficient	(Rad.hr^{-1})

CHAPTER 1

INTRODUCTION AND THESIS LAYOUT

1.1 Introduction

Tremendous progress in molecular biology and genetics during the last three decades gave birth to the rapidly evolving field of biotechnology, defined by the Spinks Report (1980) as the application of biological organisms, systems or processes to manufacturing and service industries. This new technology was rapidly applied to the industrial manufacture of biologically active and therapeutic proteins. Use of these products for therapeutic purposes puts high demands upon their quality. Whilst microbial technology enables us to produce some of these proteins, production of proteins showing true fidelity to their native form, in aspects such as glycosylation or terminal structures, is impossible in prokaryotes or simple eukaryotes. It is only with mammalian cells that we are able to produce such complex proteins.

Mammalian cells are also a preferred choice for easier down stream processing as microbial systems often lack an effective mechanism for secretion of products out of their cells. Unless the gene responsible for the secretion of product is associated with a secretory component, the product remains within the microbial cells which can in turn limit their application in production processes. Mammalian cells in culture can also be used for toxicological or pharmaceutical research, thereby reducing the need for animal tests. Dense cultures of these cells can also be used to imitate organs. Since protein production is the ultimate goal of many cell culture operations, accurate quantitative

descriptions of growth and production processes are important for simulation and optimisation of product formation. For this, it is necessary to have predictive models relating the growth and death rates and the specific rates of substrate consumption and product formation to the environmental state of the culture.

1.2 Mammalian Cell Culture

Mammalian cell technology studies deal with parts of organs or tissues or with individual cells cultured in vitro. The starting point for such cultures is an explant; as long as this retains its structure and function, one speaks of organ or tissue culture. If mechanical, chemical, or enzymatic action destroys the organisation of a tissue, transition to a true cell culture is complete. Cells and tissues taken from an organism form the primary culture. The term cell line is applied to the generations obtained after the first sub-cultivation and all subsequent ones. A cell line can become a continuous cell line by transformation. Such continuous cell lines possess the potential for unlimited sub-cultivation in vitro.

The cultivation of cells on a large scale started with BHK (baby hamster kidney) cells which were adapted to growth in suspension in 1962 and have been used industrially since 1967 in the United States, United Kingdom, Italy, Germany, France and many other countries, particularly for the production of Foot and Mouth disease vaccines. Many other vaccines, hormones, enzymes and therapeutic proteins have been produced since. However, development of such significant therapeutic proteins as interferon-γ has proceeded furthest due to tremendous current interest. There are many cell lines

established for use in cell culture processes but the CHO cell line is the best characterised and most widely used for protein production. CHO cells were first isolated by Puck in 1957 who established a fibroblastic cell line from the ovary of a chinese hamster. Since then various recombinant proteins have been commercially produced and successfully marketed using this cell line. The CHO320 cells used in this study produce interferon-γ as product. Interferons were discovered in 1960s. These are naturally occurring proteins produced by virus-infected cells, macrophages and lymphocytes. Interferons can be divided into several species. IFN-α and -β have potent general antiviral activity whereas IFN-γ is a potent activator of macrophages and is used to improve resistance to infection and phagocyte function of patients with chronic granulomatous disease.

1.3 Thesis Layout

This thesis outlines the process by which experimental results obtained using cell cycle analysis were utilized in developing dynamic mathematical models for deterministic prediction of the cell numbers of CHO320 cells in batch culture conditions. The thesis is organised into 9 chapters.

Chapter 2: The literature survey in Chapter 2 is a review of the relevant published materials on cellular physiology, cell cycle based models, theories and assumptions.

Chapter 3: Includes details of protocols of experimentation which were designed to determine the rate of change of cell cycle phases and physiological parameters associated with them, e.g., mass, volume, etc.

Chapter 4: In this chapter growth kinetics of a partially synchronised batch of CHO cells are investigated and reported

Chapter 5: Describes the investigation of the effect of substrate concentration on total cell number, cell death, cell size and cell cycle.

Chapter 6: Attention was also paid to the question of whether or not changes in cell growth (cell number, cell mass, cell volume, etc.) would be significant if cells were inoculated from different parts of the cell cycle profile.

Chapter 7: Having obtained the data required for modelling purposes, simple dynamic models based on first order differential equations were developed, simulated and their parameters optimised.

Chapter 8: Deals with more complex situations where models of the interactions between cells and their environment and the use of cell age as a regulatory parameter are discussed.

Chapter 9: In this chapter all the results are discussed and conclusions made regarding the preferred approach. Future work and developments are also suggested.

CHAPTER 2

LITERATURE REVIEW

2.1 General Pattern of Growth in CHO Cells

The growth of CHO cells in suspension cultures is shown to follow a similar profile to that observed for most organisms, (Hayter, 1991; Leelavatcharamas, 1994). Distinct growth phases can be identified. During an initial stage, known as the lag phase, cells adapt to fresh medium. In the next stage, known as the exponential phase, the cell in population increases at its maximum growth rate with a typical doubling time of 18-24 hours. Exponential growth in batch cultures is usually followed by stationary and decline phases, which are characterised by some kind of growth limitation, product inhibition or accumulation of toxic products.

2.2 Choice of Cultivation Method

Many aspects of mammalian cell physiology have been investigated using chemostat culture. A large number of published mathematical models so far are also based on continuous cultivation (Cazzador *et al*, 1993; Martens *et al*, 1995) largely because the steady-state assumptions associated with this mode of operation make the mathematical handling of the models so much easier. Continuous or chemostat cultivation is often used for research purposes as it allows the study of the effects of a change in one culture parameter to be studied, while all other parameters, including the growth rate of the cells, can be kept constant. The added advantage of steady state chemostat cultivation is that time does not play a part in formulating mass balances and developing equations.

However, batch or fed-batch operations are the preferred modes of cultivation in the biotechnology industry, as higher yields of products are obtained and metabolic direction of the growth and production processes is often easier.

2.3 Cell Synchronisation

Observation of a single cell as it passes through its cell cycle is of limited value. It is also time consuming and the amount of information provided can be restricted due to measurement difficulties. It would be more advantageous, representative and realistic to measure a property on a large number of cells rather than a few. However, at any point in time the individual cells comprising a population are at different stages of the cell cycle, so it is necessary to develop a technique that renderes study of cells of similar properties possible. Synchronization of cells is a useful technique, which enabled early researchers such as Adams(1980) to study the mammalian cell in great detail. There are several approaches to synchronization: The use of blocking agents, e.*g.* Thymidine or Hydroxurea, or of Diversity Gradient Centrifugation and Synchrony by Starvation of Cells (Toby and Ley, 1970) are other methods. Starvation synchrony in itself can be considered a stage in the batch cultivation of CHO cells. As the substrate depletes progressively more and more cells are accumulated in the G_1 stage after undergoing division.

2.4 Factors Affecting Growth Kinetics of Mammalian Cells (Nutritional Requirement)

In order to optimise growth processes in mammalian cell cultures it is imperative to explore how any particular cell line responds to defined culture conditions. The cell

culture medium must provide the nutrients required by mammalian cells for the synthesis of cell biomass and products. Quantitative studies of the effect of medium components on cell growth and product formation are essential for process development, as these vary widely with cell lines, culture systems and culture conditions.

2.4.1 Serum-Supplemented and Serum-Free Media

Growth in many mammalian cell lines is enhanced by addition of serum to the culture medium. For many applications the addition of 5 to 20 vol. % serum to the medium is still required (Dallili and Ollis, 1989). However, due to a number of disadvantages, such as economic cost (Griffiths, 1986), variation in serum consistency, complications in down stream processing (Jager, 1992) and the risk of contamination of products, the trend in industry has been to move towards completely defined culture media. One of the earlier attempts to develop a substitute for serum was that of Sato (1975), who proposed that serum supplies growth factors, hormones and trace elements, which can also be provided in a defined medium. Since then serum free media were developed (Barnes *et al*, 1984; Kitano *et al*, 1991) that were based on existing nutrient media and growth factors from defined sources. The most common additions are insulin, transferrin, selenium, fatty acids and bovine serum albumin. Monoclonal antibody production rates were found to be higher in serum-supplemented cultures of mammalian cells; However, the corresponding maximum cell densities were often lower (Glassy *et al*, 1988). Serum-free media, despite their advantages, are not always cost effective option. The cost of known supplements could exceed that of serum significantly (Griffiths *et al*, 1986).

2.4.2 Metabolism and Energy Production in Mammalian Cells

Mammalian cell cultures, in marked contrast to microorganisms, are able to grow on only a limited number of carbohydrates (Morgan, 1986). Bailey *et al* (1959), investigating carbohydrate utilization in mouse lymphoblasts, reported glucose and mannose as the best carbohydrate sources for cell proliferation. Mammalian cells are typically grown in cultures with glucose and glutamine as main energy and carbon sources (Zielke *et al*, 1978). The effects of glutamine and glucose on cell growth and productivity in a number of mammalian cell lines has been investigated (Zetterberg *et al*, 1981; Glacken *et al*, 1988; Dallili *et al*, 1989; Hayter *et al*, 1991; Zeng *et al*, 1995; Vriezen *et al*, 1996). Glucose has been found to be a biomass precursor (Dallili and Ollis, 1989) whilst glutamine is shown to be a major source of energy for the cell (Reitzer *et al*, 1979). Much of the glucose is metabolised to pyruvate and then to lactate via glycolysis to produce energy (Eagle *et al*, 1958), but limited amounts of pyruvate may be converted to acetyl CoA, which enters the tricarboxylic cycle. Although glycolysis provide cells with some of their energy requirement, it is as importantly reported to be a major source of pentose phosphates for the synthesis of nucleotides and anabolic substrates(Zielke *et al*, 1978). Glutamine is the most abundant amino acid in most cell culture media and is an essential requirement for optimal proliferation of cells due to its anabolic role as an amino donor in purine, pyrimidine, amino sugar and translational protein synthesis (Mckeehan, 1986). Glutamine can be catabolysed in a number of ways (Haggstrom, 1990). The first step is the deamination of glutamine to glutamate. This is usually accomplished through glutaminase with the release of ammonia but can also be a transamidation reaction in which the amide group from glutamine is used to synthesise

precursors for biosynthesis. The second step in glutaminolysis is the conversion of glutamate into α-ketoglutarate. This reaction can either be a deamination, catalysed by glutamate dehydrogenase, or a transamination, in which, for example, alanine is formed from pyruvate or asparate from oxaloacetate. Oxaloacetate reacts with acetyl-CoA to form citrate. Oxaloacetate may be converted into pyruvate or phosphoenol pyruvate, which in turn can be oxidised to CO_2 via acetyl-CoA. Thus the metabolic routes for glucose and glutamine partially overlap since pyruvate can be formed from glutamine as well as from glucose. The availability of glucose can reduce the utilisation rate of glutamine by mammalian cells (Zielke, 1978; Reitzer *et al*, 1979; Miller *et al*, 1989; Meijer *et al*, 1995). A decrease in glucose concentration has also been shown to increase glutamine utilisation (Zielke, 1984). The extracellular concentrations of glucose and glutamine are generally recognised to significantly influence their uptake rate (Miller *et al*, 1989; Zeng *et al*, 1995). Dallili *et al* (1989) have shown that variation of serum concentration in the medium can affect consumption kinetics of both glucose and glutamine. As the catabolic routes for glutamine utilisation are entwined with the catabolism of glucose and anabolic routes for glutamine and other amino acids, mammalian cells could have a vast array of adaptations to limiting feed concentrations of glutamine (Vriezen *et al*, 1996).

2.4.3 Metabolic By-Products and Toxicity in Mammalian Cell Culture

Ammonia and lactic acid are the most significant toxic by-products accumulated in mammalian cell culture. Ammonia is mainly derived from catabolism of glutamine by glutaminase activity whilst lactic acid is a result of metabolism of glucose by glycolysis.

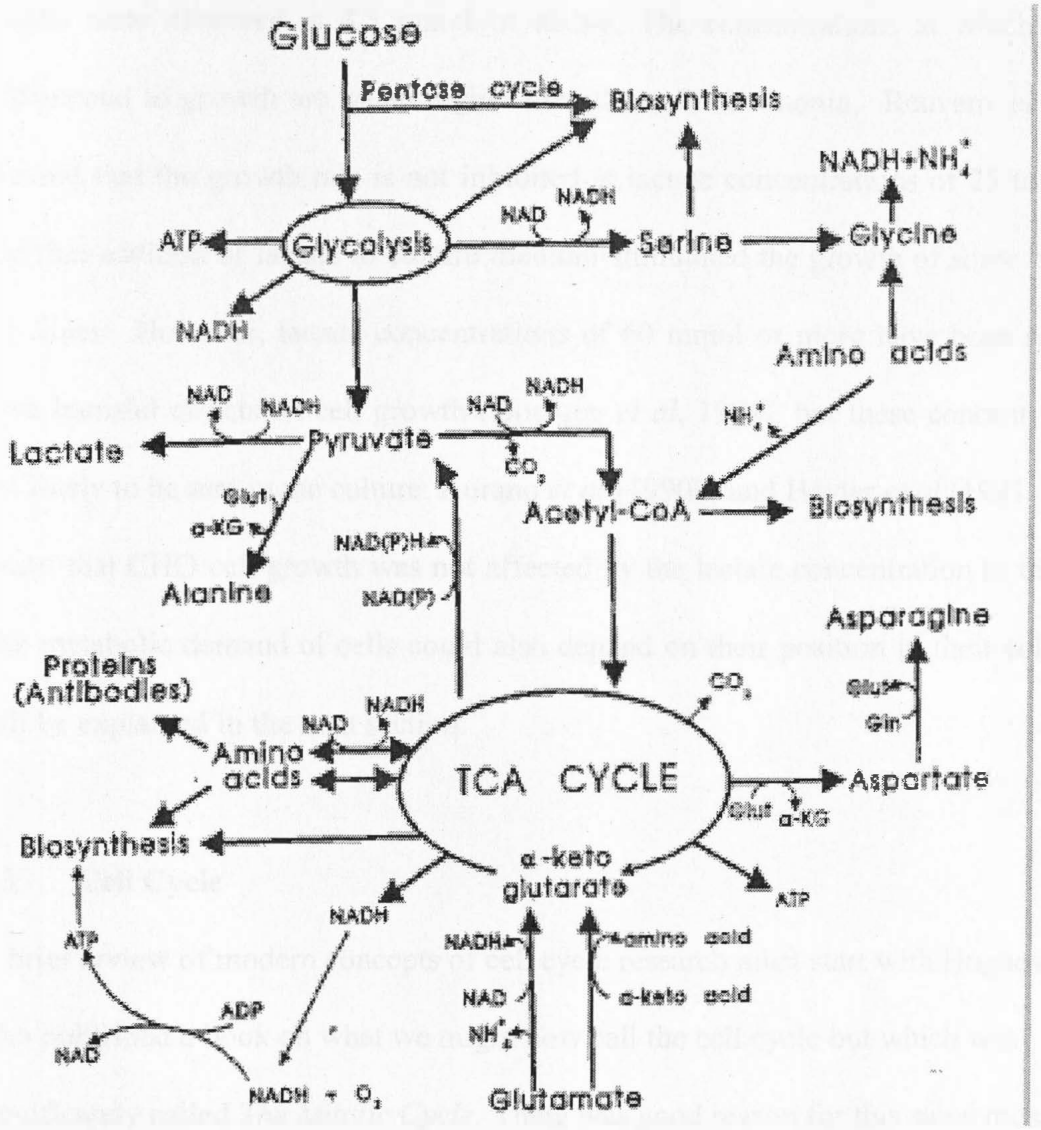

Fig 2.1 **Simplified Diagram of Metabolic Pathways for the Utilisation of Glucose and Glutamine in Mammalian Cells (Taken from Zeng et al 1995)**

Ammonia has been shown to reduce the growth rates of mammalian cells at concentration as low as 1 to 5 mmol (Miller *et al*, 1988; Goergen *et al*, 1994; Glacken *et al*, 1988; Ozturk *et al*, 1992). The work of Hayter's *et al* (1991) showed that CHO cell growth is not inhibited by ammonia at a concentration of 2 mmol although inhibitory

effects were observed at 4.5 mmol or above. The concentrations at which lactate is detrimental to growth are much higher than those for ammonia. Reuveny *et al* (1987) showed that the growth rate is not inhibited at lactate concentrations of 25 to 40 mmol and that addition of lactate to culture medium stimulated the growth of some hybridoma cell lines. However, lactate concentrations of 60 mmol or more have been reported to have harmful effects on cell growth (Goergen *et al*, 1994), but these concentrations are not likely to be met in the culture. Kurano *et al* (1990b) and Hayter *et al* (1991) have also found that CHO cell growth was not affected by the lactate concentration in the culture. The metabolic demand of cells could also depend on their position in their cell cycle as will be explained in the next section.

2.5 Cell Cycle

A brief review of modern concepts of cell cycle research must start with Hughes (1952), who published a book on what we might now call the cell cycle but which was significantly called *The Mitotic Cycle*. There was good reason for this since most of the book was concerned with cells in mitosis. In contrast, very little was known about how cells and their components grew between one mitosis and the next. With further studies using microspectrophotometry and autoradiography, it became clear that DNA synthesis took place during a restricted period in the cycles of higher eukaryotic cells. The names for these intervals were first coined by Howard and Pelc (1953), who proposed four distinct physiological phases that cells must pass through between each mitosis. They were the synthesis or S phase, the gap before synthesis and after mitosis or G_1, the gap after synthesis and before mitosis or G_2 and the mitosis period or M phase. Since then,

cell cycle based models have been increasingly the preferred choice in the development of reliable indices for prediction of cell growth, in that changes in physiology and growth kinetics in populations of animal cells can be attributed to the relative proportions of cell cycle sub-populations present in those cultures.

The cell cycle, shown in Fig 2.2, is a series of activities through which a cell passes from the time it is formed until it reproduces. It comprises the growth of a single cell and its division into daughter cells and can be divided into two sections: interphase and division. When a cell is between divisions, it is said to be in interphase. It is during this stage that the replication of DNA is completed, and the centromers, RNA and proteins needed to produce the structures required for doubling all cellular components are made. The interphase in turn can be divided into three distinct phases: S or synthesis phase, G_1 phase and G_2 phase. G_1 and G_2 are simply gaps between events in the cell cycle. G_1 is arbitrarily taken to begin the cell cycle and is the most variable phase of the cell cycle. The period during which DNA and chromosomes are replicated is called the S phase. After chromosomal replication in the S phase, there is another phase called G_2 phase. Since the G phases are periods when there are no events related to chromosomal replication they are thought of as gaps or interruptions in DNA synthesis. Most cell populations consist of dividing and non-dividing fractions. Cells can enter the non-dividing state (G_0) due to limitation of essential nutrients (Tobey *et al*, 1970) or inhibition of protein synthesis (Pardee, 1974) from a point immediately after mitosis (Lajtha, 1963). However, Al-Rubeai *et al* (1991), Ozturk *et al* (1990) and Martens *et al* (1993) have shown that even at very low or zero growth rates a considerable amount of

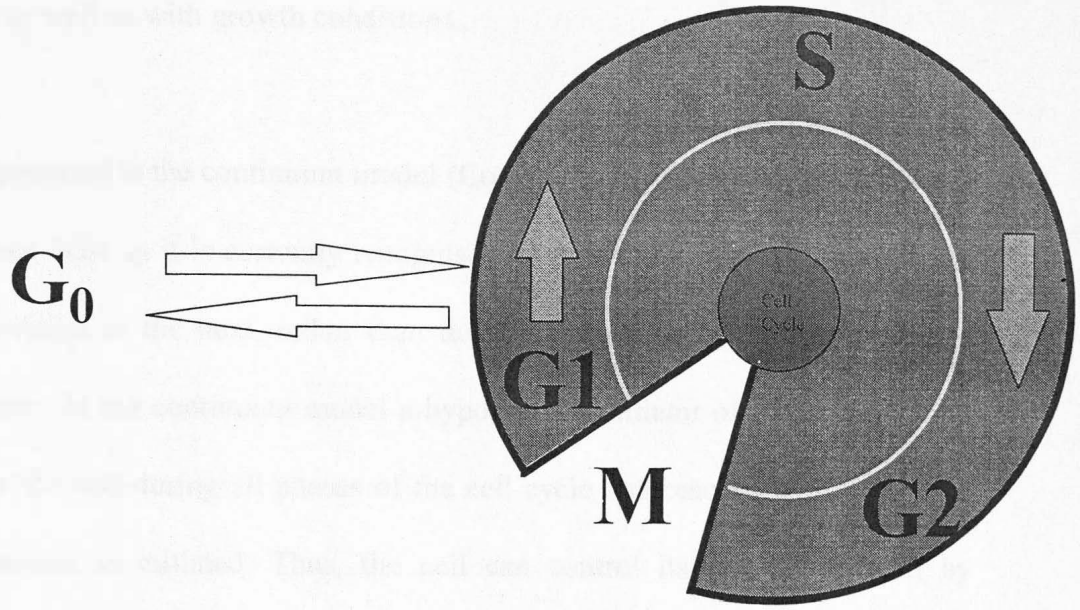

Fig 2.2 The Eukaryotic Cell Cycle

cells have an intermediate and double DNA content, indicating that cells stop cycling everywhere in the cell cycle rather than becoming arrested at a specific point.

Cells can be stimulated to re-enter the cell cycle. The point of re-entry is usually the phase from which the cells entered the quiescent stage, which is normally G_1 or mid G_1 (Baserga and Surmacz, 1987). Cells that are destined never to divide again are permanently arrested in the G_0 phase and may undergo apoptosis (Goldstein, 1990). Once a cell enters the S phase, it is committed to go through the divisional cycle. At the end of the G_2 phase, the cell is ready to enter the process called mitosis, during which it divides. For most cells, the duration of the S, G_2 and M phases are relatively constant and it is that of G_1 which is believed to be variable. In a typical cell cycle of (say) 24 hours duration G_1 would last 10 hours, S phase 9 hours, G_2 would last 4 hours and mitosis 1

hour. However, the duration of the cell cycle varies both between cell lines and individual cells, as well as with growth conditions.

An alternative proposed is the continuum model (Cooper, 1988), which suggests that the cell cycle does not exist as it is currently recognised but takes the form of a continuum from one cell division to the next, rather than discrete phases with discrete groups of regulatory proteins. In the continuum model a hypothetical initiator of DNA replication is synthesised by the cell during all phases of the cell cycle and reaches a critical value when DNA synthesis is initiated. Thus, the cell can control its rate of division by regulating the level of initiator. In this project, it was only reasonable to accept the weight of evidence for the established view of the cell cycle and base the models on the established cell cycle model. Cell cycle changes as well as the physiological changes associated with it, however, need to be accurately measured and for this purpose flow cytometric methods were developed as are described in the next section.

2.5.1 Variability in the Cell Cycle

The age at which individual cells divide is very variable even when the population as a whole is growing exponentially in steady-state (Cook *et al*, 1962). This has sometimes been attributed to a lack of uniformity within the culture or to heterogeneity of the cells. However, the variability has persisted despite many improvements in culture techniques. Variability also occurs within the first few generation of a clone. It is unlikely, therefore, to be a reflection of genetic heterogeneity (Shields, 1977). Variability thus appears to be

connected to the regulation of proliferation and it seems not unlikely that it arises as a direct consequence of the way in which the cell cycle is controlled.

There are two main viewpoints about the variability of the cell cycle: the deterministic model and the transition probability model. According to the deterministic view of the cell cycle, every cell in a population should ideally behave in an identical way, so the answer generally given to account for the variation of the cycle is that deterministic controls are 'sloppy', and this gives rise to variation around the population mean values. This does not mean that there is no control mechanism, merely that the mechanism is imprecise. In the transition probability model the variation itself is a fundamental part of the cycle. The transition is proposed to occur at random, so that the probability of the transition occurring in unit time is constant, irrespective of the past history of the cells (Burns *et al*, 1970; Smith and Martin, 1973; Shields, 1977; Shields, 1978). Deterministic models arose from investigations into the physiological and molecular mechanisms underlying the control of the cell cycle events, but such an approach by its very nature tends to stress the similarities between cells and ignores the differences. Transition probability, on the other hand, was proposed as a means to explain the differences between the cycles of the individual cells (Pardee, 1978). The two apparently different types of behaviour observed in different cell types may simply be a question of the balance of rates of two continuing processes. This view has been further discussed by Nurse (1980). In conclusion it is suggested that there need not be any major conflict between the two viewpoints as they may be describing different facets of the same underlying mechanism.

2.5.2 Molecular Mechanisms Controlling the Cell Cycle

Since the 1980s, when genetic and biochemical studies merged to identify a set of evolutionary conserved cell cycle regulators, our understanding of cell cycle control has advanced rapidly. It is now firmly established that a family of protein kinases, termed cyclin dependent kinases (cdk), controls the transition between successive phases of the cell cycle in the eukaryotic cells (Morgan, 1995). All cdk are structurally related to each other and all require associated small proteins called cyclins for their activity. Unlike simple eukaryotic organisms such as yeast, where a single cdk catalytic subunit interacts with numerous different classes of cyclin to mediate diverse cell cycle transition, mammalian cells regulatory environment is complicated by the presence of multiple cdk (Mayerson *et al*, 1992) as well as cyclins (Xiong and Beach, 1991; Lew and Reed, 1992; Hatzianikatis *et al*, 1999).

Two principal checkpoints have been identified in the cell cycle: the G_1-S checkpoint and the G_2-G_1 checkpoint (Hartwell *et al,* 1989). In the G1-S checkpoint, cdk 2, 4 and 5 start to complex with cyclins D1, D2 and D3 and become active in early to mid G_1. The level of activation of the G_1 cdk-cyclin complexes peaks at about the restriction point R, allowing cells to pass R into the S phase. Cdk2 also forms active complexes with cyclin E starting from mid G1 and peaking later than the cdk-cyclin D complexes; between R and the G_1-S phase transition. The primary substrate of the cyclin D complexes is the retinoblastoma tumour suppressor gene product Rb. Active unphosphorylated Rb complexes with and inhibits the transcription factor E2f. When Rb is phosphorylated

and inactivated, the complex dissociates releasing active E2f and hence the cells are allowed to proceed to S phase (Weinberg R.A., 1995). It has also been proposed that the cyclin E complex also phosphorylates Rb, with similar effects (Dulic *et al*, 1992). At the onset of the S phase the activation of the G_1 phase cdk-cyclin complexes decreases in the same temporal order as they increased and the complexes dissociate. As cdk2 disassociates from cyclins D and E, it complexes with cyclin A, which starts to be synthesised at about the G_1-S transition. The cdk-cyclin A complex retains its activity until the end of the S phase. At the end of the S phase the cdk2-cyclin A complex decreases and cyclin A and B then form complexes with cdk1. It is these complexes, increasing in activity throughout G_2 and continuing into mitosis, which mediate activation of the 'cell division machinery', ensuring that the cells are big enough, the environment is favourable and that DNA synthesis has been fully and accurately completed before the cell continues to mitosis and division.

2.6 Flow Cytometry

Flow cytometry is the most practised member of a family of technologies known variously as automated, analytical, or quantitative cytology. As the term implies, flow cytometry is the measurement of cellular properties as they are moving in a fluid stream past a stationary set of detectors. Diverse scientific disciplines such as computer science, laser developments, hydrodynamic focusing, ink technology and optics have been brought together in order to produce the flow cytometer.

Flow cytometry is capable of rapid quantitative, multi-parameter analysis of heterogenous cell populations on a cell by cell basis. In the simplest terms, a flow

cytometer operates by causing the cells in a fluid stream to pass in single file through a beam of light, usually generated by a laser. The photons of light, which are scattered and emitted by the cells following their interaction with the laser beam, are separated into constituent wavelengths by a series of filters and mirrors. These separated light streams fall upon individual detectors that generate electrical impulses, or analog signals, proportional to the amount of incident light striking them. Each analog signal is converted to a digital signal, a number which is accumulated in a frequency distribution, or histogram. Therefore, the resultant number is proportional to the amount of light emitted from, or scattered by, the individual cell.

Flow cytometery has evolved as a highly specialised research tool in animal cell culture technology particularly in the study of proliferating capacity and productivity in cultured cells. In addition, many flow cytometers have the ability to sort or physically separate particles of interest from a sample, which can be particularly useful.

2.6.1 Lasers and Fluorochromes

There are several laser types available that can be used on flow cytometers. The most common types are argon ion, helium-neon, krypton and dye lasers. The choice of fluorochrome to be used is influenced both by the application and the excitation wavelengths available. The most commonly used DNA dye is propidium iodide (PI) (Ormerod, 1994), which intercalates in the DNA helix and fluoresces strongly orange-red. It has the advantage that it is excited by 488 nm light and can be used on most

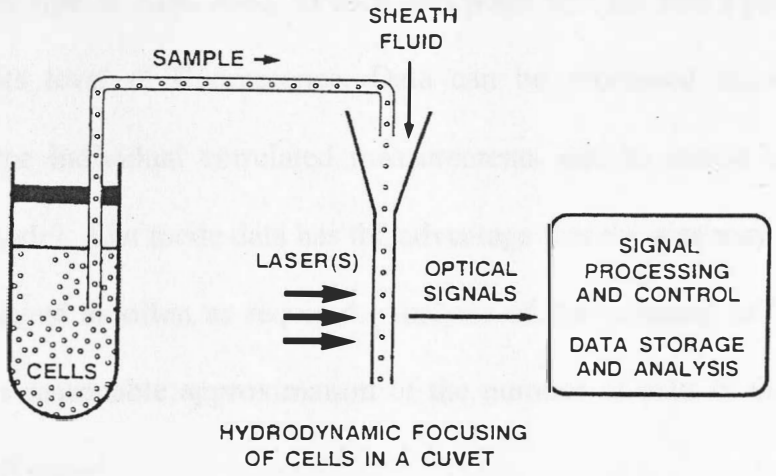

Fig. 2.3 A Schematic Representation of a Flow Cytometer.

common flow cytometers. However, it does require cells to be fixed or permeabilised and therefore non-viable. PI also stains double-stranded RNA and this should be removed with ribonuclease.

2.6.2 Data Analysis

Photomultiplier tubes (PMT) and detectors collect the photon emissions from each cell and convert them to analog voltages. The analog signals are then digitised by analog to digital converters (ADC). An analog-to-digital converter, as the name implies, has an analog input, usually a voltage in the range 0-10 volts, and a digital output, which is a binary number with 0's and 1's represented by different voltage levels (Shapiro, 1988). Each PMT/ADC circuit divides the continuous data distribution that is acquired from

cells into a discrete distribution. To do this it forms a histogram where the x axis is divided into a certain number of channels. These are either 256 or 1024 channels depending on the type of ADC used, so each data point will fall into a particular channel depending on its level of fluorescence. Data can be processed immediately into a histograms or the individual correlated measurements can be stored on disc in time sequence (list mode). List mode data has the advantage that the data may be reprocessed, gated, and displayed as often as required. Analysis of the resulting DNA histogram is used to obtain a reasonable approximation of the number of cells in G_1, S and G_2+M phases of the cell cycle.

The DNA histogram is a very simple data set that characteristically contains two peaks separated by a trough. The first peak, which is usually the larger, corresponds to cells with G_1 DNA content, and the second, which should be at double the fluorescence intensity of the first, corresponds to cells with G_2+M DNA content.

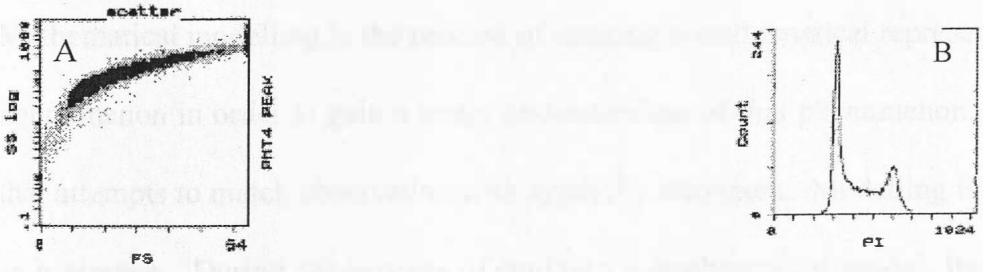

Figure 2.4 A-B Typical Scatter (A) and DNA (B) Histograms

Any cells scored in the trough have a DNA content intermediate between G_1 and G_2+M, and these usually represent cells in S phase. In order to quantify the relative proportions

of the cell cycle sub-populations in a sample the DNA histogram should be deconvoluted into its component parts, separating cells in S from those in G_1 and G_2+M phases of the cell cycle.

It is usually assumed that the cells in G_1 and G_2M phases are distributed normally so that the distributions can be described by Gaussian curves. Distribution of cells in S phase cannot be described so simply, and the algorithms used in deconvoluting use different approaches to handling the S phase cell distribution, ranging from rectilinear integration, where the S phase portion of the DNA histogram can be taken to be equivalent to a rectangle, to algorithms, through which the S phase interval is modelled with a series of closely spaced Gaussian distributions with constant coefficients of variation which are appropriately summed (Watson, 1992). Flow cytometry data obtained can then be used to develop mathematical models of the cell cycle progression.

2.7 Mathematical Modelling

Mathematical modelling is the process of creating a mathematical representation of some phenomenon in order to gain a better understanding of that phenomenon. It is a process that attempts to match observation with symbolic statement. Modelling is as much an art as a science. During the process of building a mathematical model, the modeller will decide what factors are relevant to the problem and what factors are of less significance. Of the very many model possibilities arising out of a particular application, very few can usefully illustrate the processes involved, and the useful models are not necessarily those of most intrinsic mathematical interest. Once a model has been developed, it should be

examined and modified to obtain a more accurate reflection of the observed reality of that phenomenon. In this way, mathematical modelling is an evaluating process as new insight is gained. The process begins again as additional factors are considered. "Generally the success of a model depends on how easily it can be used and how accurate are its predictions" (Edwards & Hanson, 1994).

2.7.1 Building a Model

Building a mathematical model is a challenging yet interesting task. An understanding of the underlying scientific concept is necessary. Although problems may require very different methods of solution, the following steps outline a general approach to the mathematical modelling process:

- Identify the problem, define the terms in the problem, and draw diagrams where appropriate.
- Begin with a simple model, stating the assumptions that you make as you focus on particular aspects of the phenomenon.
- Identify important variables and constants and determine how they relate to each other.
- Develop the equation(s) that express the relationship(s) between the variables and constants.

2.7.2 Variables and Parameters

Mathematical models typically contain three distinct types of quantities: output variables, input variables, and parameters (constants). Output variables give the model solutions. The choice of what to specify as input variable and what to specify as parameters is

somewhat arbitrary and often model dependent. Input variables characterise a single physical problem while parameters determine the context or setting of the physical problem.

2.7.3 Verifying and Refining a Model

Once the model has been developed as applied to the problem, the resulting model solution must be analysed and interpreted with respect to the problem. The interpretation and conclusion should be checked for accuracy by answering the following questions:

- Is the information produced reasonable?
- Are the assumptions made while developing the model reasonable?
- Are there any factors that were not considered that could affect the outcome?
- How do the results compare with real data, if available?

2.7.4 Types of Models Used in Animal Cell Culture

Models for animal cell cultures can be classified in a manner similar to that for microbial systems. The main distinctions are those of unstructured versus structured, and of unsegregated versus segregated (Tsuchiya *et al*, 1966). A third distinction can be made between deterministic and stochastic models. Each model can be classified by its type in each of the three categories. For example, Monod's model is unstructured, unsegregated and deterministic. Unstructured models do not take into account the inner structure of cells and thus acknowledge only implicitly the change of cellular physiological state with the environment (Fredrickson, 1976). Such models view the cell as a single unit, so their biological basis is limited, and their mathematical forms are generally phenomenological

or empirical. Unstructured models are of limited use in situations where significant changes in the cellular environment occur. Nevertheless, the models are relatively easy to build, and they are used extensively in simulating steady-state systems. In a structured model, the biomass is described in great detail and is divided further into more components. Such models incorporate biological knowledge by separating/lumping the biomaterial into compartments that are chemically and/or physically distinct. As is the case with microbial cells, mammalian cell populations are also heterogeneous with regard to cell age, size, growth rate and metabolic state. Whilst unsegregated models view the population as consisting of identical "average cells" segregated models build on the heterogeneous composition of a culture and offer the advantage of relating cell properties and biochemical activities with distinct parts of the population.

2.7.5 Deterministic and Stochastic Models

In deterministic models, the behaviour of the system can be exactly predicted on the basis of the known physiological state, whilst stochastic models can only specify a probability that the physiological state will be within a certain range. Since in a batch culture the concentration of the cell population is of the order $2x10^5$- $2x10^6$ cells.ml^{-1}, and the volumes we are dealing with are upwards of 10 ml, then the random behaviour of individual cells can be averaged and a deterministic approach can be utilised for model construction.

2.7.6 Models Based on Cell Cycle

During the last decade, cell cycle as a predictive index for growth of mammalian cells has been introduced into mathematical models. Cell cycle models are principally composed of 2-4 stages characterised by different cellular activity, morphology and mechanical properties. In a two phase cell cycle model (Linardos *et al*, 1992; Martens *et al*, 1995), the cell cycle is taken to consist of an indeterminate state usually denoted by A and a determinate state B, which is of fixed duration.

One of the simpler mathematical models describing the properties of cells in each phase of the cell cycle is the shell model proposed by Shioya *et al* (1999). In this model three shells, representing G1, S and M phase populations are taken and the relationship between the input to and output from each shell is described. Having developed G1, S and M equations, Shioya then determined the optimal strategy in respect of temperature and glucose concentration for rice α-amylase production.

Cell cycle models can make use of frequency functions in order to determine the number of cells or cell mass in each phase of the cell cycle at a particular time (Suzuki & Ollis, 1989; Kromenaker *et al*, 1991). Transition of cells from one phase to another in cell cycle models have also been based on the chronological age (Martens *et al*, 1995) or physiological age (Chau *et al*, 1997) of the cells. Martens' model is a combination of a cell cycle model and a model describing the growth and conversion kinetics of hybridoma cells in a steady state continuous culture. The cell cycle part of the model is an improvement on the model proposed by Cazzador *et al* (1993). Under non-balanced

growth Chau's model, in addition to A and B phases previously encountered in this chapter, consist of a pre- and a post-mitotic B phase. Transition of cells from A to B phase is assumed to be random. Influx of cells from the post-mitotic phase B_1 is dependent on the maturity velocity V_{B1}, and the number of cells at the termination of the post-mitotic B_1 phase $n_{B1}(t,T_{B1})$. In the case of balanced growth, however, the numerical value of V_{B1} is equal to one.

Cell cycle models based on the recent physiological discoveries of the cell cycle regulation (Obeyesekere *et al*, 1997; Nielsen *et al*, 1997; Novak *et al*, 1998) are the latest development in pursuing the ideal model for prediction of animal cells growth and differentiation. A number of relevant publications of interest are presented below.

The Model of Suzuki et al (1989)

Suzuki proposed a cell cycle model to provide direction for the exploration of culture conditions that enhance specific antibody production rate. In this model, the cell cycle consists of five stages, G_1, S, G_2, M and A^*. A^* is the stage in which cells are arrested. In order to determine the product yield and antibody production rates, the fractions of cells in each of the cell cycle phases had to be calculated. The latter was carried out using the relationship:

$$f_i = (1-f_A) \int 2^{(1-t/tc)}\, dx / \alpha \qquad i=G1,S,G2,M \qquad (2.7.1)$$

Where tc = the total cell cycle time, f_A is the fraction of arrested cells and α is defined as 1/ln2. In the derivation of the above equation a number of assumptions were made.

Firstly, it was assumed that all cells in the population are growing and that growth is exponential, and secondly, there is no synchrony. Having calculated the frequency and the fraction of cycling cells, a relationship between the fraction of arrested cells f_A and the specific growth rate of the population, μ, was then derived.

$$\mu = (1-f_A) \ln 2 / t_c \qquad \textbf{(2.7.2)}$$

Model predictions were tested under three different conditions:

Case 1 = when the fraction of arrested cells f_A is zero

Case 2 = where it is assumed that G_1 cells produce more product than other phases

Case 3 = when the cell cycle time t_c is taken to be constant.

In Suzuki's mathematical model, death processes are not considered. Cells are also arrested irreversibly although this does not correspond to author's theoretical assumptions.

The Model of Linardos et al (1992)

This is a steady state cell cycle model comprising of two principal phases, A and B, the former being of variable duration whilst the duration of phase B is considered to remain relatively constant. Cells that had remained in state A longer than a critical time, t_c, were considered to be arrested. The transition rate between phases A and B as well as the death rates of cycling and arrested cells are taken to be independent of the age of the population. The rate of return of arrested cells back to phase B has been taken to be equal to the rate of cycling cells exiting the cycle and is represented by λ. Based on the above criteria Equation 2.7.3 was developed for the cycling cells.

$$\omega(\alpha) = \omega(0) \exp^{-(\lambda + D + k_c)} \qquad (2.7.3)$$

where ω is the age density function for cycling cells, D is the dilution rate and k_c is the death rate of cycling cells respectively. A similar expression was developed for the arrested cells population. Fractions of cells were calculated by integrating the age density functions of cycling and arrested cells in the same manner as carried out by Suzuki *et al* (1989). Values for the death rate parameters k_c and k_o were then estimated using least squares regression. Finally, an estimated value of t_c was determined by reducing the error between the calculated fractions of cells and the values generated by the model. As previously mentioned by Cazzador (1993) and Martens (1995), the assumption of the generation time being equal to the doubling time of the population is incorrect.

The Model of Cazzador *et al* (1993)

Cazzador made use of segregated models to analyse the data related to the production of monoclonal antibodies in continuous cultures of hybridoma cells. Cazzador's model is based on three main phases; a determinate (B) phase, an indeterminate (A) phase and an arrested cells (A^*) phase. Two different models; stochastic and deterministic, and two different critical points for the arrest of cells, at the beginning and at the end of G_1 phase, were considered in this model. In the stochastic part of the publication Cazzador proposed that, at a given critical restriction point, later in phase A, cycling cells may become arrested by moving into phase A^*. Arrested cells may enter the cycle again by shifting to phase B. Cell arrest is assumed to occur after the cell has spent a fixed critical time in phase A and therefore the condition for exiting the cycle becomes rather

unreliably independent of growth conditions. According to this model the rate at which cells enter arrest is equal to the rate at which arrested cells entering the B phase. To overcome these inconsistencies he proposed a more general model, which is based on the hypothesis that there is a critical component dependent on growth condition that controls the cell arrest. Cells that do not contain the adequate critical factor will stop cycling and exit the cycle at the entrance to B, the determinate phase. However, if they accumulate the required amount for traversing the barrier between A and B phases, then they may return to the cycle. He proposed Equation 2.7.4 for the probability (P) of cell arrest.

$$P = k^n / (r^n + k^n) \qquad (2.7.4)$$

when k is the median point, namely the valve of μ at which P = ½ and n is a relative degree of smoothness around r = k . The probability for a cell to return to the cell cycle (ε_Q) is next given by:

$$\varepsilon_Q = D + B_Q / D + C_Q \qquad (2.7.5)$$

where D is the dilution rate, and B_Q and C_Q are constants. Three different scenarios were considered:

- Cells leave phase A after a constant time period T_a.
- Cells leave at a constant transfer rate λ.
- Both T_a and λ are assumed to vary with the growth rate.

Simulated results were then fitted to the Miller *et al* (1987) data. He concluded that there is an optimal value of dilution rate for maximising specific production rate of monoclonal antibodies. However, this study was not extended to establish possible relationships between sub-populations and productivity.

The Model of Martens et al (1995)

Martens' model is a combination of a cell cycle model and a model describing the growth and conversion kinetics of hybridoma cells in a steady state continuous culture. The cell cycle part of the model is an improvement on the model proposed by Cazzador *et al* (1993). In Martens' model as opposed to Cazzador's model cells cannot be arrested due to a defective control mechanism in the A phase, hence the quiescent phase Q in Cazzador's model was replaced by the O phase or apoptotic phase. The O phase is one which apoptotic cells will migrate to when growth conditions become unfavourable and the specific growth rate drops below a critical value. Moreover, the duration of phase A is taken to be dependent on specific growth rate; the higher the specific growth rate the shorter the duration of phase A. Apoptotic cells were assumed to die at a fixed time after their entry to the O phase. Martens extended the existing cell cycle model to include sub-populations using the relationship:

$$f = \int_{t1}^{t2} n_{c\,(0)} \cdot 2^{-a/tc} da \;/\; \int_{0}^{t_c} n_{c\,(0)} \cdot 2^{a/tc} da \qquad \textbf{(2.7.6)}$$

In the above equation t_1 and t_2 are the ages of the cells when entering and exiting the cell cycle phase, respectively. Measurements were carried out at the highest dilution rate, where the death rate and apoptosis are negligible and the cell cycle distribution of cycling cells is the same as that of the viable cells. Generally speaking, prediction of total cell number is poor. The total cell number is predicted too low at lower dilution rates and over-estimated at higher rates. The G_1 trend is predicted correctly; However, the values are predicted to be too high. The G_2M fractions are predicted to be too low whilst the

simulated S phase values resulted in a good fit. It is not clear how the value of $n_c(0)$ (the frequency function of cycling cells at time 0) was calculated in order to obtain N_c (the total cell number at a particular dilution rate). Changes in specific growth rate are taken to be stepwise, e.g. either at its maximum or at its minimum (critical growth rate) rather than continuous.

The Model of Chau et al (1997)

This is a cell cycle model based on the transition probability theory of Smith and Martin which has been adapted to predict cell dynamics under non-balanced as well as balanced growth conditions. Under non-balanced growth Chau's model, in addition to the A and B phases previously encountered in this chapter, consists of a pre- and a post-mitotic B phase. Transition of cells from the A to B phase is assumed to be random. Influx of cells from the post-mitotic phase B_1 is dependent on the maturity velocity V_{B1} and the number of cells at the termination of the post-mitotic B_1 phase $n_{B1}(t,T_{B1})$. In the case of balanced growth, however, the numerical value of V_{B1} is equal to one. The fraction of labelled mitotic cells was used to estimate the B phase duration, T_B and subsequently to evaluate the transition rate k_T. The concept of double transition was also introduced to give further variability in the B phase. Interruptions to the cell cycle caused by the second transition, prolong the population doubling time. In the case of non-balanced growth, recovery from quiescence has been omitted and hence transition to the quiescent phase is irreversible. The B phase is not subdivided into a pre- and post-mitotic B phase; thus, cells would enter the A state immediately after mitosis. Under non-balanced growth, the maturity

velocity V_B is taken to be a function of the limiting substrate concentration in a manner analogous to Monod Kinetics.

$$V_B = (V_{max}\, S) / (K_v + S) \qquad (2.7.7)$$

V_{max} is defined such that V_B is unity under balanced growth and K_v is the maturation saturation constant.

Similar relationships based on Monod Kinetics were also developed for the phase A to B and quiescent phase transition rates. Chau's assumption of irreversible transition to quiescent stage restricts applicability of the model (e.g. to fed batch cultivation). The mathematical model of Chau is not fitted to experimental data.

The Model of Nielsen *et al* (1997)

This cell cycle model is characterised by two events: the commitment to DNA synthesis at a point "start" late in G1 phase and mitosis. The period between start and cell division is of essentially constant length. By start is meant the point in the cell cycle when a given signal has accumulated to a prescribed level for continuation. The signal is produced when G_1 cyclins accumulate to a given critical concentration C_c, which is independent of the growth rate. When the cyclins concentration reaches C_c, the traverse of cells and the process of cyclins degradation will start instantaneously. In short, this model is an attempt to replace the complex molecular mechanisms of cell cycle transition with a simple cell mass control system. It has been assumed that the mass m of an individual cell increases according to:

$$dm / dt = \nu\,(t,m) = \mu(t)\,.m \qquad (2.7.8)$$

In other words, mass accumulation of a cell is taken to be autocatalytic, where ν is the mass accumulation rate and μ is the specific growth rate.

Following a population balance a partial differential equation in terms of cell mass density function was derived. Cell mass density function in the population balance was then replaced with an expression comprising the product of total viable cell number N_v and a frequency function. After rearrangement and simplification the following relationship was derived.

$$\mathbf{dN_v / dt = (\mu - k_d - D - 1/m_B .dm_B / dt) . N_v} \qquad \mathbf{(2.7.9)}$$

where m_B is the mass of cells at birth, D is the dilution rate, k_d is the death rate and μ is the specific growth rate of cells.

In another experiment it was demonstrated that cell number dynamics lag behind biomass dynamics. The above findings were then translated into a mathematical expression as shown:

$$\mathbf{dN_v / dt = (\mu(t-\tau_B) - k_d - D) . N_v} \qquad \mathbf{(2.7.9a)}$$

The mathematical model of Nielsen has a good predictive capability; However, introduction of a "shape preserving solution" to the frequency function in the derivation of 2.7.9 needs further elaboration and clarification.

The Model of Obeyesekere et al (1997)

This model is based on molecular mechanisms of transition between the phases in the cell cycle. It is mainly focused on the regulation of progression through the G_1 phase of the cell cycle. The proposed mathematical model is supported by experimental evidence. Experimental studies on cell cycle progression have led to the elucidation of a variety of proteins, which are required for appropriate entry into the S phase. These proteins include cyclin D, cyclin E, cyclin A and their associated kinases cdk4 and cdk2. Rb (Retinoblastoma protein) is the principal known G_1 substrate for active cdk/cyclin complexes. Rb interacts with the E2f family of transcription factors and suppresses E2f mediated transcription. Hypophosphorylated Rb sequesters E2f, forming an Rb/E2f complex. In the process of phosphorylation of Rb, Rb/E2f is disrupted and E2f is released. Free E2f in concert with cyclin E/cdk2 will initiate the S phase.

A maturation promoting factor (MPF) is included in the model to allow for completion of the remaining cell cycle phases. MPF is an activator of a phosphatase enzyme which in turn dephosphorylates Rb. Phosphorylation and dephosphorylation of Rb are taken to obey Michaelis-Menten type kinetics. In this model the beginning of the cell cycle is interpreted as the time when the cyclin D/cdk4 complex, along with unphosphorylated Rb concentrations start to increase. G_1 phase completion is believed to occur when the cyclin E/cdk2 concentration is above a threshold, close to its peak. In order to avoid modelling other phases of the cell cycle it is assumed that production of MPF is autocatalytic (though this is not based on experimental evidence). Patterns of change in simulated concentrations of Rb, E2f and cyclins are consistent with the theory; However,

the frequency and the peak of these oscillations may not correspond with a typical mammalian cell cycle. Moreover, comparison between the values generated by the model and experimental data have not been made, hence a conclusive performance analysis of this mathematical model cannot be obtained.

CHAPTER 3

MATERIALS AND METHODS

In this section an in-depth explanation is given of the protocols and biological experiments which have been used and carried out. These experiments were carried out in order to characterise the kinetics of cell growth and proliferation in CHO320 (Chinese Hamster Ovary Cells producing interferon-γ). The results were then used in the mathematical models described in the sections following.

3.1 Medium Preparation

RPMI 1640 (GIBCO UK) was selected as the basal medium for growth of CHO 320 cells. It was used in powder form and the contents of the vials supplied were first dissolved in 5 litres of deionised water. The water was deionised using an ion exchange based water purification system (Millipore Ltd. UK). The resulting basal medium was then buffered by addition of 10g of sodium bicarbonate (NaHCO3) to give a final concentration of 2g /l. The medium pH was adjusted to 7.0 using 1.0 M hydrochloric acid solution. Finally, the medium was sterilised by membrane filtration using a sterile filtering apparatus of 1 litre capacity with composite membranes of 0.2 μm pore size (Sartorius, Germany) were used in the filtration. 500 ml bottles of sterile medium were prepared kept at room temperature for 24 hours to confirm the absence of contamination , and then stored at 4^0C for future use. Glutamine and glucose free RPMI1640 media (Gibco UK) were also used. These were supplied in ready-to-use 500 ml bottles and were

used to investigate CHO320 growth kinetics after sterile addition of the prescribed amounts of either substrate.

3.2 Medium Supplement

In the batch cultivation of CHO320 cells foetal calf serum was always added to the medium to give a final concentration of 5% (v/v). Foetal calf serum was supplied by (Gibco UK) in 500 ml bottles which were then divided into 25 ml a liquotes to facilitate this process (one 25 ml aliquot per 500 ml bottle of medium).

3.3 Cell Line and Cell Maintenance

The cell line under study and investigation was a Chinese Hamster Ovary line producing interferon-γ as product, designated as CHO320. These cells were grown in suspension and maintained at 37^0C and stirred at 150 rpm in spinner flasks. Cells were resuspended in fresh medium at a concentration of $2x10^5$ cells.ml^{-1} every 4-5 days or when the cells reached a density of $8x10^5$-$1x10^6$ cells.ml^{-1}.

3.4 Growth of CHO 320 Cells

CHO cells were inoculated at ~ $2x10^5$ cells.ml^{-1} at the start of the batch culture in fresh medium (lower concentrations of CHO cells would significantly delay growth and prolong doubling time). The growth profile of CHO320 is usually sigmoid in shape. There is initially a lag period of approximately 10 hours where no change in cell number is observed, and this is followed by a period of exponential or logarithmic growth in which cells proliferate at their maximum growth rate and the death rate is minimal.

Exponential growth gradually gives way to a decline phase as the substrate concentration approaches exhaustion and waste products of metabolism accumulate.

3.5 Cell Counting Procedures

CHO cells in suspension were enumerated using a cell haemocytometer. The haemocytometer was set up by placing a cover slip on the moistened raised support arms so that the two ruled areas in the upper and lower portion of the slide were covered. 100 µl of sample was mixed with an equal volume of (0.5% w/v) Trypan Blue exclusion dye. The diluted cell suspension was triturated with a capillary pipette and a drop was placed at the opening between the haemocytometer and the cover slip ensuring that there were no trapped air bubbles under the cover slip. Cells in the top and bottom squares of each of the two grids were counted using a microscope with a magnification of 200X. Cells touching the upper and left-hand lines were counted as in the square, whilst those touching the lower and right lines were not counted. Each grid of the haemocytometer has a volume of 10^{-4} cm^3. Cell Count was determined by the following expression.

cell count/ml = average number of cells/square x dilution factor x 10^4

3.5.1 Viability Determination

Trypan Blue is one of the vital dyes used for estimation of the proportion of viable cells in a population. The reactivity of these dyes is based on the fact that the chromophore is negatively charged and does not interact with the cell unless the membrane is damaged. Hence non-viable cells will be stained blue. The percentage of viable cells (n_v) is then

determined by the expression $n/(n_v + n_d) \times 100$ where n_d is the total number of non-viable cells.

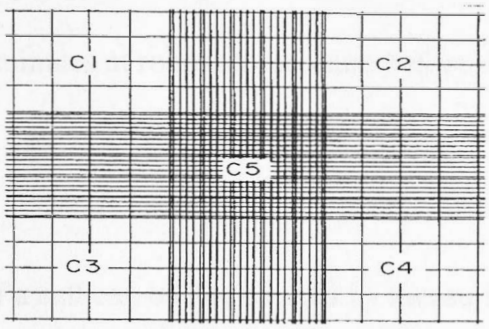

Figure 3.2 Haemocytometer : Lined Ruling of One Chamber

3.6 Cell Cycle Analysis by Flow Cytometry

3.6.1 Sampling Before Analysis

5-6 ml samples of CHO cell suspensions were removed from the spinner flasks under sterile conditions. They were placed in a universal tube and centrifuged at 1000 rpm for 5 minutes. The spent supernatant fluids were carefully discarded and 2-3 ml of cold 70% ethanol/water mixture were slowly added to each sample. The tubes containing the cell pellets were then gently shaken until the pellet disappeared and finally they were stored at -18^0C for the staining procedure.

3.6.2 Preparation of Cells for Staining

Stored samples were centrifuged at 2000 rpm for 5 minutes. After discarding the supernatant the cell pellets were washed twice with magnesium and calcium free phosphate buffer solution, as these minerals are believed to cause agglomeration of cells.

The final pellets were resuspended in 1ml of RNAase solution and the contents were transferred to small test tubes customised for use with the flow cytometer. Samples were then incubated at 37^0C for 15-20 minutes, following which 50μl of DNA staining solution (50 μg/ml of propidium iodide) was added to each sample. Finally, the samples were incubated for 5-10 minutes at room temperature before the flow cytometry analysis.

3.6.3 DNA Analysis

The cell cycle position of a cell can be determined by measuring the DNA content in that cell. This method measures the amount of DNA stained with the double stranded nucleic acid intercalating dye, propidium iodide(PI), in each cell. Following calibration, samples containing the cells and the absorbed Propidium Iodide were analysed by a Coulter Epics Elite Flow Cytometer, using an argon laser operating at wavelength 488 nm. A standard protocol for measuring the DNA content of cells was adopted and data acquisition was then initiated until at least 10,000 cells for each sample were collected. Within the acquired samples there were cell aggregates and debris that had to be excluded from the analysis by gating. The results were then saved as list mode files to be analysed for their cell cycle distributions at a later time. The relative percentages of cell cycle sub-populations were finally determined using Multicycle software (Phoenix Flow Systems). The Multicycle analysis is based on the fact that a cell cycle distribution can be deconvoluted by fitting the G_1 and G_2 peaks as Gaussian curves and the S phase by a series of overlapping Gaussian curves, as explained in section 2.6. Fitting these curves to histogram data is carried out using a nonlinear least squares routine where successive approximations are made until no further improvement to the fitted parameters is

obtained. The end result is as exemplified in Figure 3.3.

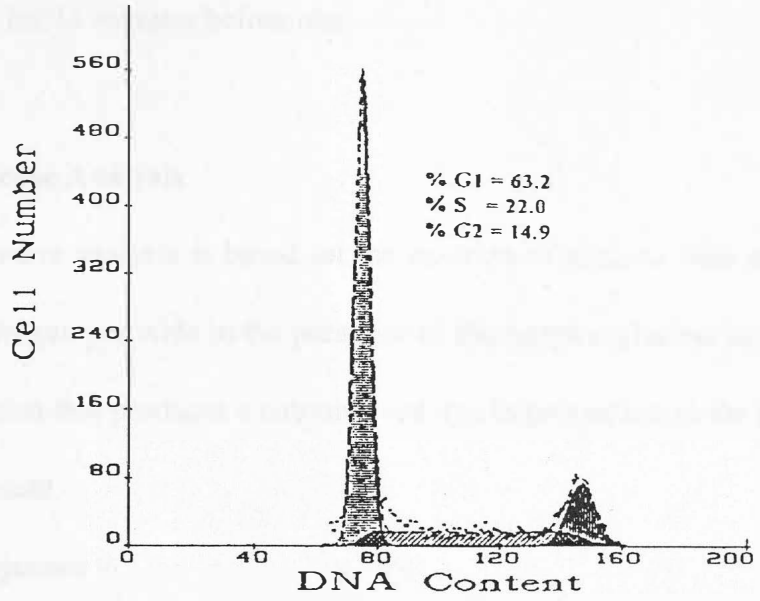

Figure 3.3 A Sample of Cell Cycle Analysis Using Multicycle Software

3.7 Metabolite Assays

Glucose, lactate and ammonia concentrations throughout the batch cultivation of CHO cells were measured by an IBI Biolyzer Analysis System using a patented dry slide technology (Kodak UK). All the reactions for quantitative measurements took place within the dry slide. A slide was used once for a single test and then was discarded.

3.7.1 General Procedure

The appropriate slide was positioned into the loading station and then pushed into the slide spotting station by the advance lever. 10μl samples were pipetted using the specialized pipette included with the IBI Biolyzer. The built-in timer was started by an optical drop detector. After completion of the incubation period (5 minutes) the slide was

conducted to the photo detector for the final stage of calculation of the sample concentrations. Unused slides were stored at -18^{0}C and were warmed to room temperature for 15 minutes before use.

3.7.2 Glucose Analysis

Biolyzer glucose analysis is based on the reaction of glucose with molecular oxygen to produce hydrogen peroxide in the presence of the enzyme glucose oxidase, followed by a second reaction that produces a coloured red dye in proportion to the peroxide (and hence glucose) present.

Reaction Sequence

$$\text{Glucose} + 0_2 + H_20 \xrightarrow{\text{Glucose Oxidase}} \text{Gluconic Acid} + H_20_2$$

$$2\ H_20_2 + \text{4-Aminoantipyrine} + \text{1,7-Dihydoxynaphthalene} \xrightarrow{\text{Peroxidase}} \text{Red Dye}$$

3.7.3 Lactate Analysis

Lactate levels in the sample are measured by following the catalysed conversion of L(+) lactate to pyruvate and hydrogen peroxide in the presence of oxygen. As in the glucose analysis above, the hydrogen peroxide generated, oxidises a 4-aminoantipyrine, 1,7-dihydroxy- naphthalene chromagen system in the horseradish peroxidase catalysed reaction, to form a dye complex.

$$\text{L(+) Lactic Acid} + 0_2 \xrightarrow{\text{Lactate Oxidase}} \text{Pyruvate} + H_20_2$$

$$2\ H_20_2 + 4\ \text{Aminoantipyrine} + \text{1,7-Dihydroxynaphthalene} \xrightarrow{\text{Peroxidase}} \text{Red Dye}$$

3.7.4 Ammonia Analysis

Biolyzer ammonia analysis is based on selective migration of ammonia through the semi-permeable membrane to react with the indicator dye in a second reagent layer. Ammonia solutions were diluted between 2-5 fold as the Biolyzer effective range for ammonia concentration is between 1-500 mmol(s).

NH_3 + Bromphenol Blue $\longrightarrow$ Blue dye

3.7.5 Glutamine Assay

Determination of the glutamine concentration in the medium was made using a calorimetric assay kit (Sigma Bio-sciences UK). The assay is based on the reductive deamination of L-glutamine by a proprietary enzyme. Quantification is accomplished by linking a dye directly to the reductive reaction. The reaction is specific to glutamine and does not cross-react with other amino acids or ammonia. In order to account for the differences associated with any inhibition or enhancement effects of the media an internal standard was used with every sample.

Reference Curve

Duplicate samples of standards ranging from 0 mmol to 6 mmol of glutamine were prepared and a reference curve was plotted.

Assay Procedure

2 ml samples were pipetted into two Eppendorf centrifuge tubes and spun at 10000 rpm for 5 minutes. 300µl of the supernatant medium from each Eppendorf was added to a

tube along with 50µl of reaction buffer and 500 µl of diluent buffer. Then, 150µl of enzyme preparation was added to each tube and the samples were incubated for 1 hour at 37^0C. Following the incubation period, 100 µl of colour reagent was added to each tube and mixed thoroughly. The mixture was then allowed to stand at room temperature for 5 minutes before transferring the contents of each tube to a 1 ml cuvette for spectrophotometric analysis at 550 nm. In the preparation of the internal standard, instead of 500 µl of diluent buffer, 490µl was used and the remaining 10µl was replaced with 10µl of L-glutamine standard (60 mmol L-glutamine).

Calculations

The quantity of L-glutamine in the sample was determined using the following formula:

D = (A-B)/C Where

A = glutamine in sample with internal standard (mmol)

B = glutamine concentration in sample without internal standard(mmol)

C = glutamine concentration added as internal standard (2 mmol)

D = recovery value

E = Uncorrected glutamine concentration in sample (calculated from the reference curve)

The corrected glutamine concentration is then obtained by dividing the calculated value from the curve (E) by the recovery value (D)

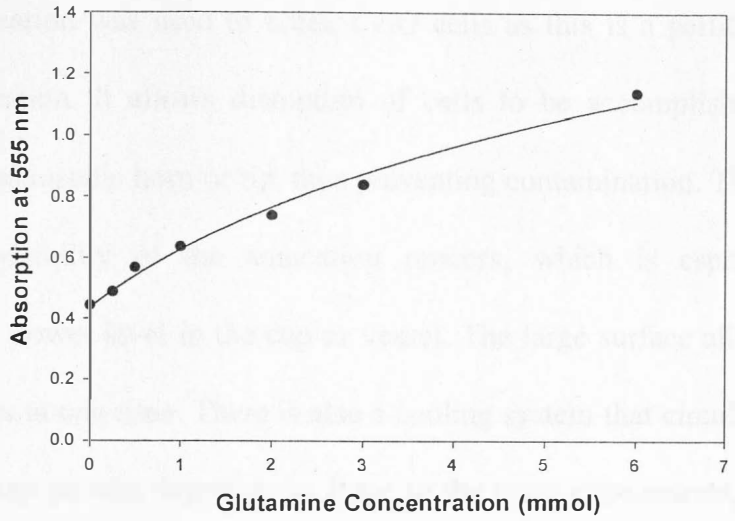

Fig 3.4 **Glutamine Standard Curve**

3.8 Cell Mass Content

3.8.1 Protein Content by Bradford Method

The total soluble protein content was taken to be an indicator of a change in the mean cell mass of the CHO cell population. Pierce Coomassie Protein Assay Reagent, a ready-to-use modification of the well-known Bradford Assay, was used in this experiment.

Sampling and storage of cells for analysis

2-3 ml samples of CHO cells in suspension were removed and centrifuged at 1000 rpm for 5 minutes and washed twice with phosphate buffer saline (PBS). After discarding the supernatants a few drops of 70% cold ethanol/water mixture were added to the tube. Samples were then labelled and kept at -18^0C for further treatment.

Sonication

Cup Horn sonication was used to break CHO cells as this is a particularly convenient means of sonication. It allows disruption of cells to be accomplished without direct exposure to an ultrasonic horn or tip, thus preventing contamination. The transparent cup provides full visibility of the sonication process, which is especially helpful in determining the power level in the cup or vessel. The large surface allows sonication of multiple samples at one time. There is also a cooling system that circulates cold water to minimise/stop any protein degradation. Prior to the main experiments, a small study of the effect of sonication at different settings and durations on cells was carried out to determine the optimum operating conditions for sonication. Among the five settings available setting 3 was chosen as it was in the middle of the range. The results are shown in Figure 3.5.

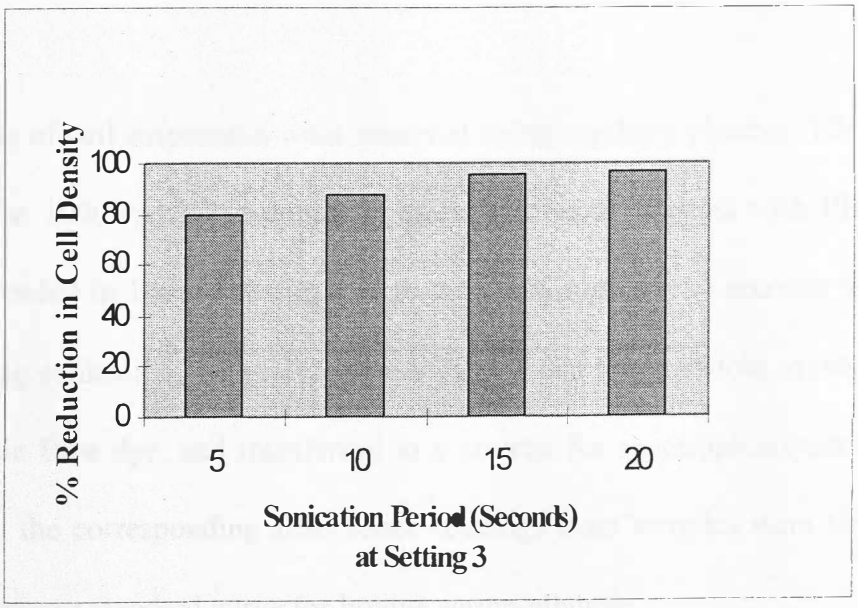

Fig 3.5 Sonication Calibration Chart

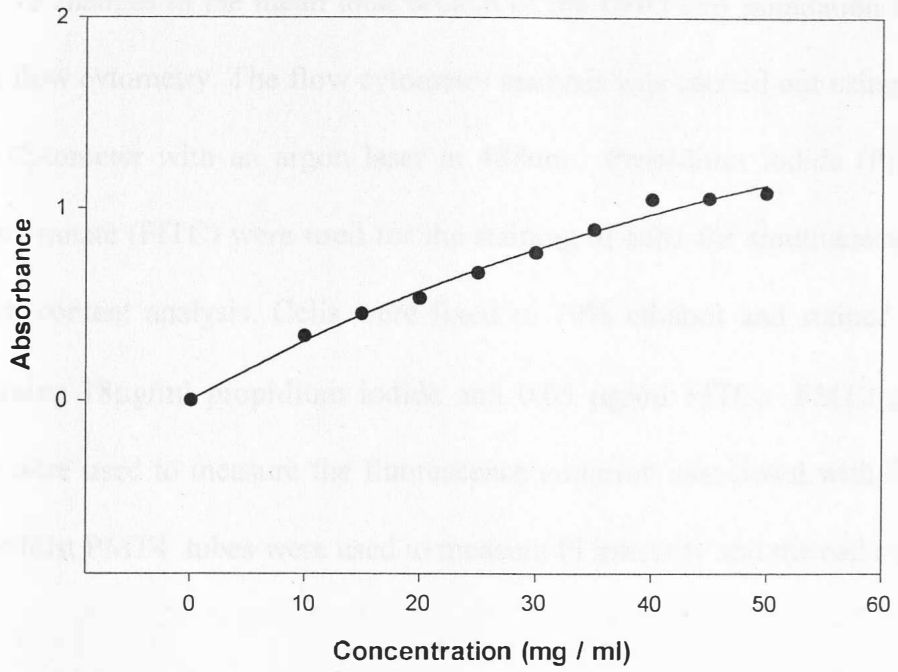

Fig 3.6 Bovine Serum Albumin Microtitre Calibration Curve

Analysis

2 ml samples of cell suspension were removed using capillary pipettes. These were then centrifuged at 1000 rpm for 5 minutes and subsequently washed with PBS. The cells were resuspended in 1 ml of distilled water and sonicated for 30 seconds to break them up. Following sonication, the samples were diluted one hundred-fold, mixed with 500µl of Coomassie Blue dye, and transferred to a cuvette for spectrophotometric analysis at 595 nm. All the corresponding absorbance readings from samples were then converted into µg/ml using a standard curve for bovine serum albumin.

3.8.2 Protein Content by Flow Cytometry

Relative changes in the mean total protein of the CHO cell population were determined using flow cytometry. The flow cytometry analysis was carried out using a Coulter Epics Elite Cytometer with an argon laser at 488nm. Propidium iodide (PI) and fluorescin isothiocyanate (FITC) were used for the staining of cells for simultaneous cell cycle and protein content analysis. Cells were fixed in 70% ethanol and stained with a solution containing 18μg/ml propidium iodide and 0.05 μg/ml FITC. PMT2 photo multiplier tubes were used to measure the fluorescence emission associated with FITC staining of cells whilst PMT4 tubes were used to measure PI intensity and the cell cycle fraction.

3.9 Cell Size Analysis

Measurement of cell volume was made by three different methods in order to study variation of the mean cell size over a doubling time, to measure the mean size of cell cycle fractions and the changes of cell volume throughout batch cultivation under various environmental conditions.

3.9.1 Coulter Multisizer

Apparatus

The apparatus consists of a glass tube with a small orifice on its side at the end which is between 20-200 μm in diameter. This is immersed into a glass container in which the cells to be counted or sized are suspended in an electrically conducting fluid. As a result of suction created by the vacuum pump, electrolyte flows into the tube transporting the cells through the orifice, which in turn brings about changes in electrical resistance.

These changes in electrical resistance are then transformed into a pulse shaped electrical signal. The height of the pulse is proportional to the volume of cells.

Procedure

The apparatus was calibrated using latex beads. Tubes of 100 μm orifice diameter were chosen and installed for this analysis. 1-2 ml of CHO cells were sampled at various intervals and diluted in 170 ml of Isoton II (Coulter Electronics UK). Stirring of the diluted suspension was maintained throughout the analysis to keep the cells in suspension. Data from cells were obtained in the form of graphs and bar charts and were analysed using ACCUCOMP software.

3.9.2 Cell Sizing by Flow Cytometry

The Coulter Epics Elite Flow Cytometer was used to determine the mean cell size of CHO320 cells. A test tube containing the cell suspension is placed on the instrument from which the sample passes down tubing due to the action of a high velocity injection nozzle. The nozzle, containing sheath fluid under pressure, hydrodynamically focuses the cells so that they exit the nozzle in single file. Laser light is then focused onto the stream where each cell is interrogated as it passes through the laser.

Photo multiplier tubes (PMTs) collect the photon emissions from each cell and convert them to analog voltages. Light scattered at the same wavelength and direction as the laser light correlates with the relative size of the cells (Forward Scatter). Data were collected

and presented in the form of single parameter histograms of cell count versus forward scatter, from which the mean size of the population was obtained.

3.9.3 Centrifugal Elutriation

The technique of centrifugal elutriation was applied to produce cell cycle enriched fractions from normally growing heterogeneous batch cultures. The cell size and cell cycle states of elutriated fractions were then investigated. Centrifugal elutriation offers advantages with respect to the speed of separating cells. The method is rapid in that a large number of cells can be separated within a relatively short period of time. It is also an alternative to starvation synchrony and a less "interruptive" technique in terms of cell biochemistry. Asynchronous CHO cells were separated by centrifugal elutriation using a Beckman J-6 M/E centrifuge equipped with a JE-6B elutriation rotor and standard elutriation chamber. The rotor speed was kept at 1950 rpm at 20^0C. Cells were introduced into the chamber using phosphate buffer saline (PBS) as eluant. All cells were elutriated under aseptic conditions. Pump speed was progressively increased during fractionation of cells. Approximately $2x10^8$ cells were harvested from exponentially growing CHO cells in culture and loaded into the elutriation chamber with eluant running at a pump setting of 0.75 units on the scale. The eluant pump setting was increased by 0.25 units for every 50 ml fraction collected. 2-3 ml of each fraction was removed for cell size analysis by Coulter Multisizer and the remaining amount was used to carry out the cell cycle analysis using flow cytometry. Results from cell cycle analysis and cell sizing were then analysed in order to determine the mean diameters of the cell cycle fraction.

3.10 Modelling and Tuning Methods

The building of mathematical models and subsequent simulation using them were accomplished using Matlab 4.2c. Matlab stands for MATRIX LABORATORY. It is a technical computing environment for numeric computation. Matlab also features a family of application specific solutions called tool boxes. The Simulink 1.3c toolbox, which was used extensively, enables diagrammatic representation of dynamic systems. A simulink block diagram for a simple dynamic model is shown in Fig 3.7. The optimisation tool box was also used for tuning purposes. It consists of functions that perform minimisation or maximisation on general nonlinear functions. A least squares routine was used to tune each model's parameters. A sample optimisation routine is shown in the appendix I.

Overview of Optimisation Routine

- The model is simulated over the time period of reference data using a fourth order Runge-Kutta algorithm.
- Output values are interpolated to obtain simulated values corresponding to the reference time data set.
- The difference between the measured and simulated values constitutes the error which will be reduced in order to get the best fit to the experimental data.

Validation of Model

Wherever possible, models were tuned and validated against another set of data not previously used in the tuning.

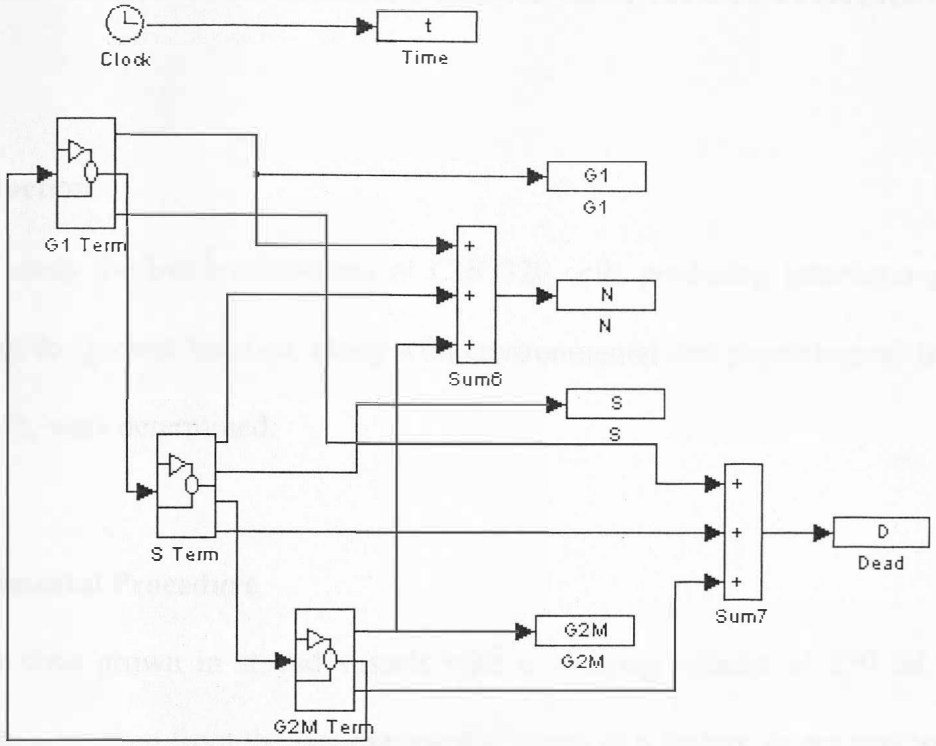

Figure 3.7 A Simulink Block Diagram for a Dynamic Model

CHAPTER 4

GROWTH KINETICS OF CHO320 CELLS IN BATCH CULTIVATION

4.1 Introduction

In this initial study the batch cultivation of CHO320 cells producing interferon-γ was carried out and the growth kinetics, along with environmental and physiological factors affecting growth, were determined.

4.2 Experimental Procedure

CHO320 cells were grown in stirred vessels with a working volume of 250 ml. The initial inoculum was taken from the late exponential phase of a culture grown previously, spun down and resuspended in 250 ml of fresh medium to give a CHO cell concentration of approximately $2x10^5$ cells.ml^{-1}. The medium used was RPMI 1640 supplemented with 5% foetal calf serum. Stirred vessels were incubated at 37^0C and magnetically stirred at an agitation rate of 150 rpm. 7-9 ml samples were removed at various intervals from the culture and analysed. The variation of cell number was determined using a haemocytometer and cell viability was determined using trypan blue exclusion dye. Metabolite concentration profiles during batch culture were quantified by colorimetric methods (Kodak Biolyzer). Cells were also fixed with 70% ethanol after centrifugation at 1000 rpm for 5 minutes, labelled and stored at -18^0C for cell cycle analysis by flow cytometry.

4.3 Results and Discussion

4.3.1 CHO 320 Growth Profile

A typical growth profile of CHO320 cells is presented in Figure 4.1. As expected the growth curve is sigmoid in shape with three distinct lag, exponential and stationary phases. A typical batch using RPMI 1640 medium lasted between 100-120 hours before a significant reduction in viable cell number was observed. CHO320 cells in stirred vessels reached maximum viable concentrations of 1-1.2 x 10^6 cells.ml^{-1} after 93-100 hours. The maximum specific growth rate during exponential growth was found to be 0.03 h^{-1}. A decline in viability at the beginning of batch culture, as shown in Figure 4.1, is believed to be in part due to adhesion of cells to the inner surface of the spinner flasks and partly as a result of cell death. After the initial decline, viability increases again until the onset of the exponential phase where a decrease in viability is observed. The sharp decline at the end of the culture time is associated with cell death due to substrate exhaustion.

4.3.2 Glucose Metabolism

The specific glucose consumption and lactate production rates are shown in Figure 4.2. They were calculated by evaluating the rates of consumption and production of glucose and lactate using the correlation $(c_2-c_1)/(t_2-t_1)$ where c and t correspond to the concentration and time of measurement of metabolites. To obtain the specific consumption or production, the calculated rates were divided by the mean cell number corresponding to t_1 and t_2. As is evident, both glucose and lactate specific consumption and production rates decline as the cultivation time progresses and the number of viable cells increases. The rate of decline is more marked between 41-80 hours, lactate

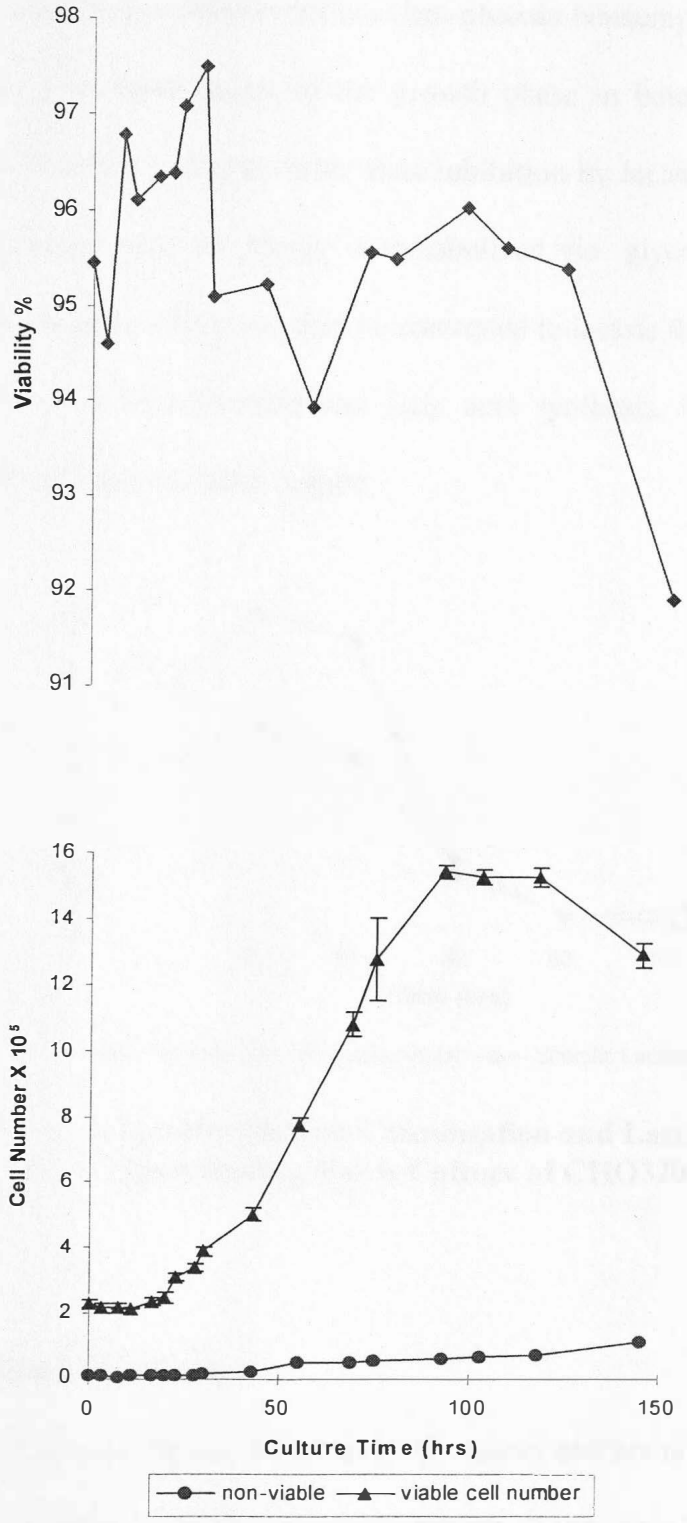

Fig 4.1 **Viable Cell Number, Non-viable Cells and Viability for CHO320 Batch Culture. Error Bars Represent the Standard Deviation of Six Cell Number Measurements**

production exhibiting a sharper decline than glucose consumption. Reduction in specific growth rate in the later stages of the growth phase in batch cultures is attributed to depletion of essential nutrients rather than inhibition by lactate and ammonia (Hayter *et al*, 1991). Glucose used for energy is metabolized via glycolysis to pyruvate, the end product of glycolysis, which can then be converted to lactate that is excreted. Glucose may also be used in nucleotide and fatty acid synthesis. Glucose was found to be exhausted by 120 hour of batch culture.

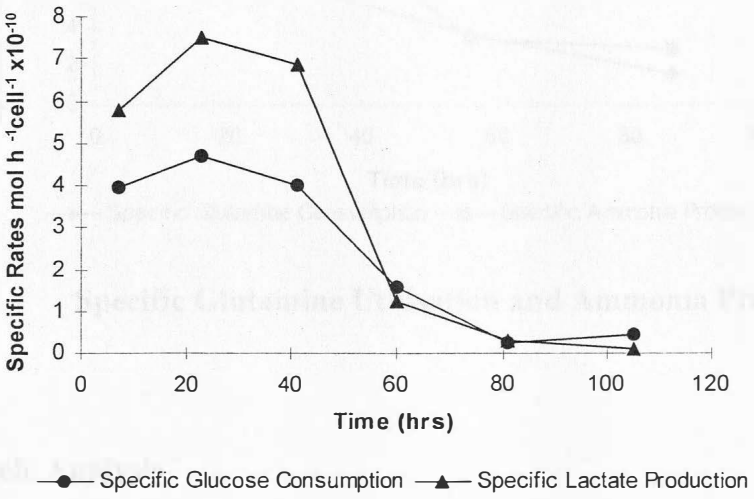

Fig 4.2 **Specific Glucose Consumption and Lactate Production Rates During Batch Culture of CHO320 Cells**

4.3.3 Glutamine Utilisation

Glutamine is the most rapidly depleted energy source and amino acid in the culture and is therefore often taken to be the limiting substrate. It was found to be exhausted by 100 hours, which corresponded with the end of the exponential phase. Patterns of change in the concentration profile of glutamine during the batch culture resembled that of glucose. The rates of consumption and production of glutamine and ammonia respectively were

also found to be declining with time. The glutamine is catabolised in a number of ways and the major end products of metabolism are a variety of intermediates entering the tricarboxylic cycle e.g. (asparate, alanine) and ammonia whose specific production rate is also graphically shown in Figure 4.3.

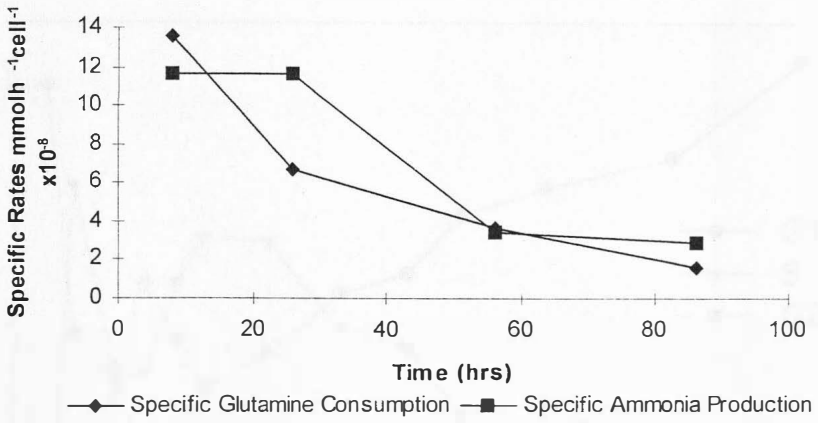

Fig 4.3 **Specific Glutamine Utilisation and Ammonia Production Rates**

4.3.4 Cell Cycle Analysis

The results of cell cycle analysis are shown in Figure 4.4. The percentage of G1 cells at the start of the batch process is the highest as cells were partially synchronised before inoculation. This partial synchrony was primarily brought about by depletion of substrates in the inoculum stage. As is shown, cells start accumulating in the G1 phase after somewhere between 43 and 50 hours of batch culture. It is believed that the concentration of the substrate in the medium plays an important role in determining the fate of G1 cells, whether they pass through the restriction point or simply stay in G1 phase and possibly undergo apoptosis. S cell behaviour is shown to be inversely related to G1; a decrease in G1 is followed by an increase in S cells almost to the same extent. In

some instances at the end of a recuperative period, G_2M transition to G1 and G1 transition to S events are synchronised. The fraction of G2M cells, however, remains constant (~15-19%) for most of the duration of batch fermentation.

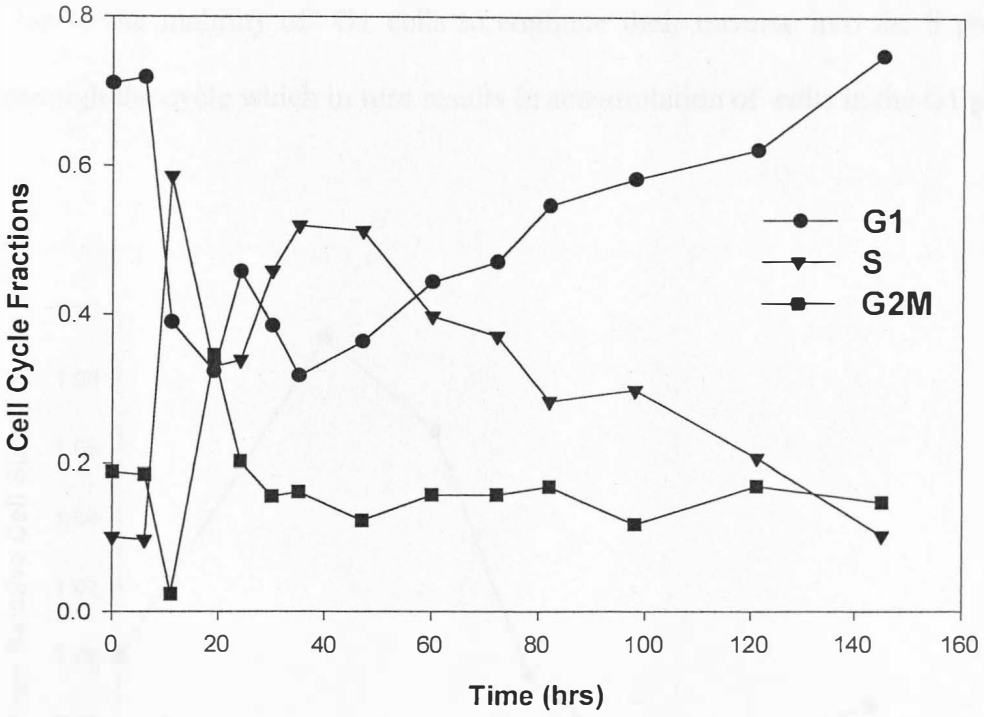

Fig 4.4 **Profile of Cell Cycle Fractions of a Partially Synchronised CHO320 Batch after Inoculation in Fresh Medium**

4.3.5 Cell Size Variation During a Batch Culture

The mean cell size of partially synchronised CHO cells was measured by means of forward scatter on a flow cytometer and the values for the relative mean size with respect to the initial mean size of the population were evaluated. The higher the forward scatter value the larger is the mean volume of cells. Results are shown in Figure 4.5. In partially

synchronised culture being high in G_1 cells at the start of inoculation, the relative mean cell size increased as the cells progressed through the cycle. The maximum mean relative size of cells was achieved at 20-30 hour of culture time following which there was a steady decline in the mean relative size until the termination of the batch fermentation. The fact that cell size does not increase again after the first doubling period, may be partly due to the inability of G1 cells to continue their traverse into the S phase and hence through the cycle which in turn results in accumulation of cells in the G1 phase.

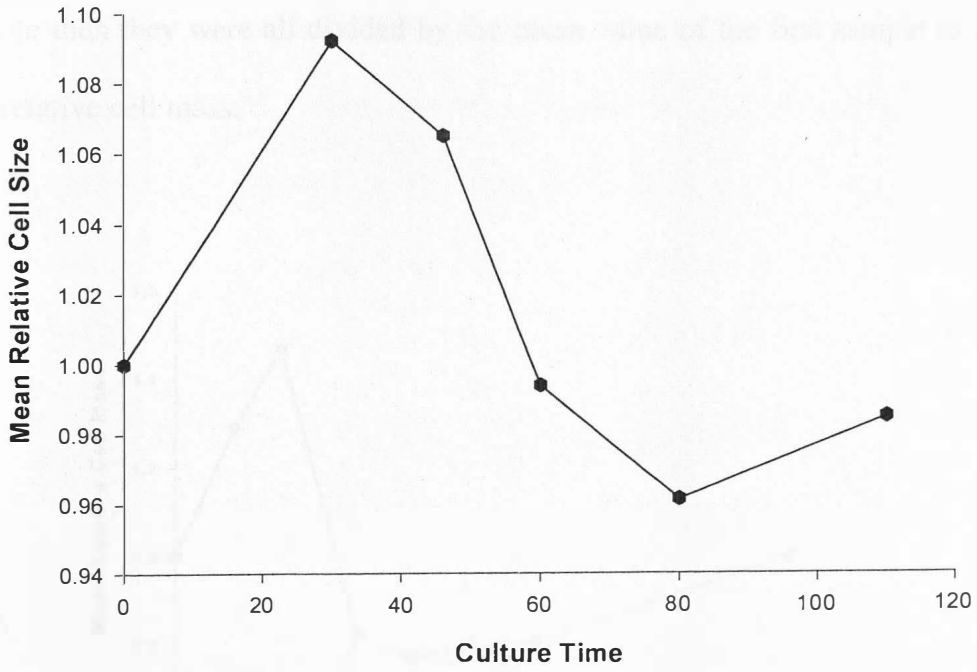

Fig 4.5 **Mean Relative Size of CHO320 Cells at Different Times of Batch Cultivation in Stirred Flask**

4.3.6 Mean Relative Cell Mass

Figure 4.6 presents the flow cytometry analysis results for the variation in the mean relative mass of CHO cells in batch culture with time. As has previously been shown by Hu *et al* (1989), the mean relative cell mass of cells is shown to mimic mean relative cell size or volume patterns of change with time and their relationship is linear. To obtain the mean relative cell mass of CHO cells, measured fluorescence emissions associated with FITC staining (refer to section 3.8.2) were saved as histograms of cell count vs. FITC intensity from which data corresponding to peak heights and mean values of each peak for each sample were obtained. Once all the mean values for a batch of cells were available then they were all divided by the mean value of the first sample to obtain the mean relative cell mass.

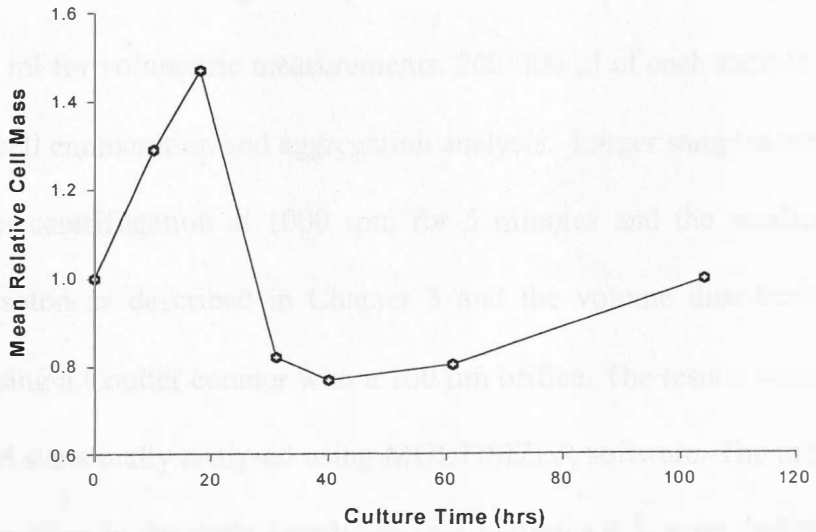

Fig 4.6 Mean Relative Mass of CHO320 Cells in Batch Cultivation

4.4 Volume Distribution of CHO320 Cells by Electrically Sizing Transducers

4.4.1 Introduction

Cell size and mass can be used to distinguish between similar but distinct populations of animal cells. Increase and decrease of mean cellular volume or mass and their respective distributions in the study population are connected with and are reflective of the environmental and physiological conditions the cells are in. Volume and mass also play important roles in the modelling of a population either as independent single parameters or as basic parameters in multi-parameter analyzing systems.

4.4.2 Experimental Procedure

A partially synchronised batch culture of CHO320 cells containing RPMI 1640 as medium and 5%(v/v) of foetal calf serum was started and 6-7 ml samples were aspirated using a pipette at various intervals within a doubling time. The original samples were further subdivided into a larger sample of 5ml for cell cycle analysis and a smaller sample of 2 ml for volumetric measurements. 200-300 μl of each sample was placed in a cuvette for cell enumeration and aggregation analysis. Larger samples were fixed in 70% ethanol after centrifugation at 1000 rpm for 5 minutes and the smaller samples were diluted in isoton as described in Chapter 3 and the volume distribution of cells was measured using a Coulter counter with a 100 μm orifice. The results were acquired on an IBM PC and statistically analysed using MULTISIZER software. The mean diameters of cell cycle fractions in the study population (see section 4.4.3) were derived using the cell cycle analysis and volume distribution data and the resulting system of equations were solved for each fraction. Various factors can affect the volume distribution and add to the difficulty of interpreting the volume distribution data. In this study, the presence of cell

aggregates in the sample had to be taken into account. In order to quantify the cell aggregates they were divided into doublets, triplets and larger aggregates and their average frequency in the culture was determined using a microscope.

4.4.3 Results and Discussions

Figure 4.7 (0-31hrs) shows the volume distributions of a typical batch of a partially synchronised CHO320 cells. A gradual increase in the degree of skewedness of the volume distribution curves to the right (away from the origin) which is associated with corporeal progression of cells through the cycle was observed. Mean and median values of the above distributions were determined and are plotted against the culture time in Figure 4.8. The qualitative behaviour of the means is similar to that of median and mode, increasing after inoculation, reaching a peak value at around 20 hours and decreasing as new G1 cells enter the cycle after division. The diameters of the cell cycle fractions G1, S and G2M were determined by developing a system of equations using cell cycle analysis and volume distribution data. A typical equation is shown below :

$$\textit{G1 fraction} \times d_{G1} + \textit{S fraction} \times d_S + \textit{G2 M fraction} \times d_{G2M} = \textit{Mean diameter of population} \qquad (4.4.1)$$

where d_i is the diameter of the appropriate cell cycle phase which is multiplied by its fraction obtained by cell cycle analysis, and the right hand side of each equation is the experimental mean diameter value of the total population acquired using the Coulter counter . To calculate the figures in Table 4.1 three equations containing the measured cell cycle data and their corresponding coulter counter measurements of the mean diameters of the total cell populations were developed as follows:

$$0.65\, d_{G1} + 0.244\, d_S + 0.1\, d_{G2M} = 12.13 \qquad (4.4.2)$$

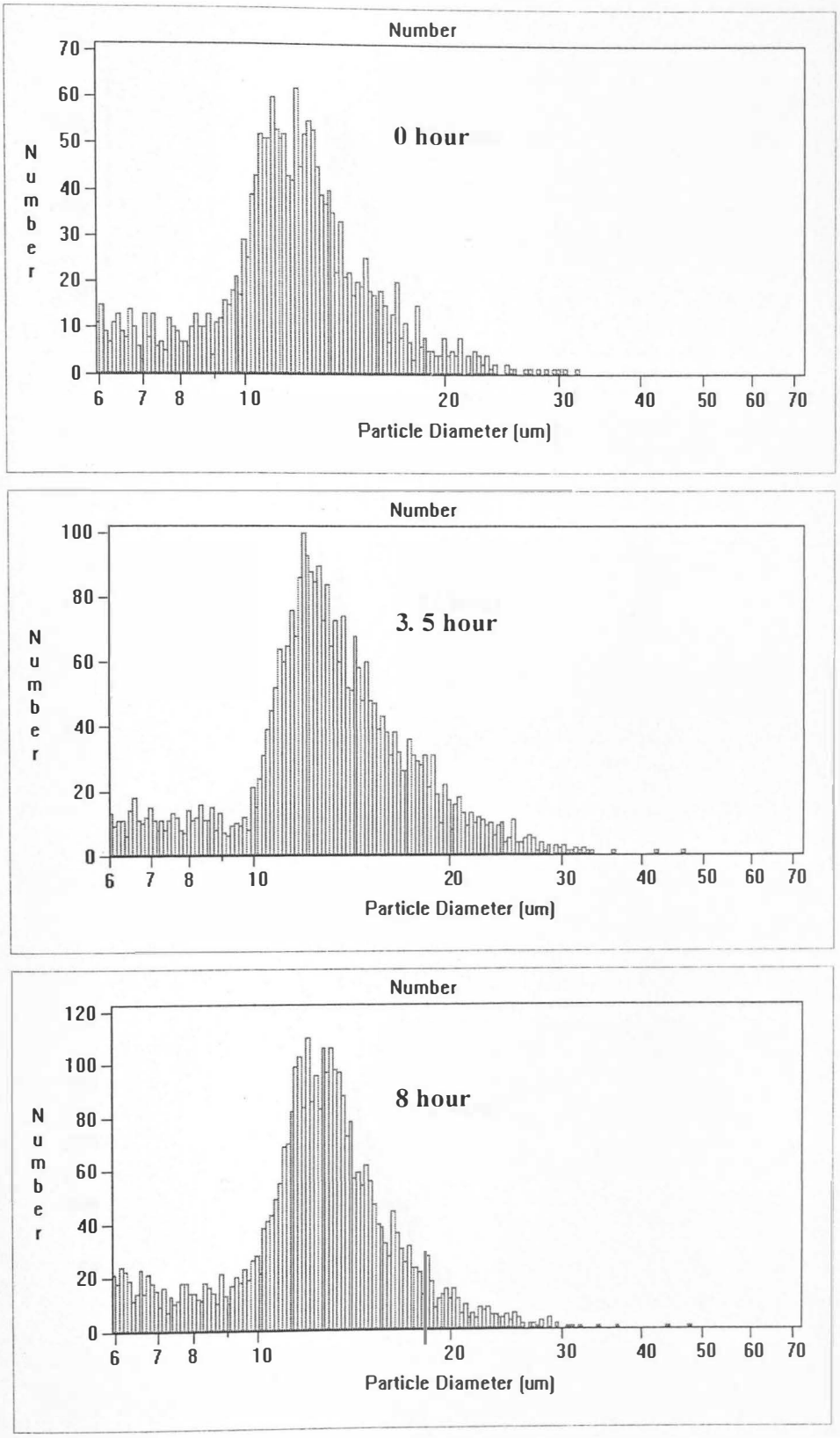

Fig 4.7 (0 - 8 hrs) Volume Distributions of CHO320 Cells in a Doubling Time

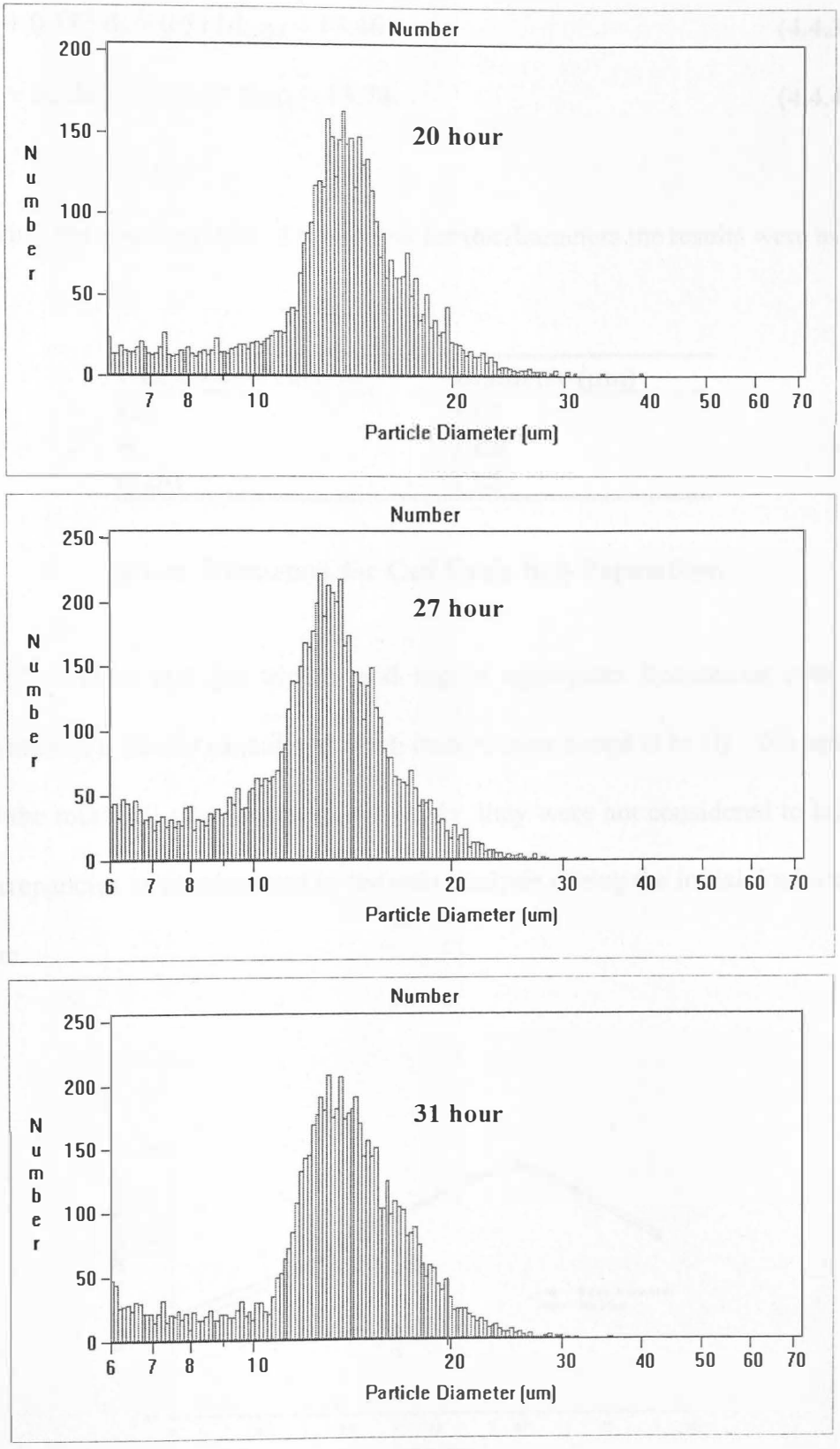

Fig 4.7 (20 - 31 hrs) Volume Distributions of CHO320 Cells in a Doubling Time

$$0.504\, d_{G1} + 0.185\, d_S + 0.311 d_{G2M} = 13.46 \quad \textbf{(4.4.3)}$$

$$0.307\, d_{G1} + 0.524\, d_S + 0.169\, d_{G2M} = 13.74 \quad \textbf{(4.4.4)}$$

After solving the above system of equations for the diameters the results were as follows:

Cell Cycle Fraction	Diameter (μm)
G1	10.7
S	14.3
G2M	17.5

Tab 4.1 **Mean Diameters for Cell Cycle Sub-Populations**

Average (i) doublet and (ii) triplets and higher aggregates frequencies over the first doubling time of a freshly inoculated batch culture were found to be (i) ~ 6% and (ii) < 1% of the total cell population. In this study, they were not considered to bring about large discrepancies or inaccuracies in the data analysis during the initial doubling time of the culture.

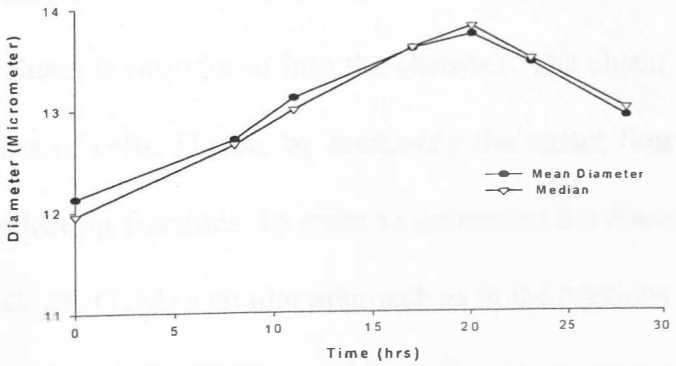

Fig 4.8 **Variation of Mean and Median Distributions of CHO320 Volume in Batch Culture**

4.5 Evaluation of Diameter in CHO320 Cells by Centrifugal Elutriation

4.5.1 Introduction

As discussed earlier, starvation synchrony may have some effect on the intracellular biochemistry and as a result may bring about changes in the degree of hydration and hence the volume of cells. This study was carried out for comparison with that of the starvation synchrony method.

4.5.2 Experimental Procedure

Fractionation of CHO320 cells was carried out by centrifugal elutriation using a Beckman J-6M/E centrifuge equipped with a JE-6B elutriation rotor. The temperature of operation was 20^0C, the eluant used was phosphate buffer saline (PBS) and the centrifuge was operated at 1950 rpm. $2x10^8$ cells were allowed into the chamber with the eluant running at a pump setting of 0.75 units. Pump speed was increased after each 50 ml fraction was obtained. At the end of the process the seven fractions collected were analysed for their cell cycle and volumetric distributions.

4.5.3 Results and Discussions

The results of fractionation of a heterogeneous CHO320 population by centrifugal elutriation are shown in Figure 4.9. The horizontal axis (fraction number) represents the rate at which the eluant is introduced into the chamber. The eluant role is to oppose the centrifugal retention of cells. Hence, by increasing the eluant flow rate, larger cells are passed into the collecting fractions. In order to determine the diameters of the cell cycle sub-populations (G1, S, G2M) a similar approach as in the previous section was made. Mean values of the total CHO320 population diameters obtained by analysing their respective volume distributions are shown in Figures 4.10(A-C) and their cell cycle data

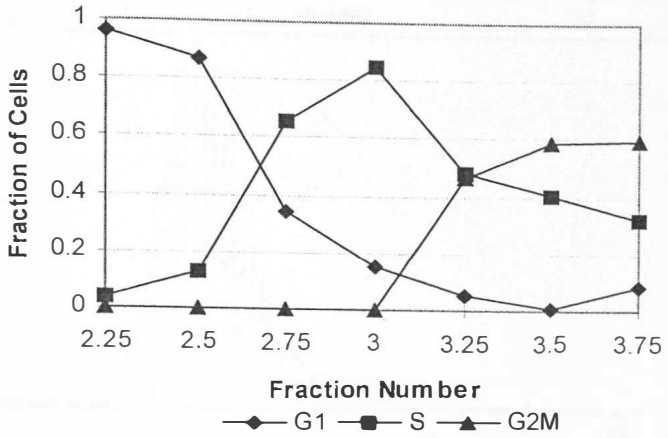

Fig 4.9 **Proportions of Each Cell Cycle Phase in Each Fraction**

were used to develop three equations from which the diameters were determined. The results are shown in the Table 4.2 below.

Cell Cycle Fraction (elutriation)	Diameter (μm)
G_1	11.2
S	15.5
G2M	14.5

Tab 4.2 **Mean Diameters for Cell Cycle Sub-Populations Obtained by Elutriation**

The discrepancy between the calculated diameters for the two methods was found to be significant as shown in Tables 4.1 and 4.2. G1 cells being the least and G2M cells being the most variable in the diameter. The diameters of G1 and S cells obtained by centrifugal elutriation were found to be higher. With reference to G2M cells, calculated

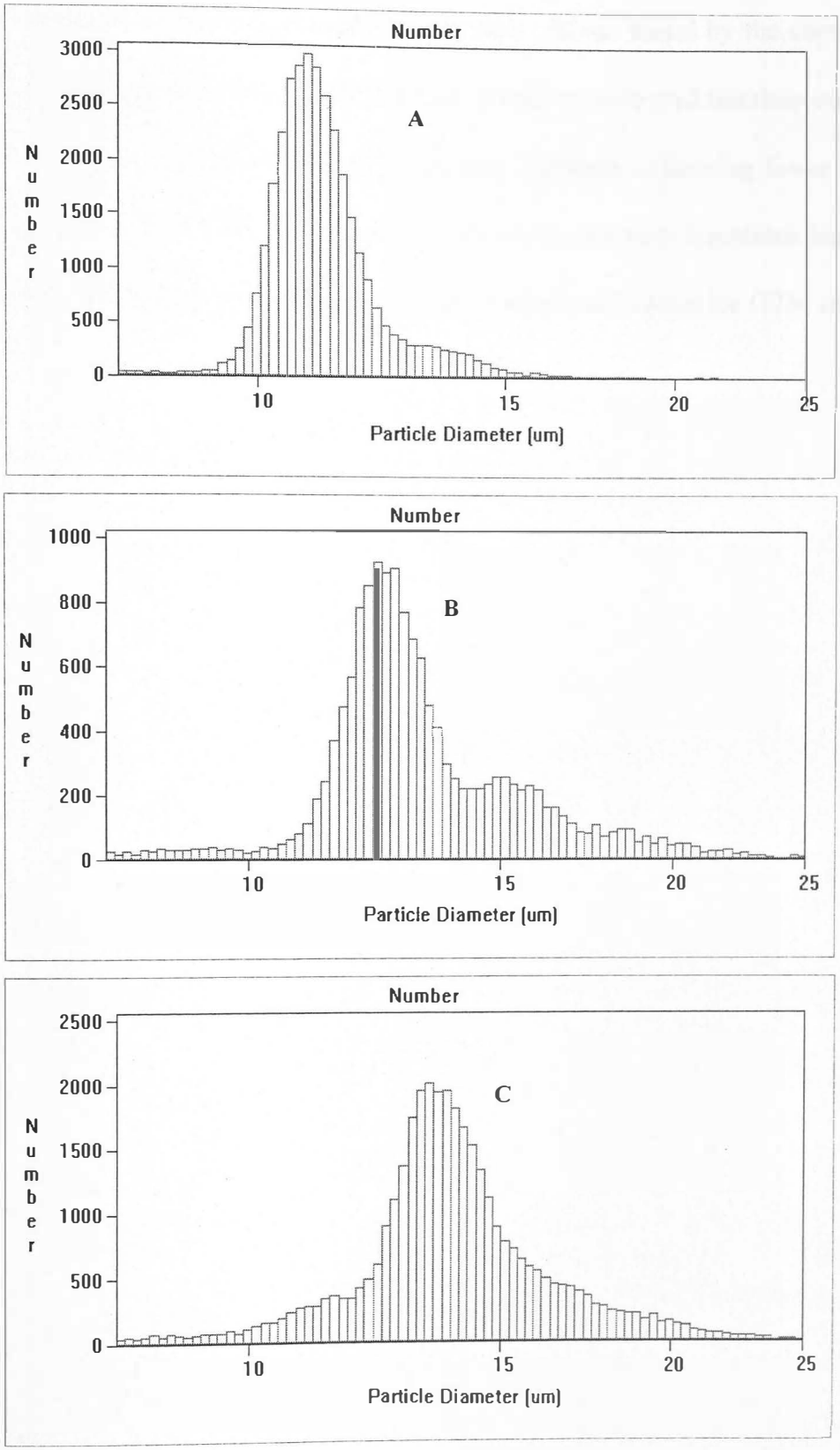

Figure 4.10 (A-C) **Volume Distributions of Some Elutriated Fractions**

diameters by elutriation are significantly lower than those found by the corresponding starvation synchrony method. It is believed that not all the collected fractions containing cells were included in the analysis and hence later fractions containing fewer but larger cells (particularly rich in G2M cells) were not taken into account. Equations based on the early and middle fractions therefore produce underestimated values for G2M cells.

CHAPTER 5

THE EFFECT OF INITIAL SUBSTRATE CONCENTRATIONS ON CHO320 CELLS GROWTH KINETICS

5.1 Introduction

Chinese Hamster Ovary cells use both glucose and glutamine as energy and carbon sources. The use of these substrates both as energy and carbon sources provides CHO cells with a certain degree of flexibility. Increasing the concentration of one substrate could lead to a decrease in the uptake rate of the other, as shown by Meijer et al (1995) where a low supply rate of glucose was followed by higher consumption of glutamine. This chapter describes the growth kinetics of partially synchronised and of asynchronous cultures of CHO320 cells using various initial concentrations of the substrates in the medium.

5.2 Experimental Procedure for the Study of Glutamine Effects on CHO320

CHO cells from a previously grown culture (from the late exponential phase in the case of partially synchronised cultures) were counted by the haemocytometer method. An appropriate amount of cells in suspension was removed and then centrifuged at 1000 rpm for five minutes. The pellet of cells formed by centrifugation was resuspended in a small volume of fresh medium and, after thorough mixing, was divided into three parts and inoculated into three media of different glutamine concentrations to give three batches each of initial concentration ~ $2x10^5$ cells.ml^{-1}. The medium used was RPMI 1640 without glutamine so that adjustment to glutamine concentrations could be made. Prior to inoculation, concentrated glutamine (x100) was added to glutamine free medium to

give final glutamine concentrations of 2, 1 and 0.5 mmol in each culture. Stirred flasks for this study were of 250 ml capacity with 150 ml working volumes. For every run, 5-6 ml samples were removed from the culture out of which 3-4 ml of cells were spun down, and fixed with cold 70% ethanol and stored at -18^{0}C for cell cycle, cell size and cell mass analysis. The remaining part of the samples were used for cell count and viability analysis.

5.3 Results and Discussions

5.3.1 Growth and Death Rates

Figures 5.1A-B and 5.2A-B show the growth and death profiles of CHO320 within the first doubling time in partially synchronised and asynchronous cultures. With respect to viable cell number, batches with higher initial glutamine concentrations gave rise to higher total viable cell number at the end of culture time for both partially synchronous and asynchronous cultures of CHO320 cells. The highest increase in cell numbers in both cases is seen to be that of batch cultures with 2 mmol glutamine concentration. With the exception of the 0.5 mmol glutamine batch, the maximum numbers of viable cells reached in the partially synchronised cultures were higher than those of the asynchronous batches at the end of the culture time, but their respective values remain fairly close to each other up to 18 hours after the inoculation. In both partially synchronised and asynchronous cultures, the profiles of non-viable cells for all glutamine concentrations are shown to decline after inoculation. Whilst the profiles of non-viable cells in the asynchronous batches for all glutamine concentrations stabilised after the initial decline, those of partially synchronised cultures did not and exhibited greater fluctuations.

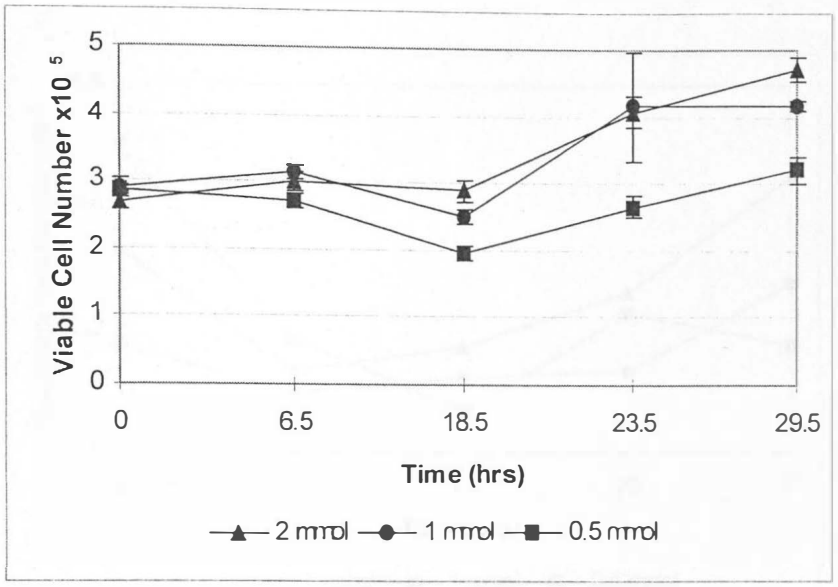

Fig 5.1A **Growth Profiles of CHO320 Cells at Various Initial Glutamine Concentrations in a Partially Synchronised Culture. Error Bars Represent the Standard Deviation of Six Cell Number Measurements.**

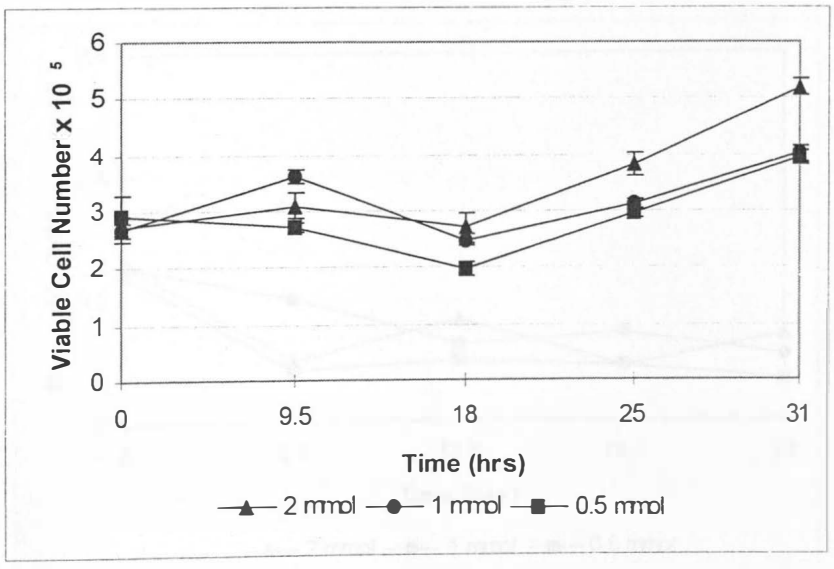

Fig 5.1B **Growth Profiles of CHO320 Cells at Various Initial Glutamine Concentrations in an Asynchronous Culture. Error Bars Represent the Standard Deviation of Six cell Number Measurements.**

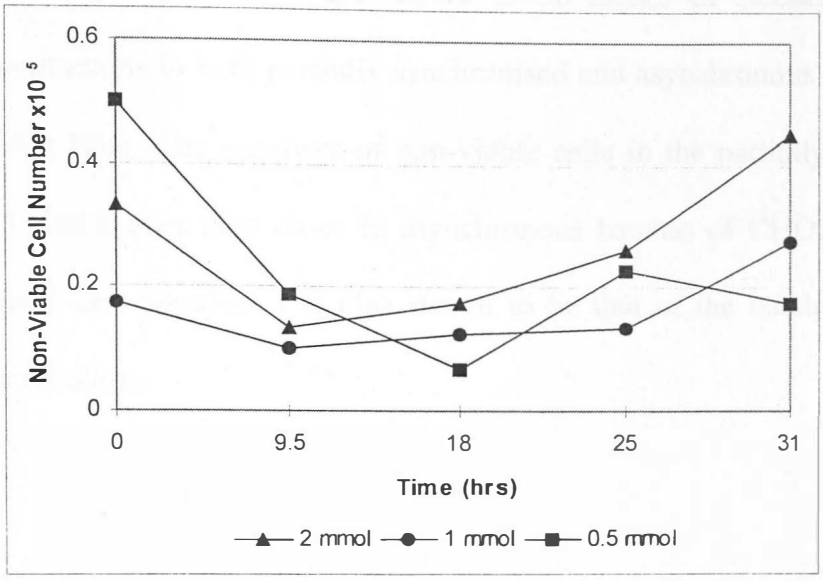

Fig 5.2A **Non-Viable Cell Populations at Various Initial Glutamine Concentrations in a Partially Synchronised Culture.**

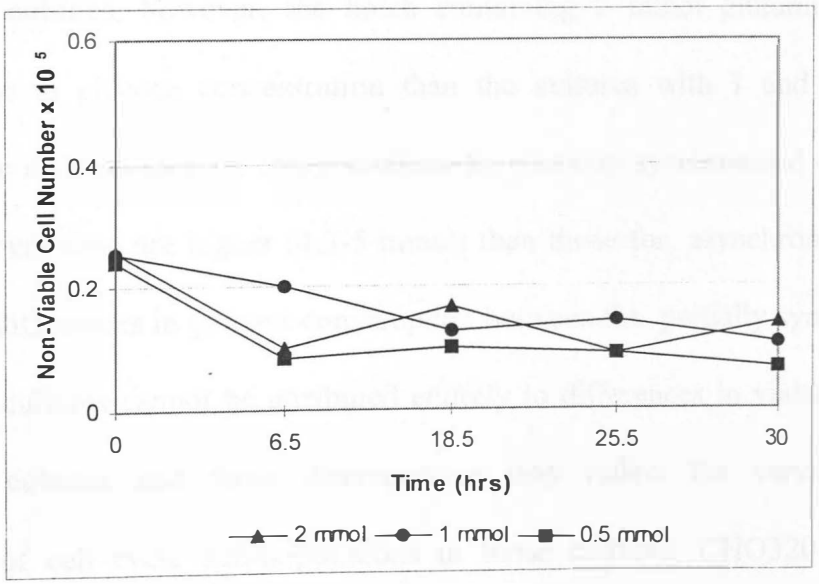

Fig 5.2B **Non-Viable Cell Populations at Various Initial Glutamine Concentrations in an Asynchronous Culture**

Concentrations of non-viable cells are shown to be higher in batches with higher glutamine concentrations in both partially synchronised and asynchronous cultures at the end of the culture time. The numbers of non-viable cells in the partially synchronised batches are 2-3 fold higher than those in asynchronous batches of CHO320 cells. The highest non-viable cell population is also shown to be that of the batch with 2 mmol glutamine concentration.

5.3.2 Glucose Utilisation

Glucose concentration profiles for partially synchronous and asynchronous batches of CHO320 cells with different initial glutamine concentrations are presented in Figures 5.3A-B. In the partially synchronous cultures the changes in glucose concentration with time for all the glutamine concentrations are shown to be very similar. In the asynchronous cultures, however, the batch containing 2 mmol glutamine exhibits a steeper decline in glucose concentration than the cultures with 1 and 0.5 mmol of glutamine. The residual glucose concentrations for partially synchronised cultures at the end of the culture time are higher (4.3-5 mmol) than those for asynchronous ones (2-3 mmol).These differences in glucose consumption between the partially synchronised and asynchronous cultures cannot be attributed entirely to differences in viable cell number between the cultures and these discrepancies may reflect the varying metabolic requirements of cell cycle sub-populations in those cultures. CHO320 cells at low glutamine concentrations (0.5 mmol) do not appear to exhibit the higher glucose consumption rates observed in some cell lines (Vriezen et al, 1997) .

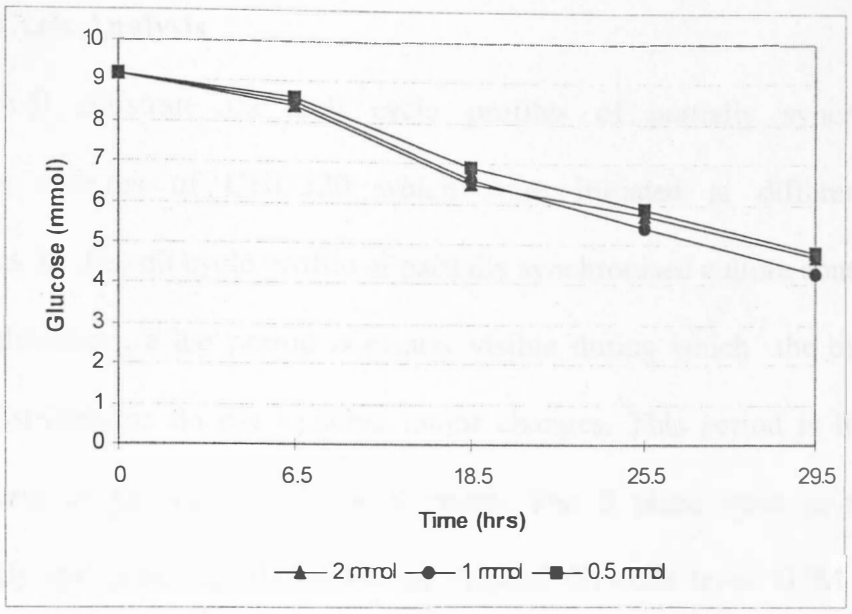

Fig 5.3A **Glucose Metabolism by CHO320 Cells at Various Glutamine Concentrations in a Synchronous Culture**

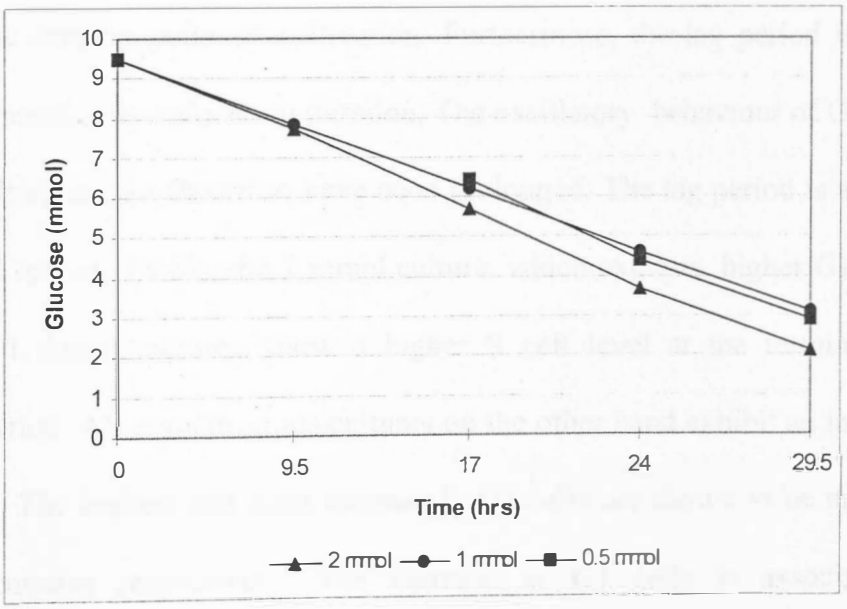

Fig 5.3B **Glucose Metabolism by CHO320 Cells at Various Glutamine Concentrations in an Asynchronous Culture**

5.3.3 Cell Cycle Analysis

Figures 5.4A-B illustrate the cell cycle profiles of partially synchronised and asynchronous cultures of CHO320 which were initiated at different glutamine concentrations. In the cell cycle profile of partially synchronised culture containing 2 mmol of glutamine, a lag period is clearly visible during which the cell cycle sub-population distributions do not undergo major changes. This period is followed by a general traverse of G1 cells into the S phase. The S phase cells in turn increase proportionately and peak slightly below the original G1 cells level. G2M cells show a slight increase following the influx of S cells into and through the G2M. The cell cycle profile of the culture with 2 mmol of glutamine behaved as would normally be expected of a partially synchronised culture. The partially synchronised culture containing 1 mmol of glutamine however has the most unexpected results. Firstly, the results of cell cycle analysis of the 1 mmol sample show a much higher level of S cells than the other two batches at the starting point of cultivation. Furthermore, the lag period is either non-existent or dramatically reduced in duration. The oscillatory behaviour of G1 and S cells in 1mmol culture is also shown to have been prolonged. The lag period is also absent in the 0.5 mmol culture. Unlike the 2 mmol culture, which exhibits higher G1 cells levels, 0.5 and the 1 mmol cultures show a higher S cell level at the termination of the cultivation period. All asynchronous cultures on the other hand exhibit an increase in G1 cells initially. The highest and least increase in G1 cells are shown to be those of 1 and 0.5 mmol cultures respectively. The increase in G1 cells is associated with a proportionate decrease in S cells in all asynchronous cultures. The increase in G1 cells and the proportionate decrease in S cells within the first 10 hours of culture time suggests

that, whilst S cells are able to traverse G2M phase into G1, G1 cells are not traversing from G1 into S phase during that period. G2M profiles remain constant for the first 9.5 hours of culture time after which, with the exception of the 0.5 mmol culture, they drift into the G1 phase. To summarise, it is not believed that changes in medium glutamine concentrations have an affect on the cell cycle of CHO320 cells. The variation observed (Fig 5.4A), particularly between batches of partially synchronised cultures, may have been caused by accidental changes in settings of the flow cytometer during data acquisition.

5.3.4 Mean Relative Cell Size

Changes in the mean relative cell sizes for the three batches are shown in Figure 5.5. Cultures with 2 mmol and 1 mmol of glutamine are similar in their size profile. The results for the 0.5 mmol culture however deviate from the other two cultures after 6.5 hour; the 0.5 mmol culture is rich in S cells whilst the other two cultures are high in G1 cells. As the S cells in the 0.5 mmol culture traverse through G2M into G1 a significant reduction in cell size, associated with cell division, is observed that accounts for the sharp decline in the relative size of the 0.5 mmol culture. The mean relative size of the 0.5 mmol culture increased again after the G1 cells passed into the S phase as shown in Figure 5.5. Data corresponding to the size of cells in batches of asynchronous cultures was not available.

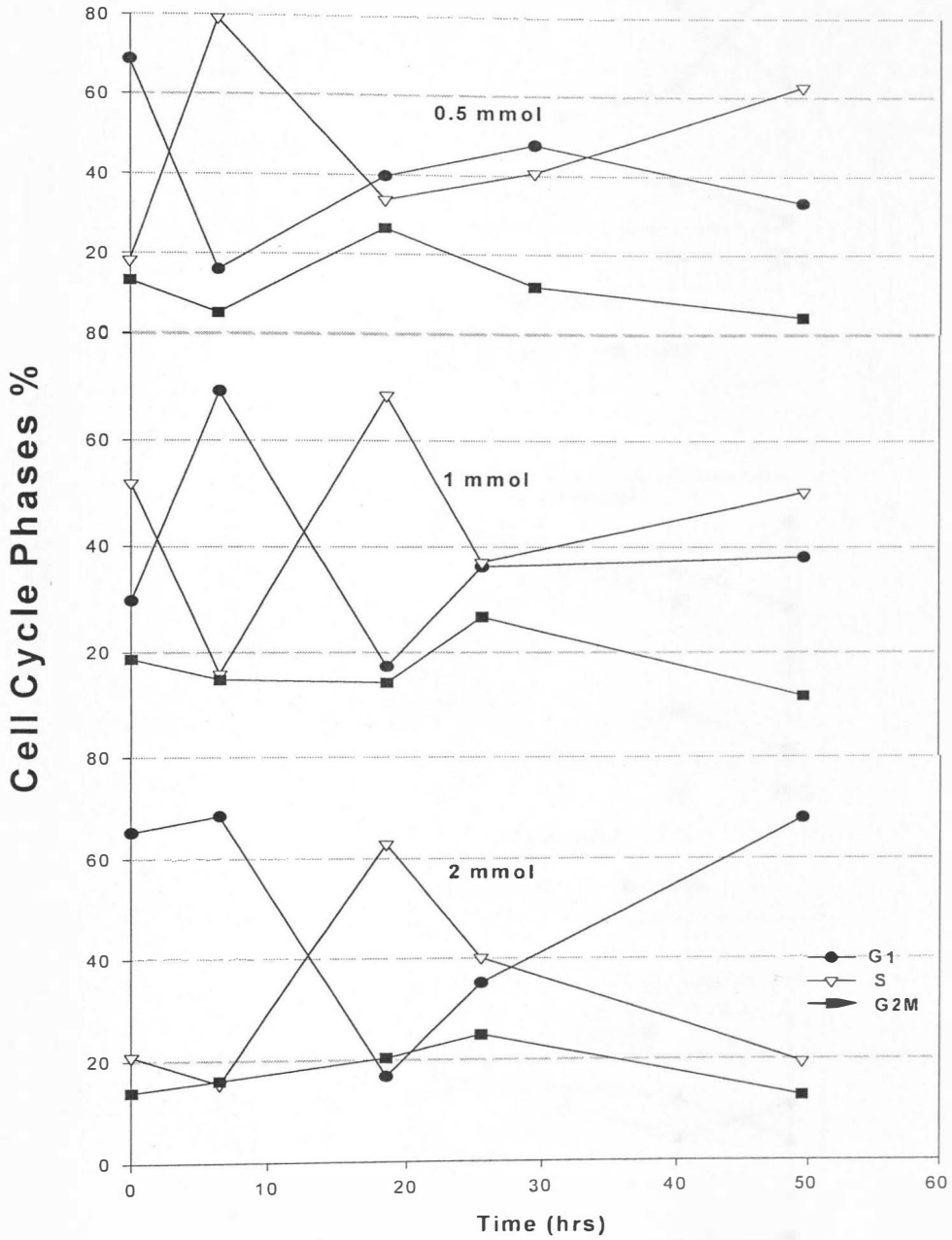

Fig 5.4A **Cell Cycle Changes in a partially Synchronised Batch of CHO Cells at Various Glutamine Concentrations**

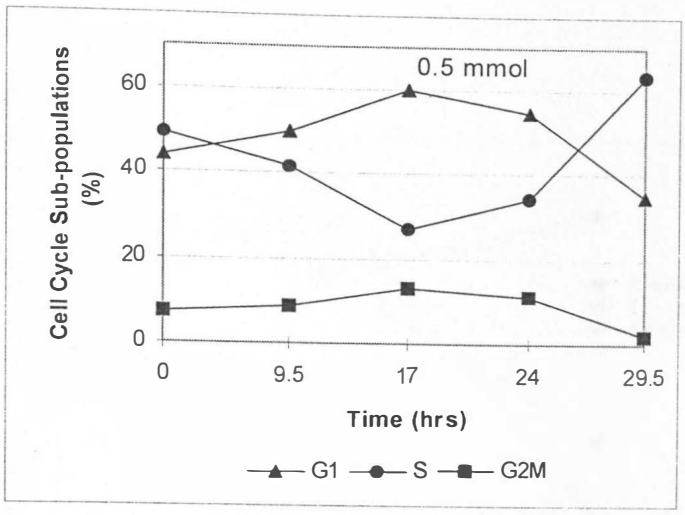

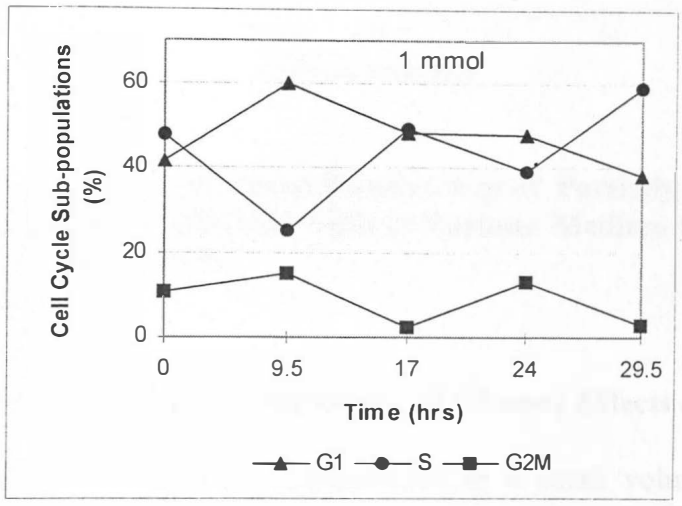

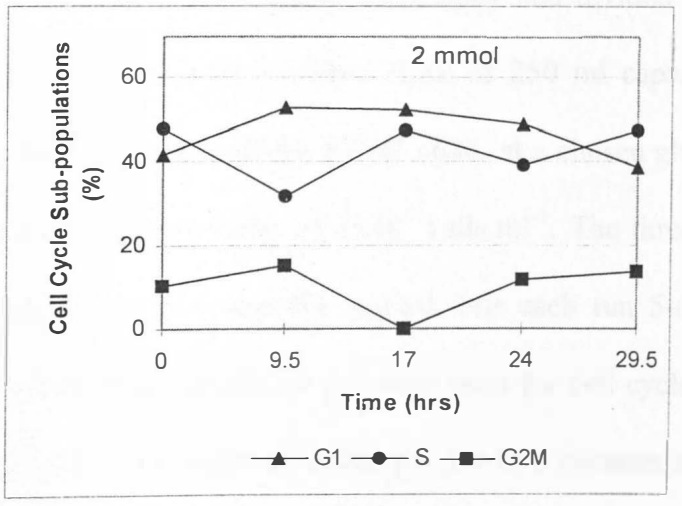

Fig 5.4B **Cell Cycle Changes in Asynchronous Batches of CHO320 Cells at Various Glutamine Concentrations**

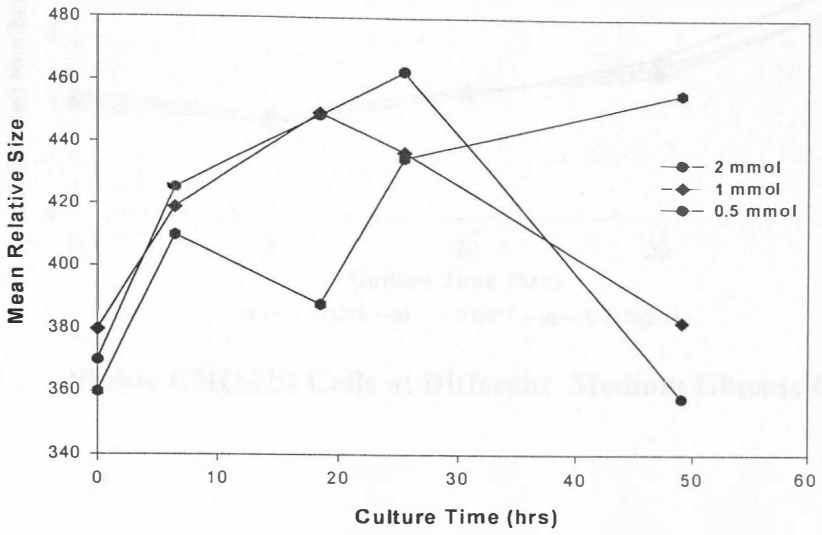

Figure 5.5 **Changes in the Mean Relative Size of Partially Synchronised Batches of CHO320 Cells at Various Medium Glutamine Concentrations**

5.4 Experimental Procedure for the Study of Glucose Effects on CHO320 Cells

CHO320 cells were centrifuged and resuspended in a small volume of glucose-free medium following which they were mixed thoroughly and divided into equal volumes each of which was transferred into a stirred flask of 250 ml capacity and a working volume of 150 ml containing the medium RPMI 1640 at a chosen glucose concentration to give a final CHO cell concentration of $2x10^5$ cells.ml^{-1}. The three different medium glucose concentrations were 2, 1 and 0.6 mg/ml. For each run 5-6 ml samples were removed from each flask from which 3-4 ml were used for cell cycle, cell size and cell mass analysis after being centrifuged at 1000 rpm for five minutes and fixed with cold 70% ethanol. The remaining 2 ml of the samples were used to determine cell count and the viability of the cultures.

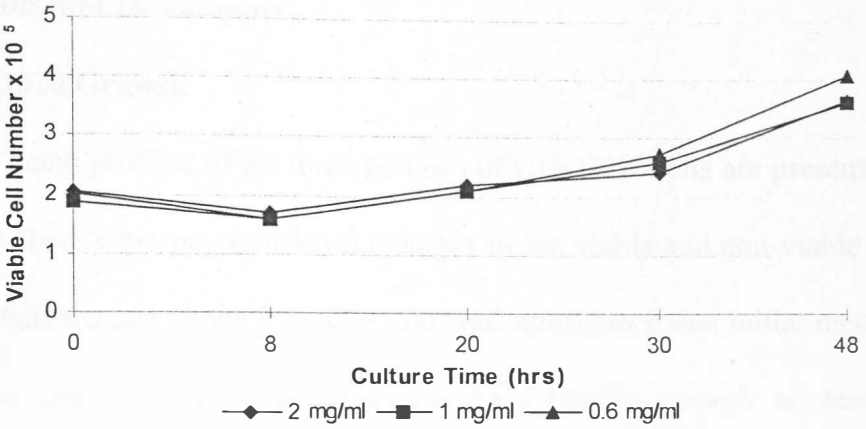

Fig 5.6 **Viable CHO320 Cells at Different Medium Glucose Concentrations**

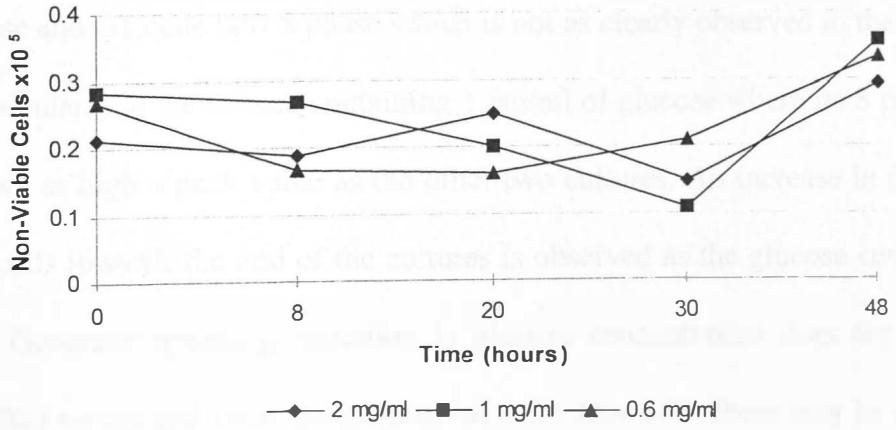

Fig 5.7 **Non-Viable CHO320 Cells at Different Medium Glucose Concentrations**

5.5 Results and Discussions

5.5.1 CHO320 Growth

Growth and death profiles of all three batches of CHO320 Cells are presented in Figures 5.6 and 5.7. There were no significant changes in the viable and non-viable cell numbers of the three batches and hence it can be said with confidence that initial medium glucose concentration does not have an affect on the CHO320 growth or death processes. Fluctuations between the non-viable curves may be due to the fact that many non-viable cells, being less dense, float to the top and form a thin film at the surface of the culture medium and therefore are not uniformly mixed in the suspension culture.

5.5.2 Cell Cycle Analysis

Figure 5.8 shows the cell cycle profiles of three batches of CHO320 cells initiated at different glucose concentrations within their first doubling time. Cell cycle profiles in all three cultures are very similar. The duration of the lag period is identical in all three cultures. The culture with 2 mg/ml of glucose exhibits synchronised release of G2M cells into G1 phase and G1 cells into S phase which is not as clearly observed in the remaining cultures particularly in the culture containing 1 mg/ml of glucose where its S phase curve does not have as high a peak value as the other two cultures. An increase in the amount of S phase cells towards the end of the cultures is observed as the glucose concentration is reduced. Generally speaking, variation in glucose concentration does not appear to have any effect on the cell cycle progression of cells. However, there may be an indirect link between the G2M-G1 check points and the glucose concentration that could be investigated further but for the modelling purposes it is considered appropriate to stop at

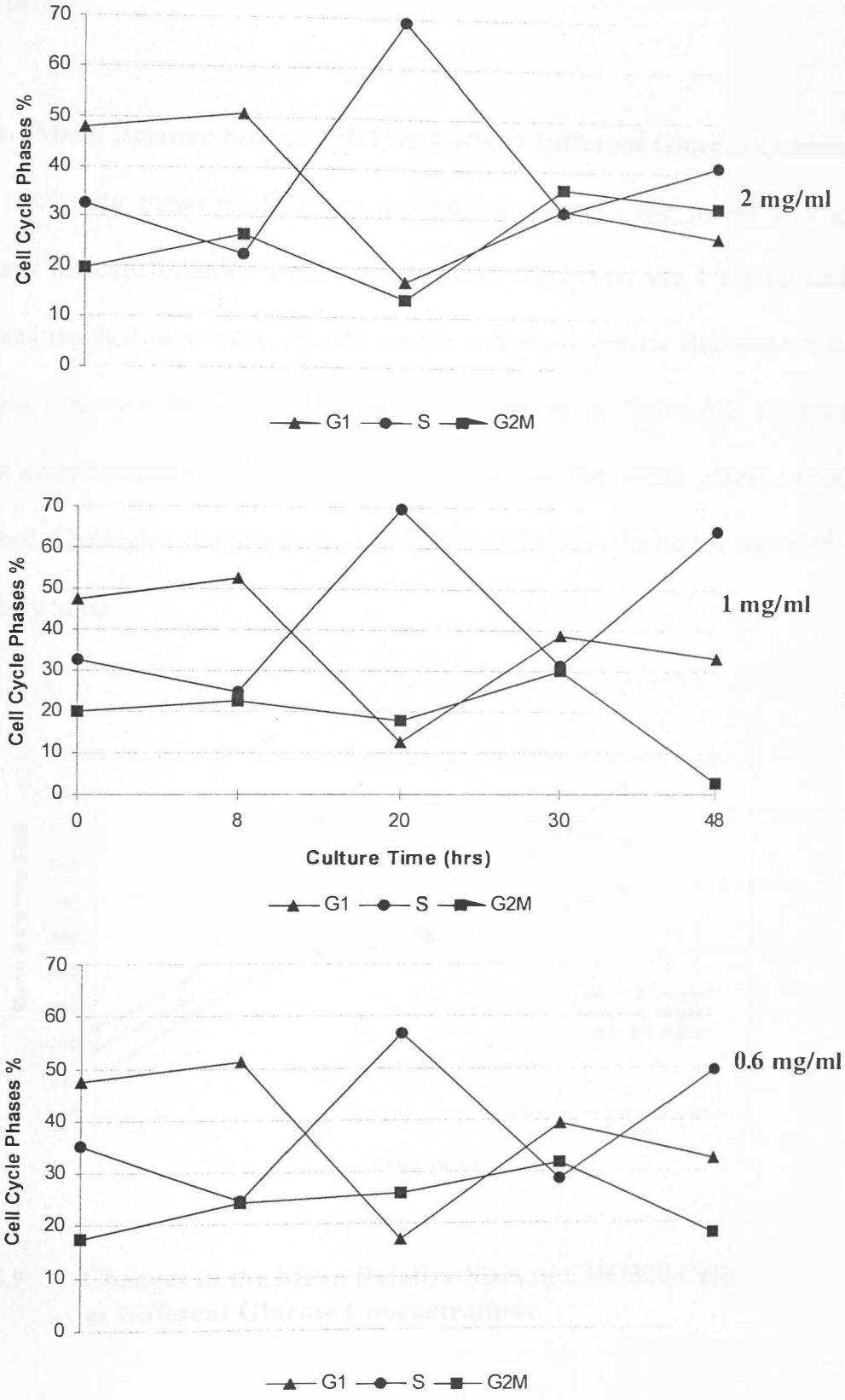

Fig 5.8 **Cell Cycle Profiles of CHO320 Cells at Different Medium Glucose Concentrations**

this point.

5.5.3 Mean Relative Size of CHO320 Cells at Different Glucose Concentrations

The results for mean relative size analysis of the cells are shown in Figure 5.9. All cultures increase initially in size as expected. However, the 1 mg/ml and 0.6 mg/ml cultures reached their peak in size sooner and show greater fluctuations in their mean relative size than the 2 mg/ml culture. As is shown in Figure 5.8, the proportion of S phase cells increases and G2M cells decreases as the initial glucose concentration is reduced. The higher the proportions of S and G2M cells the higher the relative mean size is likely to be.

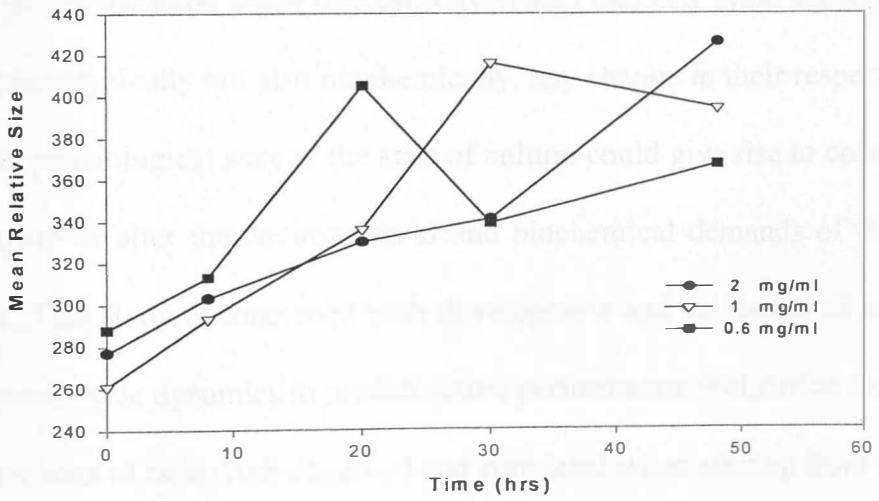

Fig 5.9 Changes in the Mean Relative Sizes of CHO320 Cells at Different Glucose Concentrations

CHAPTER 6

A COMPARATIVE STUDY OF THE GROWTH KINETICS OF CHO320 CELLS AT VARIOUS POSITIONS IN ITS CELL CYCLE

6.1 Introduction

The fundamental process underlying all biological growth is the cell division cycle. Subdivision of the intermitotic period into discreet phases has provided a strong framework for attempts at analysing the processes controlling cell proliferation. Moreover, most of the experimentally induced changes seen in population growth of mammalian cells have been shown to be mainly due to changes in the duration of their cell cycle phases. The possibility of using information on the cell cycle fractions of cells at the start (inoculation) of a culture to predict later rates of proliferation and cell loss has increasingly attracted much interest. Given also that cell cycle subpopulations differ not only phenotypically but also biochemically, any change in their respective proportions or in their physiological state at the start of culture could give rise to changes in the kinetics of growth or alter the environmental and biochemical demands of that population as a whole. This study is concerned with development and validation of models that attempt to use cell cycle dynamics to predict future performance. Validation therefore depends on comparisons of behaviour observed and simulated when starting from different cell cycle and cell physiological states. The next experiment was therefore devised in order to allow a succession of inoculation states to be generated so that each subsequent stage of the culture produced a new data set for model development and validation purposes.

6.2 Experimental Procedure

Cells are allowed to accumulate up to the late exponential phase of growth of a culture so that a high proportion of them (72%) is in the G1 phase. Cells from this partially synchronous populations are then inoculated into fresh medium to give a cell concentration of $2x10^5$cells.ml^{-1} in a stirred flask of 1litre capacity and this is taken to be the reference culture with respect to subsequent inoculations. Fresh batch cultures are then inoculated using cells taken at 0, 10, 18, 30 and 46 hour from this reference culture by inoculation into fresh medium in stirred flasks of 250 ml capacity. 6-7 ml samples were drawn for each analysis, 3-4ml of which were fixed by 70% ethanol and used for cell cycle and size analysis by flow cytometry at a later date and the remaining 2-3 ml were used for the cell enumeration, viability and metabolite assays.

6.3 Results and Discussions

CHO320 cells producing interferon-γ have been extensively studied by Hayter et al (1991-1992), who determined the effects of the physiological state of CHO cells on both the production and the quality of the heterologous protein. He also investigated the effect of serum, glucose, glutamine, ammonia and lactate concentrations on the proliferative state of the CHO cells. Hayter's studies on CHO cells were further complemented by Leelavatcharamas (1996) who investigated these parameters in the light of their cell cycle profiles. Previous studies, including those of the cell cycle of CHO cells by Leelavatcharamas mainly used partially sunchronised cultures. Cells were taken from the late exponential phase of the culture, inoculated in fresh medium and their growth and cell cycle profiles under controlled conditions were studied. The partially synchronised cultures used were high in G1 and low in S and G2M cells. Typically, a cell

cycle profile consists of a lag period of 9-10 hours during which there is no traverse of cells between the cell cycle phases and hence there is no increase in the total viable cell number and cells are simply recuperating and adjusting to new conditions. The next stage of the cycle is characterised by rapid traverse of cells from G1 into S and G2M and finally cell division. As culture time progresses, substrates are depleted and waste products accumulate, CHO cells become progressively arrested in G1 phase of the cell cycle and S phase cells gradually decline till the end of cultivation period. G2M cells on the other hand remain fairly stable and only minor fluctuations in their profile are observed.

This study was therefore initiated to investigate whether, as well as physico-chemical factors in the immediate environment of CHO cells, their position in this cell cycle profile alone could have an effect on their proliferative state. Hence, cells from distinct stages of the cell cycle profile such as at the end of the lag period, after the rapid traverse of G1 cells into S phase (high S phase) and when the cells are asynchronous, were taken and inoculated in fresh medium to determine how they would grow in comparison to the partially synchronised cultures. The data for CHO320 cells taken from 0, 10, 18, 30 and 46 hour of the reference culture are shown in Figures 6.1(a) to 6.1(e). 100-105 hour of cultivation time in each batch was assigned as the point of termination of the culture for facilitation of the comparative study.

Batch I - The Reference Culture (Fig 6.1(a))

This has a partially synchronised inoculum rich in G1 cells. As this reference culture progresses, it provides in turn inocula of different cell cycle distributions for the subsequent batches 2-5 in fresh medium. We begin by looking at the growth of the cells in this reference batch. The cell growth profile in this batch is sigmoid in shape reaching a maximum of 9.3×10^5 cells.ml^{-1} at 80 hours of culture time, after which a decrease in cell number is observed. Non-viable population of batch I remain fairly constant at about 0.2×10^5 cells.ml^{-1} for the first 50 hour of the culture time after which a steady increase in the dead cell population is observed approaching 1.3×10^5 cells.ml^{-1} at 104 hour of culture time. The cell cycle profiles exhibit what is normally expected from a culture partially synchronised by starvation. The cell cycle show a lag period of about 10 hours after which the G1 cells begin to enter the next stage or S phase rapidly causing an increase in S phase cells which maximises at around 18-20 hour of cultivation time. The fraction of G2M cells however remains relatively unchanged and its value at any time along the cultivation period can be taken to be constant. The G1-S transition stops when the G1 cell fraction is reduced by approximately half from 73% to 38%.The next stage is a period described previously as the G1 enrichment phase where G1 cells begin to increase again as a result of substrate exhaustion and the cells need to be inoculated in fresh medium. The mean relative size of the cells exhibits a 27% increase within the first 30 hours of the culture time after which a steady decrease in mean relative size till the end of culture time is observed. This steady reduction in size is the result of G1 cells being unable to traverse the cell cycle and therefore remaining trapped in the G1 phase until the conditions are favourable again. The reduction in mean relative size at the end

of the culture time with respect to the starting point is found to be 25%. The glucose consumption curve shows a steady decline in concentration as the culture time progresses approaching exhaustion (below 0.5 mmol) at 79 hours of culture time.

Batch II (Fig 6.1(b))

The Batch II cell culture, inoculated with cells taken at 10 hours of the reference culture, is similar in profile to that of batch I. Its maximum value is found to be 8.8 x 10^5 cells.ml^{-1} and this occurs interestingly at 80 hour of cultivation time. The progress of the cell cycle distribution of this inoculum was essentially identical to that of the reference culture. The difference was that 10 hour had passed (what has been generally termed a lag or recuperative phase) so, as is shown in Figure 6.1(b), the lag period is absent as perhaps might now be expected and hence cells begin to traverse as soon as they are inoculated. The expectation that Batch II cells would then attain a higher population density than Batch I as a result of having more time and substrate available for growth is however shown not to be met. Cell death shows a steady increase as the culture time progresses, reaching a value of 0.73x 10^5 cells.ml^{-1} at 101 hour of culture time and this is lower (almost half) than that of the reference culture. The fraction of G1 cells decreases from 72% to 27% (a reduction of 62.5%) in 19 hours. An interesting observation is that, despite the absence of a lag period in Batch II cells, the fraction of G1 cells at 19 hours of the culture is similar to that at the same time in batch I. The increase in S phase cells is very much proportional to the decrease in G1 cells. The fraction of G2M cells remains fairly constant through the batch culture time but the average value is higher than in Batch I by 7-10%. The time progression of mean relative size remains the same as in

Batch I with the time taken for the cells to reach their maximum size being effectively the same followed by the same rate of decline. The glucose consumption curve is shown to be very similar to that of Batch I.

Batch III (Fig 6.1(c))

The cell growth profile in batch III, inoculated with cells taken at 18 hours of the reference culture, reaches its maximum value of 7.66 $x10^5$ $cells.ml^{-1}$ at 84 hours of the cultivation period, which is slightly lower than in the previous cultures. The inoculum for this culture showed a quite different cell cycle distribution, since the population released from its partially synchronised state now had progressed through the S phase. Its corresponding value at the end of the culture (105 hr) was found to be 7.066 x 10^5 $cells.ml^{-1}$. Non-viable cells reach a value of 1.22 x 10^5 $cells.ml^{-1}$ at 105 hour of cultivation time. No lag period is seen and transition between the phases of the cell cycle occurs as soon as the cells are inoculated. One notable difference is that the fraction of G2M cells remains at a low value (~ 3-4%) after the first 18 hour of the batch. In the early hours of the cultivation period (<12 hour) the cells in this batch show a sharp increase of up to 16% in their mean relative cell size. After 30 hours of cultivation, however, the mean relative size exhibits a steady decrease till the end of the culture. The mean relative cell mass declines throughout the culture from time zero, initially sharply (up to 18 hour), and later more gently. The overall decline in relative mean size at the end of the culture time with respect to the starting point was found to be 25% whilst the decline in mean relative mass is shown to be continuous throughout the Batch III culture, achieving a final reduction in relative mass of 60 % at the end of the culture. The glucose

consumption curve declines less rapidly and hence its exhaustion occurs at 105 hour of cultivation as opposed to 79-80 hour encountered in Batch I and Batch II.

Batch IV (Fig 6.1(d))

The total viable cell concentration in Batch IV peaks at a cell density of 7.93 $x10^5$ $cells.ml^{-1}$ at 96 hour of the cultivation period. The formation of non-viable cells shows an abrupt increase towards the end of culture reaching a value of 0.255 x 10^5 $cells.ml^{-1}$ at the end of the batch period. In Batch IV the relative proportions of G1 and S cells at the start of the culture are close which is believed to be the underlying reason for the rapid occurrence of S-G2M transition (which is not seen in the cultures with proportions of G1 cells considerably higher than of the S cells) at the beginning of the culture, prior to G1-S or G2M-G1 transitions. G2M cells remain low throughout most of the cultivation period. There does not appear to be a lag phase and the G1 enrichment phase occurs at more or less the same position with respect to other cultures during the cultivation period. Another interesting feature was that the relative mean mass profile showed two distinct peaks at 31 and 71 hour of culture time with increases in relative mean mass of 37% and 92% respectively. These protein synthesis peaks are associated with higher substrate consumption, particularly of glucose which is exhausted some 10 hours earlier than in the reference culture. The mean relative size on the other hand shows a steady decline till the end of the cultivation period but the rate at which the reduction in size occur appears to be slower in comparison to other cultures. The final reduction in size however was found to be 19%.

Batch V (Fig 6.1(e))

The maximum viable cell density was found to be 7.09 x 10^5 cells.ml^{-1} which occurred after the 80 hours of culture. The non-viable cells profile is very similar to that for Batch IV with a sharp increase in the non-viable cell population at the end of the culture (104 hrs) giving a maximum value of 3.4 x 10^5 cells.ml^{-1}. Cell cycle profiles resemble that of the reference culture with the exception of G2M which remain very low during the culture. The reduction ratio in the G1 cells as a result of transition within the first 19 hours of culture was found to be 2.47. The lag phase is reestablished in Batch V and the G1 enrichment is similar to that in all the previous cultures. The relative mean size profile is unchanged up to 60 hours after which an overall reduction in size of 20% is observed. The mean relative mass exhibits a very similar pattern to that of Batch IV but the peaks are shifted to the left by 16 hours, which is the time difference between the inoculation of the two cultures. The cells at the end of the culture have the same mean relative mass and exhibit no real difference with respect to the starting point. Glucose is shown to deplete even more rapidly than in the previous cultures.

6.4 Summary

The final viable cell number appears to decrease slightly as the cultures move away from the reference culture profile towards asynchrony. These variations in final cell number may be partly due to the number of G1 cells at the start of the culture as the G1 phase is the period in which proliferation is regulated (Smith et al, 1973) or they may be due to the exhaustion of substrate particularly in Batches IV and V. The non-viable cell populations, however, remain fairly constant throughout the culture period, and their

magnitude is higher in Batches I, II and III than in Batches IV and V. In terms of their cell cycle profiles, only Batch I and V appear to have distinct lag phases. In Batch II the lag phase is totally absent. The presence or absence of the lag phase in cultures, as well as the physiological state of the cells, could also be dependent to some extent on their relative proportions at the start of the cultures. All cultures exhibit G1 enrichment in their profiles. The mean relative cell size profiles can be explained with reference to the relative fractions of cell cycle populations at any particular time in culture. Generally G2M size > S size > G1 size. Glucose consumption was found to be the least in Batch III which can be attributed to the high percentage of S cells in that culture which are likely to have completed their biomass synthesis associated with doubling of cellular machinery for their subsequent division ahead. The highest glucose uptake on the other hand was found to occur in Batch V. The latter principally is believed to be due to the presence of two protein synthesis peaks which occur during the culture (also occuring in Batch IV). It is not clear what factors are contributing to these peaks and more experiments may be needed to establish the cause. However, dye-protein interference may be a contributory factor to the mass and size variations shown in Batch IV and Batch V. The results of the above experiment point to the conclusion that the make up of the population in terms of its cell cycle sub-populations together with their respective positions in the cell cycle at the time of inoculation and the presence or absence of periods of intense cell mass accumulation are the principle reasons for variation in substrate exhaustion, cell proliferation and death rates encountered in this study.

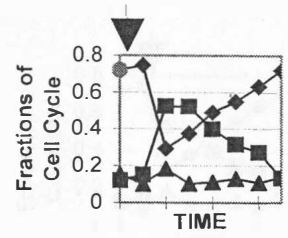

Reference Culture

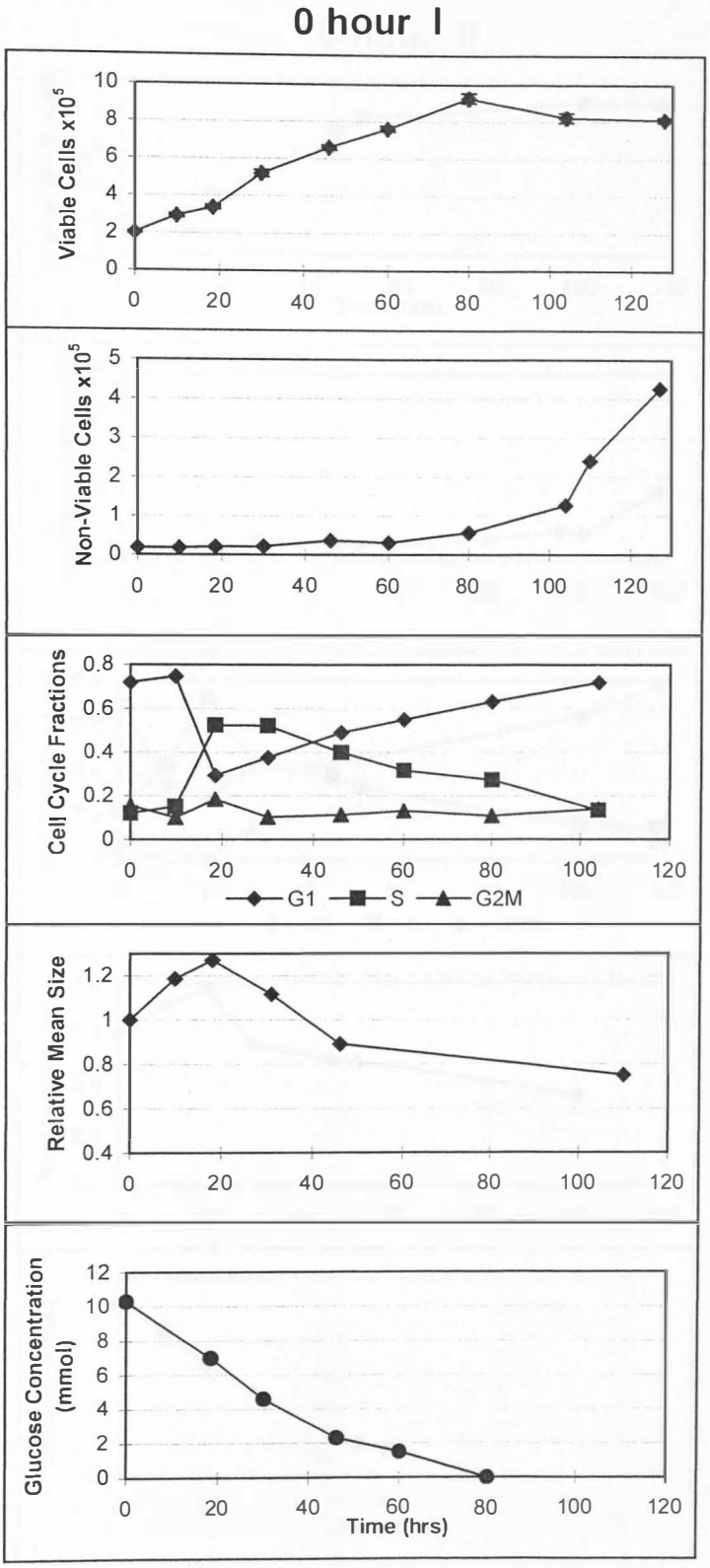

Fig 6.1(a)

Multi-parameter Presentation of Batch Cultivation Results of CHO320 Cells at Time Zero of Reference Culture. *(Error Bars Represent the Standard Deviation of Six Cell Number Measurements)*

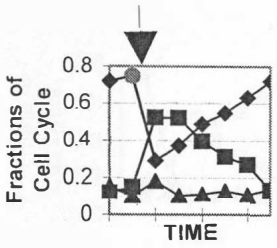

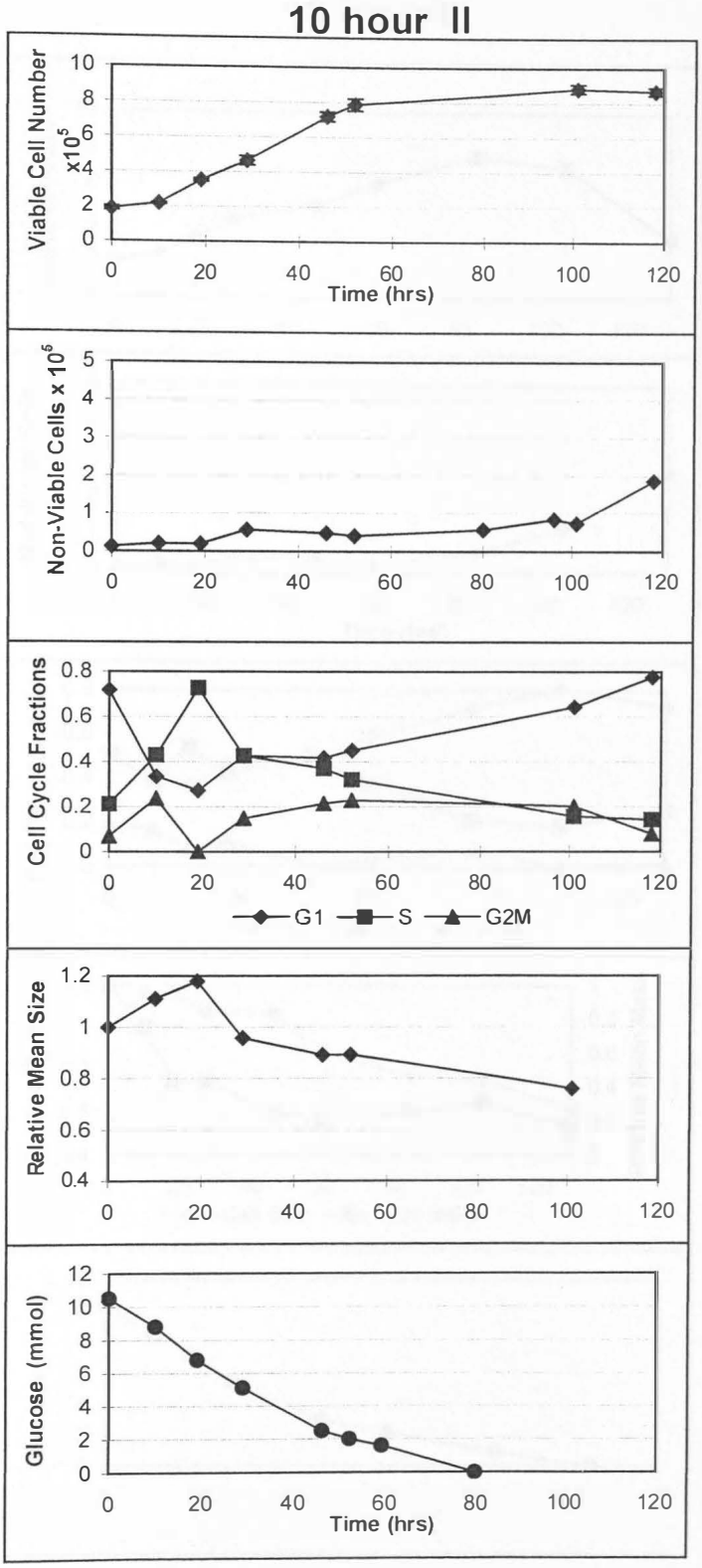

Fig 6.1(b)

Multi-parameter Presentation of Batch Cultivation Results of CHO320 Cells at 10 Hour of Reference Culture. *(Error Bars Represent the Standard Deviation of Six Cell Number Measurements)*

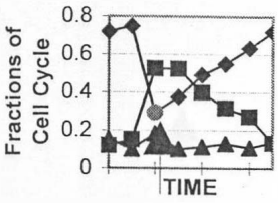

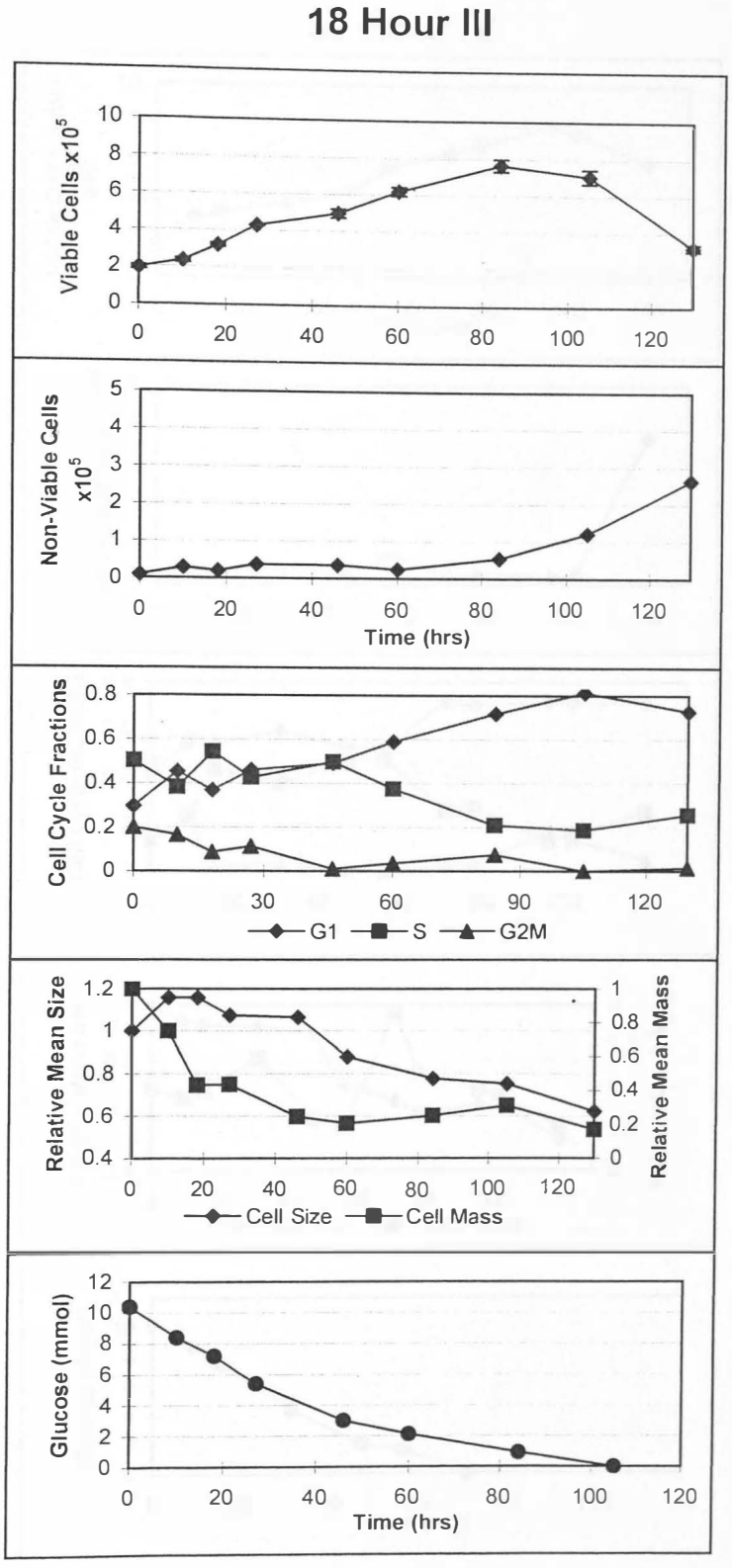

Fig 6.1(c) **Multi-parameter Presentation of Batch Cultivation Results Culture of CHO320 Cells at 18 Hour of Reference Culture.** *(Error Bars Represent the Standard Deviation of Six Cell Number Measurements)*

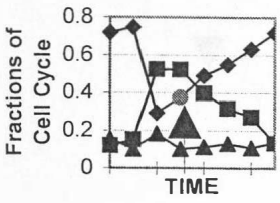

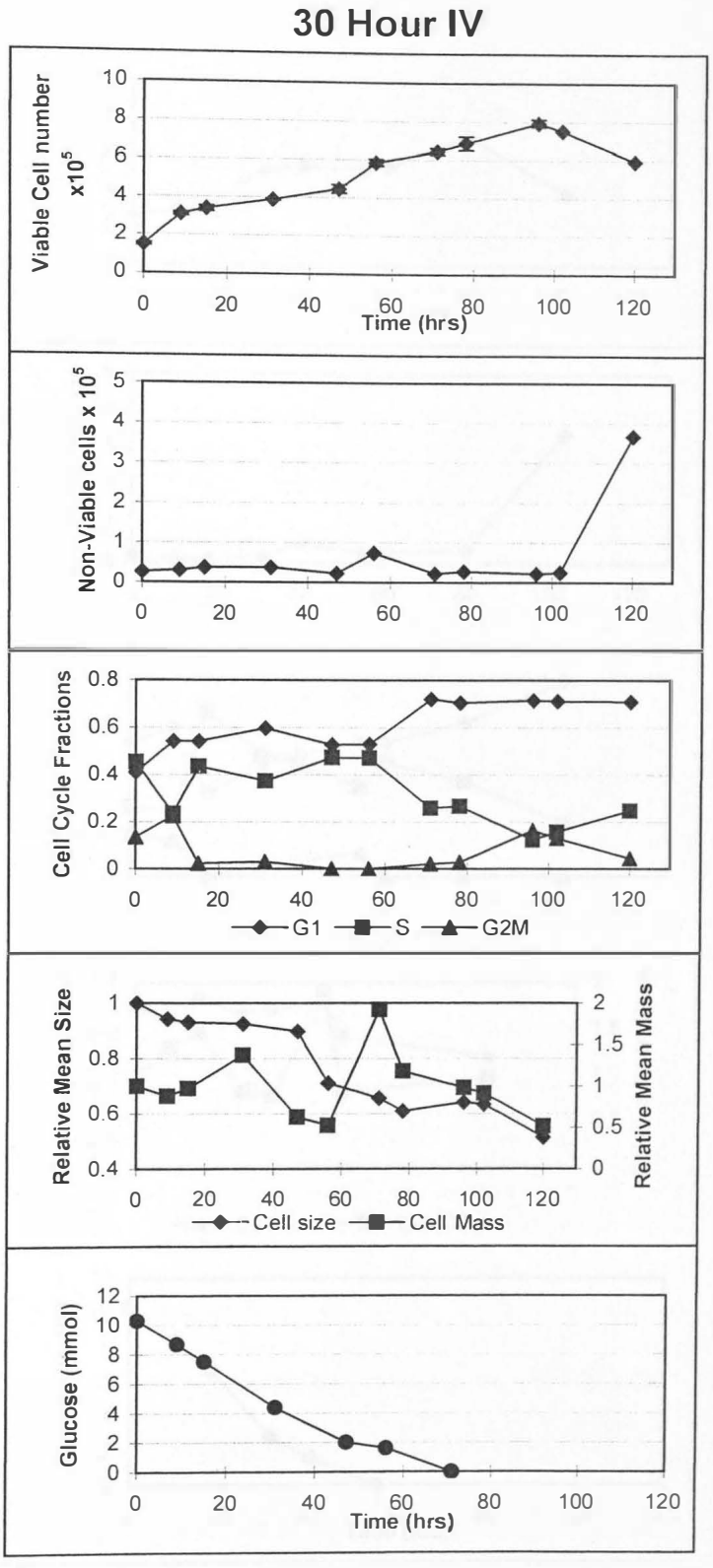

Fig 6.1(d) **Multi-parameter Presentation of Batch Cultivation Results of CHO320 Cells at 30 Hour of Reference Culture.** *(Error Bars Represent the Standard Deviation of Six Cell Number Measurements)*

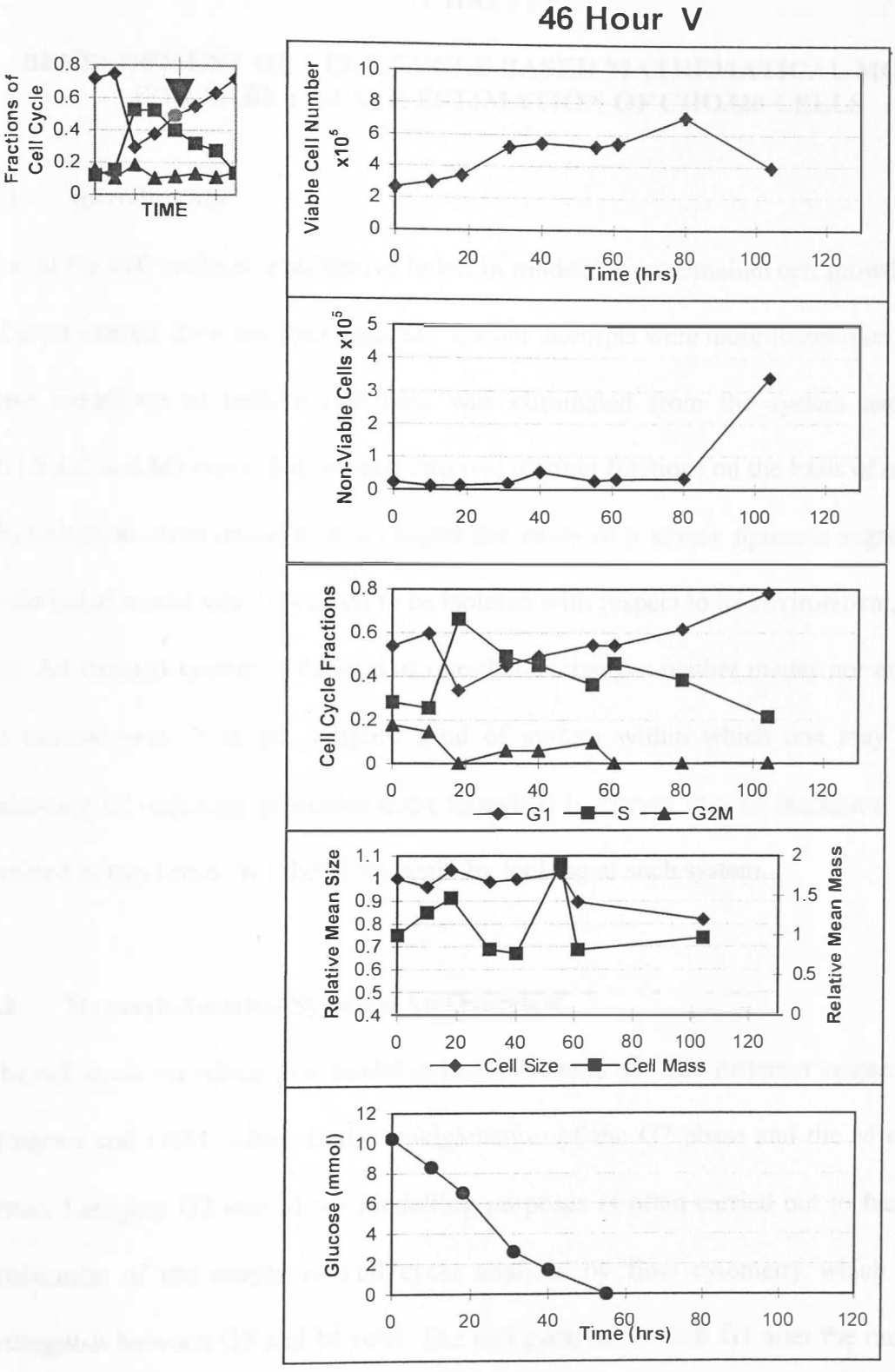

Fig 6.1(e) **Multiparameter Presentation of Batch Cultivation Results of CHO320 Cells at 46 Hour of Reference Culture.** *(Error Bars Represent the Standard Deviations of Six Cell Number Measurements)*

CHAPTER 7

DEVELOPMENT OF CELL CYCLE BASED MATHEMATICAL MODELS FOR EARLY STATE ESTIMATION OF CHO320 CELLS

7.1 Introduction

Use of the cell cycle as a predictive index in modelling mammalian cell growth has been of great interest for more than a decade. Earlier attempts were more focused on the steady state modelling of cells where time was eliminated from the system and biomass (G1,S,G2 and M) was often lumped into two distinct fractions on the basis of measurable physiological differences. In this chapter the study of a simple dynamic segregated cell cycle based model which is taken to be isolated with respect to its environment, is carried out. An isolated system is defined as one that exchanges neither matter nor energy with its environment. It is the simplest kind of system within which one may study the balancing of opposing processes even though it is known that no biological system is isolated in this sense. We therefore begin by looking at such system.

7.2 Dynamic Isolated Systems-An Overview

The cell cycle on which this model is based consists of three different stages: G1, S or synthesis and G2M, which is the amalgamation of the G2 phase and the M or Mitosis phase. Lumping G2 and M for modelling purposes is often carried out to facilitate the application of the results of cell cycle analysis by flow cytometry which does not distinguish between G2 and M cells. The cell cycle starts with G1 after the immigration of divided cells from the preceding G2M phase. During the G1 phase, cells prepare to duplicate themselves for the next S phase, during which cells precisely and accurately

duplicate their genome by synthesizing DNA and the associated nuclear protein components. Once the DNA replication is complete the cycling cells enter G2M, during which the cells synthesize the proteins required to direct chromosome segregation and cell division. After G2M cells return to the G1 phase to start a new cell cycle. Cells also die and enter the dead cell population D by necrosis.

7.3 System Features, Components and Variables

In this model three distinct features are identified:

- total biomass, Σ N
- total biomass decay, Σ D
- Formation and inter-conversion rates between the biomass sub-populations

The total viable biomass growth is determined by simply summing up the individual viable biomass sub-populations G1, S and G2M. Change in total biomass in a fixed region of space thus can only occur for four reasons (defined by rates):

- **B**irth of new cells
- **D**eath processes
- **I**mmigration
- **E**migration

In a small time interval Δt the change in population ΔN can thus be written as:

$$\Delta N = (B-D+I-E)\,\Delta t \qquad (7.3.1)$$

Also included in this model are conversion and decay terms to describe the rates at which cells traverse through each physiological state of biomass, say from being G1 to G2M, and exit the cycle as dead cells denoted as D.

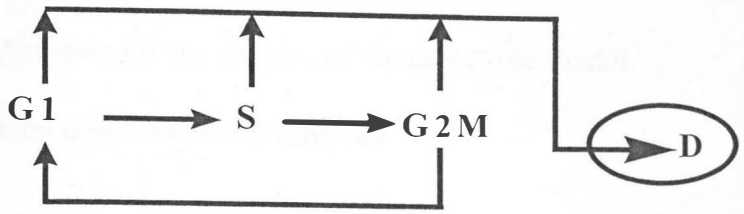

Fig 7.1 **Signal Flow Diagram Showing Stages of the Cell Cycle Model**

7.4 Development of Model Equations

A cell cycle model was developed by firstly writing a generalised statement of the component balance for the system and then expressing each balance term in mathematical form using first order reaction rate equations to characterise each transition as shown below.

(Accumulation of cells) = (Cells entering) - (Cells leaving) - (Cells lost by death)

$$\frac{dG1}{dt} = 2.K_{G2mG1}[G2M] - K_{G1S}[G1] - K_{DG1}[G1] \qquad \textbf{(7.4.1)}$$

$$\frac{dS}{dt} = K_{G1S}[G1] - K_{SG2M}[S] - K_{DS}[S] \qquad \textbf{(7.4.2)}$$

$$\frac{dG2M}{dt} = K_{SG2M}[S] - K_{G2MG1}[G2M] - K_{DG2M}[G2M] \qquad \textbf{(7.4.3)}$$

Where K_{G1S}, K_{SG2M} and K_{G2MG1} are transition rates constants and K_{DG1}, K_{DS} and K_{DG2M} are death rate coefficients for the phases of the cell cycle model.

7.5 Assumptions and General Remarks

This subsection sets out the assumptions made in constructing this model.

- In this non-homogeneous population the individuals within each subpopulation behave identically and independently from each other (Gold, 1977).
- The system is not affected by its environment and hence cells are not arrested in a quiescent stage as the environmental conditions become unfavourable.
- Cell death occurs throughout the cell cycle and is not confined to a particular phase of the cell cycle (Al-Rubeai, 1991).
- Cells freely traverse between phases of the cell cycle unidirectionally.

7.6 Components of Tools for Model Analysis

Reference Data

The data used in simulation, optimisation and validation of models were obtained from batch cultivation of CHO320 cells. Batch data, as shown in Figure 7.2, has been divided into three sections: *Recuperative, Oscillatory* and *Enrichment* periods to facilitate comparative assessment of the models.

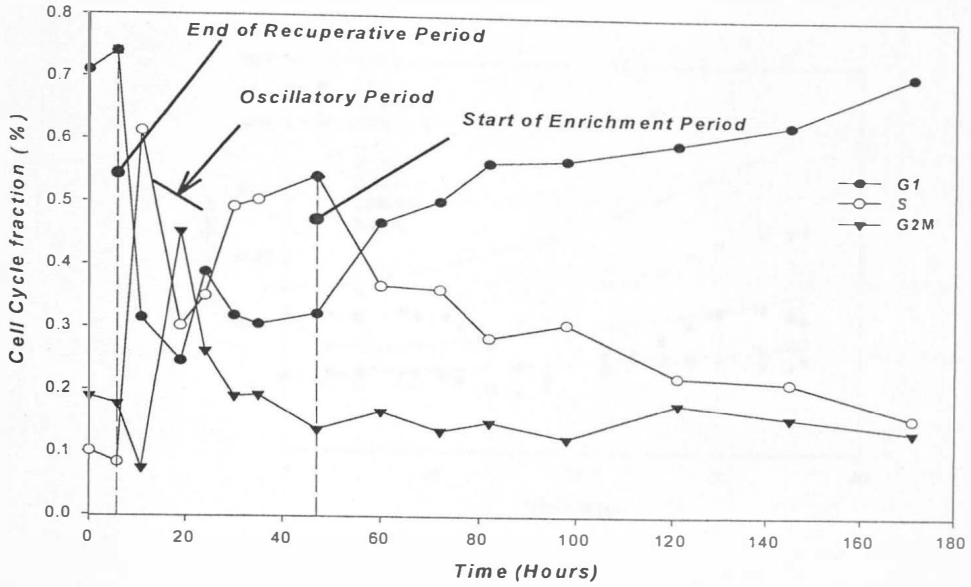

Fig 7.2 Reference Data Used in Tuning and Optimisation of Models

Construction and Tuning Models

Models were built and optimised using Matlab and its accessory Simulink and Optimisation tool boxes. The system of equations developed above were solved numerically using a Runge Kutta 4th order algorithm. Initial estimates for transition and death rates were made using average experimental values as tabulated in Table 7.1 below.

Rate Constants	hr^{-1}
K_{G1S}	0.3405
K_{SG2M}	0.238
K_{G2MG1}	0.418
K_{DG1}	0.015
K_{DS}	0.015
K_{DG2M}	0.015

Tab 7.1 Average Experimental Parameter Values for Transition and Death Rate Constants

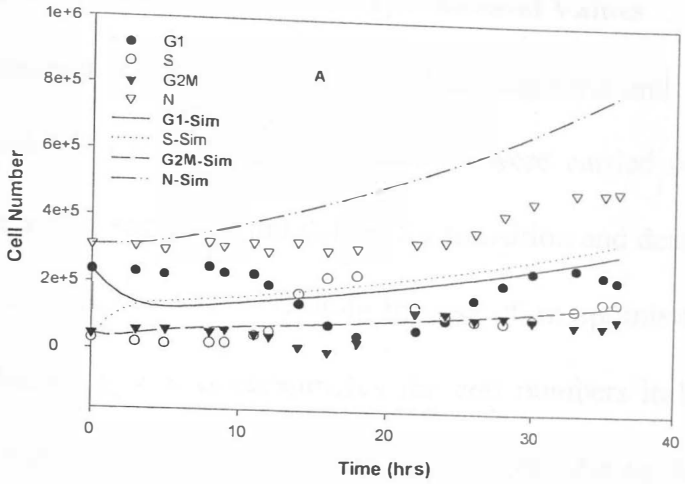

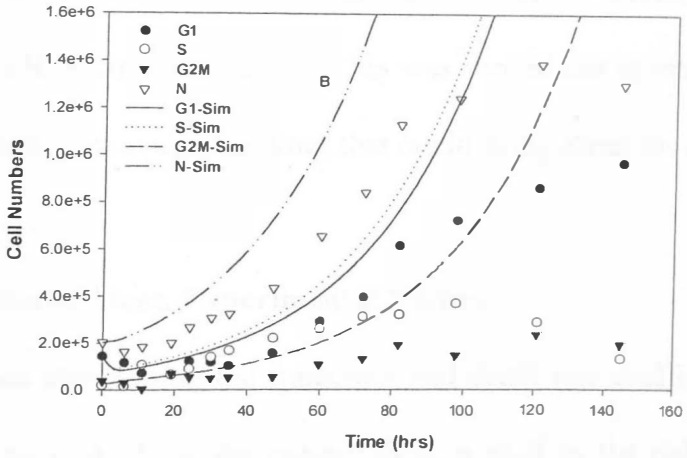

Fig 7.3A-B **Measured and Predicted Values of Cell Cycle Fractions and Total Cell Number Using Mean Experimental Values**

7.7 Results and Discussions

7.7.1 Simulation of Model Using Mean Experimental Values

Simulated and measured values over the first doubling time and the entire batch are presented in Figures 7.3 (A-B). These simulations were carried out to determine the extent to which the actual experimental values for transition and death rates are useful in predicting the concentrations of cells without the use of an optimisation routine. As can be seen, the simulation grossly overestimates the cell numbers in both short and long term simulations. Simulated results correlate very poorly during the recuperative and oscillatory period with the experimental results. However, it must be said that the recuperative period was never anticipated to be predicted correctly under the current assumption of cells being able to move freely from one phase to another. Before making any further attempt to change the existing model or the assumptions used on it, the parameters used in the simulation were optimised by writing a script file which allowed globalisation of the parameters and reduction of error between the measured and predicted data by a least squares method. This was carried out to establish whether there was any combination of parameters values that could bring about the desired outcome.

7.7.2 Optimisation of Mean Experimental Values

The results obtained after tuning the transition and death rate coefficients are shown in Figures 7.4 A-B. As a result of the optimisation, a shift to the right of the simulated curves over the entire batch time is observed whilst there is no significant change in the simulated results for the first doubling time of the culture. In the longer term simulation

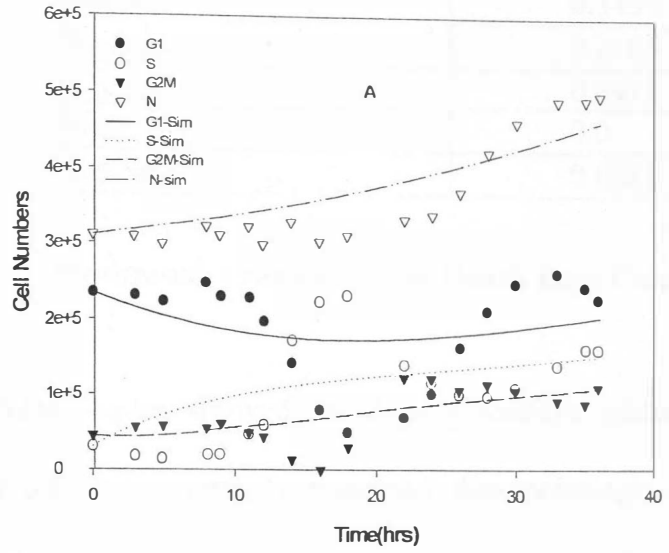

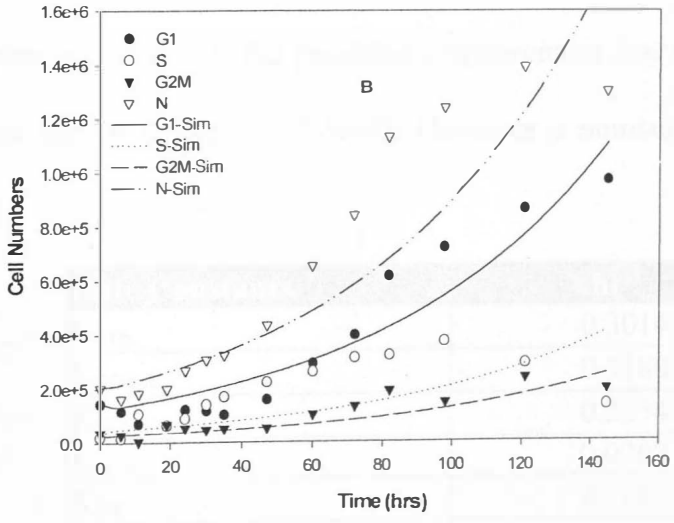

Fig 7.4 A-B **Results of the Model Simulations Using Optimised Experimental Parameters**

Rate Constants	hr^{-1}
K_{G1S}	0.0281
K_{SG2M}	0.3453
K_{G2MG1}	0.2403
K_{DG1}	0.0933
K_{DS}	0.0
K_{DG2M}	0.0281

Tab 7.2 **Optimised Transition and Death Rate Constants**

of the model, G2M values showed some improvement whereas predictions in the recuperative and oscillatory periods remained disappointingly inadequate. To move forward from this point, as a first step, the recuperative period was omitted from the reference data as the model was clearly unable to predict it, and new starting values for the parameter set were chosen to establish whether better optimisation results and convergence between the measured and predicted data could be obtained.

7.7.3 Omission of Recuperative Period

Having omitted the recuperative period and with optimisation of transition and death rate constants as shown in Table 7.3, the resulting improvement was found to be negligible and inadequate as shown in Figures 7.5A-B. However a number of problems came to light, as follows:

Rate Constants	hr^{-1}
K_{G1S}	0.3014
K_{SG2M}	0.3180
K_{G2MG1}	0.2234
K_{DG1}	0.0207
K_{DS}	0.1085
K_{DG2M}	0

Tab 7.3 **Optimisation Results after Omission of Recuperative Period**

Plots of the total cell number and G1 cells overshot the reference data. This was attributed principally to the assumption that cells traverse between phases freely. In other words the assumption of unhindered passage of cells through the cell cycle is the main cause of overestimation in long term simulation. Intuitively, there must be an expectation that the changing environment (particularly substrate limitation) will change the rates of transition. In the case of short term simulation the same assumption is believed to be instrumental in the distortion of the oscillatory pattern of the data. It became evident that in order to get ahead, it was necessary to adapt the existing model to account for changes both in the long and short term simulations. Since it was unlikely that the assumptions to be made could be applied to both long and short term data, they would be dealt with separately using two different models. In the light of the amendments to be implemented, the model describing the short term data could still be categorised as an isolated system, whilst modelling of the long term growth entered a new category, referred to as an open system, which will be discussed in Chapter 8. Going back to the short term data and the problem of oscillation, it was decided to introduce a delay term into the model which not only permits reintroduction of the recuperative period but also offers some resistance to the free passage of cells through the cell cycle.

7.8 Delayed Regulation

There are different types of models with time delay terms but by far the most plausible type of delayed regulation is based on a population birth rate which, because of developmental delays, depends on N_D and not on N.

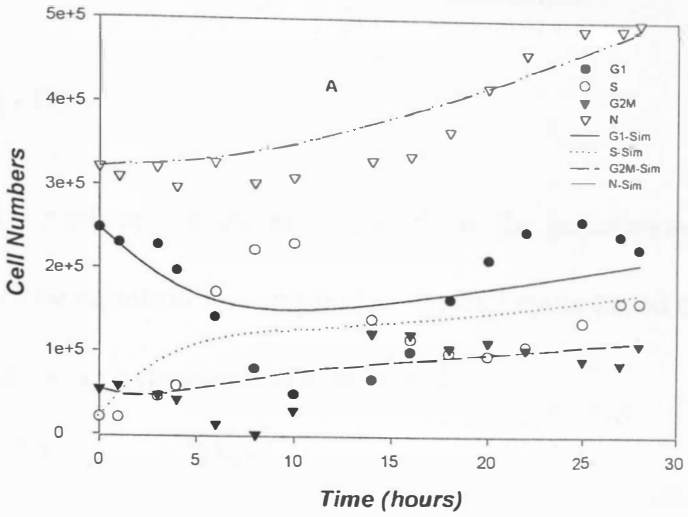

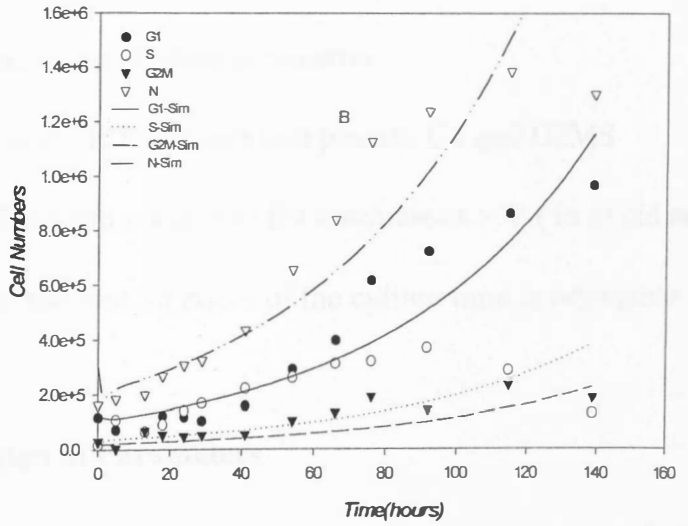

Fig 7.5 A-B **Simulated Values of Total Viable Cells and Cell Cycle Fractions After Omission of Recuperative Period**

7.8.1 Development of Model Equations

The above assumption yields a general equation of the form:

$$\frac{dN}{dt} = B(N_D) - D(N) \qquad \textbf{(7.8.1)}$$

where B and D are birth and death rates and N_D is the population at $t < 0$, or delayed population. The above equation was applied to the cell cycle based model in the previous section and the following expression was obtained.

$$K_{G1S}[G1]\,(t - \Psi) = 2\,K_{G2MSG1}\,[G2MS] \qquad \textbf{(7.8.2)}$$

which is translated in words as: " the rate at which new cells appear at time t is proportional to the number of cells at $t-\Psi$ where Ψ is the average cell division time." Equation 7.8.2 was incorporated into the cell cycle model by substituting for $K_{G1S}[G1]$.

7.8.2 Assumptions and General Remarks

- No cell division occurs before time zeros
- The cell cycle is made up of just two phases: G1 and G2MS
- Equation 7.8.2 is valid subject to the constraint $\mathbf{t > \Psi}$ (to avoid negative values)
- Cell death over the first 36 hours of the culture time is negligible.

7.8.3 Optimisation of Parameters

After substitution for K_{G1S}, K_{G2MG1} and Ψ were the parameters which were optimised. The results of the optimisation are shown in Table 7.4.The death rate were taken to be negligible.

Parameters	
K_{G2MG1}	0.2259 hr^{-1}
Ψ	14 hr

Tab 7.4 **Optimised Parameters for Cell Cycle Model with Delayed Regulation**

7.8.4 Results and Discussion

Having examined the simulated results shown in Figures 7.6 and 7.7 it can be said that the beginnings of an improvement in the prediction of the recuperative period can be seen except towards the end of the period. The effects at t >10 hours are due to the fact that, while transition between G1 and G2MS was prevented by the delay term, transition from G2MS into G1 was not, and so a slight decrease in the G2MS and a proportionate increase in G1 was observed. However, the ensuing simulated oscillatory period remains incomplete and amplitude of oscillation falls short of the corresponding measured data. The transition between the recuperative period and the latter is also somewhat sharp. This is believed to be due to the constraints imposed on the model as explained above. This rigidity from the point of view of biological systems is not natural or realistic, and hence it was decided to introduce a new assumption to eliminate the rigidity of the system and improve its ability to predict the oscillation. So far we have examined systems which are comprised of constant rate coefficients but now a new case is explored where the coefficients for the transition rates are changing with time.

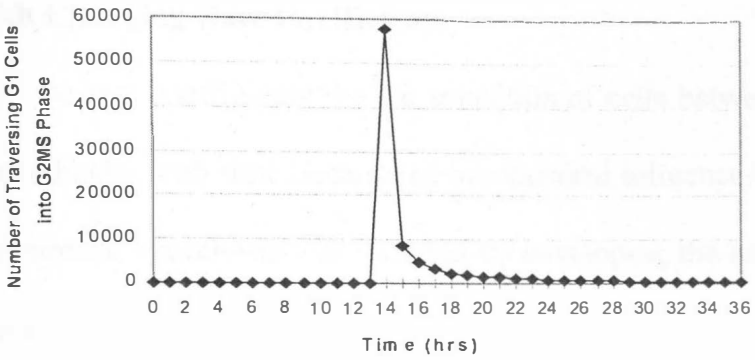

Fig 7.6 **Simulated Rate of Transition Between G1 and G2MS Using the Model with Incorporated Delay Term**

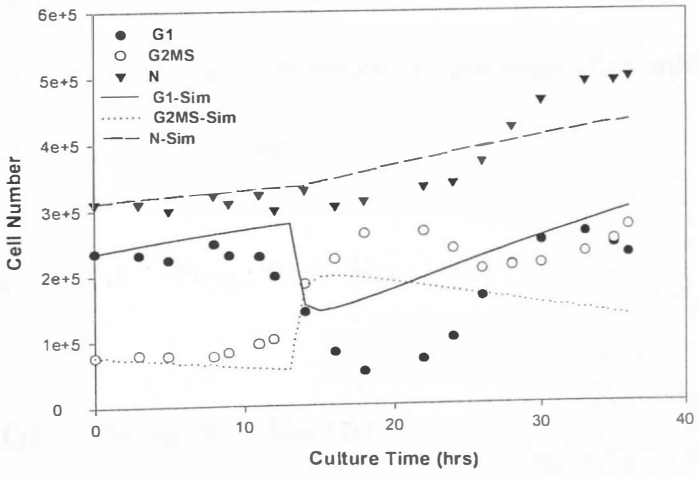

Fig 7.7 **Simulated Total Cell Number and Cell Cycle Sub-Populations Produced by Introduction of Delay Term**

7.9 Model with Changing Rate Coefficients

It is supposed that the rate coefficients for the transition of cells between phases of the cell cycle vary periodically with time because of biochemical influences within the cells. Testing of this theoretical hypothesis was initiated by developing the new assumption(s) into mathematical expressions as shown below.

7.9.1 Development of Model Equations

If T_n is taken to be the period of the oscillations of the rate coefficients then the frequency f of the oscillation is defined by $1/T_n$, and the angular frequency ω is defined by $\omega=2\pi f=2\pi/T_n$. The units of ω are radians per unit time. The simplest possible example of a rate coefficient oscillating with angular frequency ω without creating negative values is obtained by assuming:

$$\Theta(t) = \Theta(0)(1+\alpha\sin\omega t) \qquad (7.9.1)$$

Where Θ_i is the rate coefficient, α_i is the amplitude of oscillation and ω_i is the angular velocity of stage i. The resulting mathematical equations after substitution for the new rate coefficients are as shown overleaf.:

$$\frac{dG1}{dt} = 2.\Theta_{G2MG1}[G2M] - \Theta_{G1S}[G1] - K_{DG1}[G1] \qquad (7.9.2)$$

$$\frac{dS}{dt} = \Theta_{G1S}[G1] - \Theta_{SG2M}[S] - K_{DS}[S] \qquad (7.9.3)$$

$$\frac{dG2M}{dt} = \Theta_{SG2M}[S] - \Theta_{G2MG1}[G2M] - K_{DG2M}[G2M] \qquad (7.9.4)$$

7.9.2 Assumptions and General Remarks

- The death rate (unlike transition rates) does not oscillate (and is still taken to be negligible)
- The population is partially synchronised

7.9.3 Optimisation of Parameters

Optimised parameter sets for the model with oscillatory transition rates with and without the lag period are presented below.

Optimised Parameters		
$\Theta(0)_{G1S}$	0.2190	hr^{-1}
$\Theta(0)_{SG2M}$	0.2937	"
$\Theta(0)_{G2MG1}$	0.2455	"
K_{DG1}	0.0183	"
K_{DS}	0	"
K_{DG2M}	0.015	"
ω_{G1S}	0.1005	$Rad.hr^{-1}$
ω_{SG2M}	0.3323	"
ω_{G2MG1}	0.2790	"
α_{G1S}	0.1764	hr^{-1}
α_{SG2M}	0.2406	"
α_{G2MG1}	0.3376	"

Tab 7.5 Optimised Parameters (Set A) for the Model with Oscillatory Transition Rate Coefficients

Optimised Parameters	
$\Theta(0)_{G1S}$	0.2707 hr^{-1}
$\Theta(0)_{SG2M}$	0.4937 "
$\Theta(0)_{G2MG1}$	0.6677 "
K_{DG1}	0.2258 "
K_{DS}	0.0021 "
K_{DG2M}	0.000 "
ω_{G1S}	0.5988 $Rad.hr^{-1}$
ω_{SG2M}	0.3323 "
ω_{G2MG1}	0.2022 "
α_{G1S}	0.1548 hr^{-1}
α_{SG2M}	0.900 "
α_{G2MG1}	0.430 "

Tab 7.6 **Optimised Parameters (Set B) for the Model with Oscillatory Transition Rate Coefficients**

Optimised Parameters	
$\Theta(0)_{G1S}$	0.325 hr^{-1}
$\Theta(0)_{SG2M}$	0.24 "
$\Theta(0)_{G2MG1}$	0.261 "
K_{DG1}	0 "
K_{DS}	0.034 "
K_{DG2M}	0.00 "
ω_{G1S}	0.279 $Rad.hr^{-1}$
ω_{SG2M}	0.270 "
ω_{G2MG1}	0.343 "
α_{G1S}	0.297 hr^{-1}
α_{SG2M}	0.149 "
α_{G2MG1}	0.349 "

Tab 7.7 **Optimised Parameters for the Model with Oscillatory Transition Rate Coefficients after the Removal of the Lag Period**

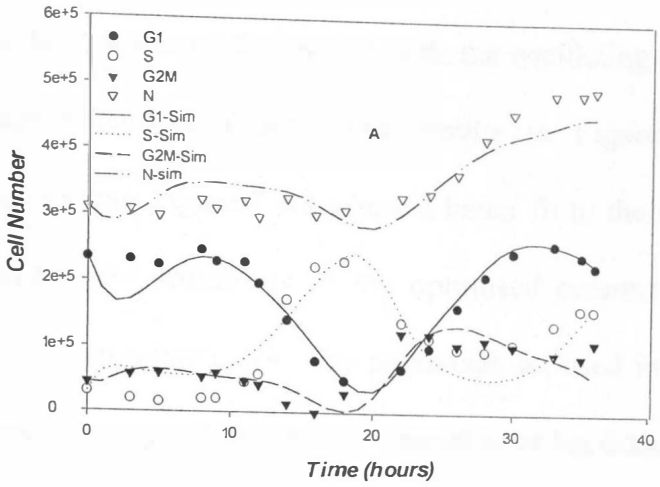

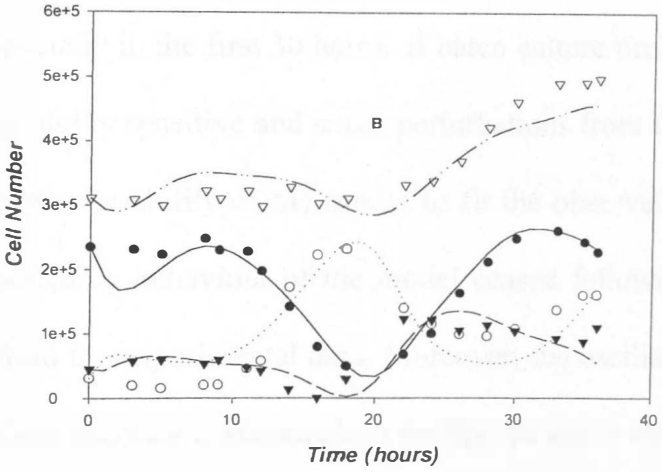

Fig 7.8 A-B **Predicted and Measured Data for Model with Oscillatory Transition Rate Coefficients Using Two Different Optimised Parameter Sets**

7.9.4 Results and Discussion

Figures 7.8A-B show the results of the model with the oscillating transition rates two with different optimised parameter sets. The results in Figure 7.8A predict the recuperative period better than Figure 7.8B where a better fit to the oscillatory period is observed. With respect to the suitability of the optimised parameter sets used in the simulation, each has its own advantages. The parameter set used in the case of Figure 7.8A exhibits its superiority in predicting the recuperative or lag period but its prediction of the oscillatory phase is less satisfactory. For instance, the simulated G1 profile appears to be slightly out of phase and its corresponding simulated S phase profile does not quite reach its peak as set by the observed data. Synchronised transition of G2M cells into G1 and G1 cells into S phase at around 18 hour of culture time is also not predicted. The prediction of the lag period using parameter set B, as shown in Figure 7.8B, is less plausible; however, its fit to both S and G2M phases excels that of the parameter set A simulation results especially in the first 30 hours of batch culture time. This points to the fact that this model is highly sensitive and small perturbations from the previously tuned data could totally impair the ability of the model to fit the observed data, as shown in Figure 7.9, where oscillatory behaviour of the model ceased following omission of the recuperative period from the experimental data. Moreover, the oscillatory functions built into the rate expressions produce a symmetrical profile, which is rarely the case in the biological measurements, and hence the closeness of the fit between different experimental and simulated data sets could be very variable depending on the degree of symmetry in the experimental data.

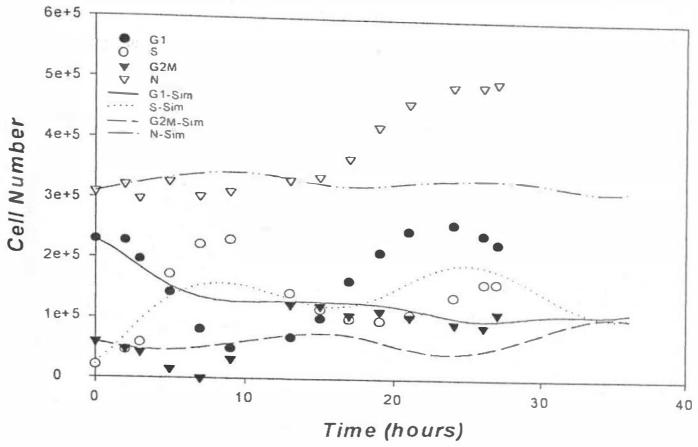

Fig 7.9 **Showing the Inability of the Model to Oscillate after Omission of the Lag Period**

Validation of the Oscillatory Model

This is the stage where the model is tested in order to establish whether it adequately fulfils the purpose for which it was designed, in other words gives predictions that are sufficiently accurate to be useful. To do that a different set of batch data was chosen and the results of simulation using the previously tuned parameters were compared with the new set of data as shown in Figure 7.10. Similar results were obtained in the validation process as presented in Figure 7.10. The profile of G1 cells is predicted well during the lag period, but on commencement of the oscillatory phase deviation between the measured and predicted data becomes significant. The S phase cells show the same effect as G1 cells but reciprocally. The simulated G2M profile is a good fit, particularly in the beginning, but towards the end of cultivation time it begins to overestimate the corresponding measured data. To summarise, it is believed that the use of an oscillatory

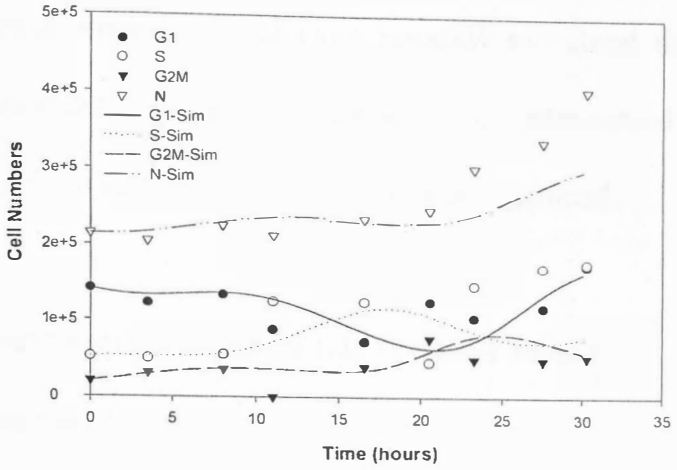

Fig 7.10 **Validation Results of Model with Oscillatory Transition Rates.**

rate coefficient was a step forward with respect to the predictive models based on estimating the initial doubling time of the culture in a partially synchronised culture. However, this model is shown to be highly sensitive and hence unstable when some perturbation is introduced into the system; besides it can only estimate the cell cycle population of cells which are highly synchronised and hence it could not be used to estimate changes in an asynchronous culture of cells where the lag or recuperative period is not so well defined or is absent and the amplitudes of the oscillations in the rate coefficients are significantly different. Symmetry in the measured data is also another confounding factor that could cause broadening of the margin of error.This model, however, laid the foundation for the next stage of model development which makes use of the oscillatory nature of rate coefficients but is based on a more plausible and experimentally proven mechanism rather than a purely pragmatic approach. In this way,

by introducing a type of feedback mechanism into the model, it is hoped to overcome the problems encountered previously and even possibly to extend the application of the model to the full batch data. In the following section, mathematical models based on the molecular mechanisms of cell cycle transition will be examined.

7.10 Physiological Models (Based on Obeyesekere Model)

7.10.1 Introduction and Overview

The creation and analysis of cell cycle oriented models based on physiological interactions between cellular components could provide better control strategies in biotechnology. However, formulation and study of such models must also be simplified as far as possible to enable effective analysis and avoid over-specification of the system. This work was initiated by assuming a simple relationship between two principal proteins involved in cell cycle transitions: retinoblastoma protein (Rb) and E2F, an important transcription factor of RNA polymerase II. Transition between phases is controlled by the successive sequestration and releasing of the E2F molecules by Rb. Sequestration takes place when the retinoblastoma protein (Rb) is in its hypophosphorylated form (Rbs) so that, upon phosphorylation to (PRb), releases the sequestered E2F molecules and hence allows transcription and proliferation processes to follow. Phosphorylation and dephosphorylation of retinoblastoma proteins is carried out by a family of proteins known as cyclin dependent kinases. At this stage the effects of cyclins are not taken into account and changes between states are assumed to obey first order kinetics as shown below, rather than the saturation type kinetics (Michaelis-Menten) of enzyme catalyzed reactions. Most of the interactions presented in Figure 7.11 which are supported by

experimental evidence are shown with solid lines and all the assumed reactions with dotted lines.

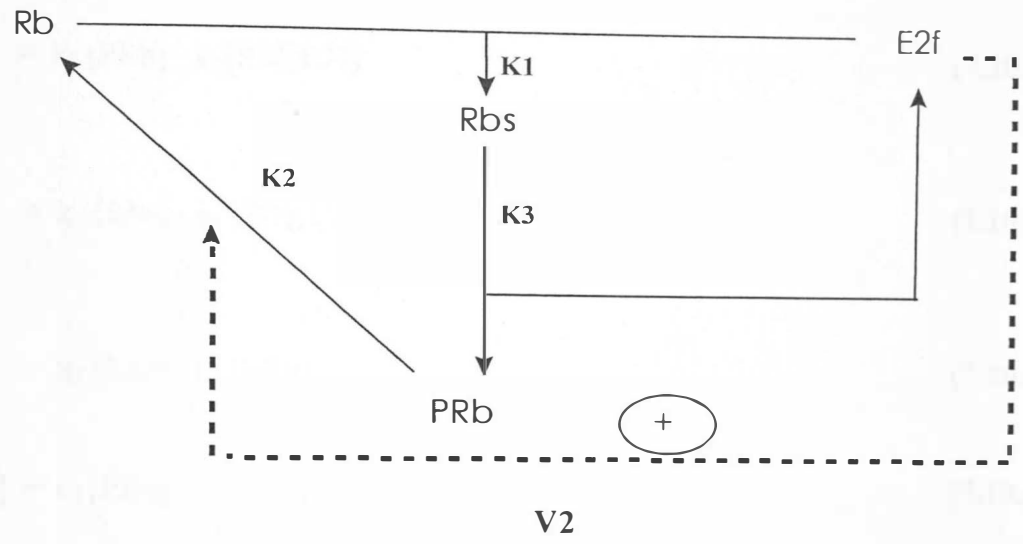

Fig 7.11 **Signal Flow Diagram for the Proposed Molecular Mechanism of Cell Cycle Transition**

7.10.2 System Features, Components and Variables

The mechanism is translated into four mathematical equations which describe the concentration profiles of Rb, PRb and E2F. The beginning of the cell cycle is interpreted as the time when the concentration of unphosphorylated retinoblastoma protein is high and increasing, whereas passage through the G1-S checkpoint and hence through the rest of the cycle is considered to occur when the E2F concentration is at its maximum and the unphosphorylated retinoblastoma concentration is on the decrease.

7.10.3 Development of Model Equations

The mathematical expressions describing synthesis and interconversion of the species are as follows:

$$\frac{dRb}{dt} = k_2 [PRb] - k_1[Rb][E2f] \quad \textbf{(7.10.1)}$$

$$\frac{dE2f}{dt} = k_3 [Rbs] - k_1 [Rb][E2f] \quad \textbf{(7.10.2)}$$

$$\frac{dPRb}{dt} = k_3 [Rbs] - k_2 [PRb] \quad \textbf{(7.10.3)}$$

$$k_2 [PRb] = c_2 [PRb] + v_2[E2f] \quad \textbf{(7.10.4)}$$

Where k_i, v_i, c_i are rate constants

7.10.4 Assumptions and General Remarks

- Total Rb (Rb_T) concentrations are constant
- Rates of degradation of chemical species are negligible
- The G1-S transition rate is proportional to the E2f concentration
- Population is partially synchronised (partially synchrony was incorporated into the model by specifying the initial conditions before the simulation and optimisation began).

7.10.5 Optimisation of Parameters

Optimisation results for the physiological model with first order kinetics are presented in Table 7.8. Since experimental data for the chemical species were not available, these

parameters were fitted using a least squares routine to produce the closest fit to the cell cycle data.

Optimised Parameters		
K_{SG2M}	0.0613	hr^{-1}
K_{G2MG1}	0.0626	hr^{-1}
k_1	0.9	hr^{-1}
k_3	0.2	hr^{-1}
c_2	0.0163	hr^{-1}
v_2	0	hr^{-1}
Rb_0	0.0032	C*
$E2f_0$	4	C
Prb_0	0.4	C
Rb_T	5	C

Tab 7.8 **Optimised Parameter Set for the Physiological Model with First Order Kinetics**
** C is an arbitrary concentration*

7.10.6 Results and Discussions

Figures 7.12 and 7.13 demonstrate the performance of the proposed physiological model. Given the assumptions and the level of complexity of the proposed model, predictions in the lag or recuperative period along with G2M and total cell number profiles show some promise but G1 and S transitions are slower than anticipated. Since the rate of transition between G1 and S phases was assumed to be proportional to the free E2f concentration, it is best to look into the predictions of these chemical species by the model in order to find the cause of the discrepancies of the data. The first noticeable deviation seen on examining Figure 7.13 was the manner in which these chemical species fluctuated during the cultivation time. Before constructing the model it was assumed that the beginning of the cell cycle is associated with a high concentration of free Rb and the onset of

transition by free E2f concentration is at its maximum value. Although the E2f concentration curve exhibits an increase at the beginning of the culture time, the curve soon levels off and remains so until the end of the simulation period. The free Rb curve on the other hand remains very close to zero throughout the culture time whilst its behaviour should have shown some similarity to that of the E2f. The decrease in Rbs (Phosphorylation) and the corresponding increase in PRb also occurs too rapidly. In the next step the initial Rb concentration is altered whilst the others remain the same in order to see whether an improvement in its profile can be made by changing its initial pre-simulation value. Furthermore, the first order rates describing phosphorylation and dephosphorylation of Rb will be replaced with Michaelis-Menten expressions as, in reality, these reactions are catalysed by enzymes whose activity more closely resembles the Michaelis-Menten relationship (Obeyesekere, 1997).

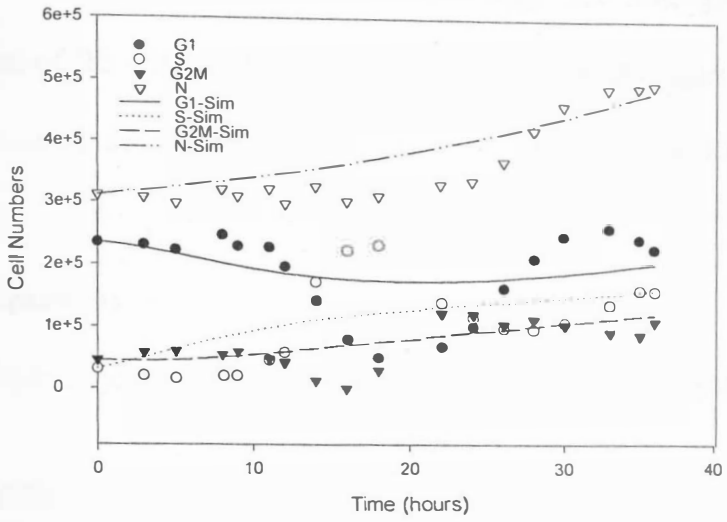

Fig 7.12 **Simulated Results of Cell Cycle Fractions in the Physiological Model**

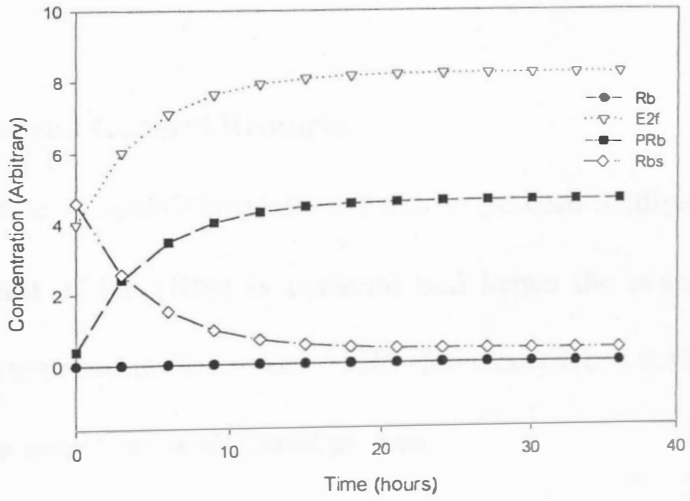

Fig 7.13 **Numerical Simulation of the Rb, E2f, PRb and Rbs Profiles by the Proposed Physiological Model**

7.11 Physiological Model Based on Michaelis-Menten Kinetics

It was decided to replace the first order rates for the phosphorylation and dephosphorylation of Rb with a Michaelis-Menten type of rate equations to see whether any improvement in the concentration profiles of PRb, Rb, E2f and Rbs could be made.

7.11.1 Model Equations

The modified phosphorylation and dephosphorylation rates are as follows;

$$\frac{dRb}{dt} = \frac{c_2 \quad [PRb]}{j_2 + [PRb]} + V_2[E2f] - k_1[Rb]\,[E2f] \qquad (7.11.1)$$

$$\frac{dE2f}{dt} = \frac{k_3 \quad [Rbs]}{j_3 + [Rbs]} - k_1[Rb][E2f] \qquad (7.11.2)$$

$$\frac{dPRb}{dt} = \frac{k_3 \quad [Rbs]}{j_3 + [Rbs]} - \frac{C_2\ [PRb]}{j_2 + [PRb]} - V_2\,[E2f] \qquad (7.11.3)$$

7.11.2 Assumption and General Remarks

- Phosphorylation and dephosphorylation reactions proceed unidirectionally
- The total amount of Rb (Rb_T) is constant and hence the concentration of Rbs is replaced by the expression $Rbs = Rb_T - PRb - Rb$ where Rb is the concentration of the free and unsequestered retinoblastoma protein

7.11.3 Optimisation of Parameters

Parameters along with their optimised values for the physiological model based on the Michaelis-Menten kinetics are presented in Table 7.9.

Optimised Parameters		Optimised Parameters	
K_{SG2M}	0.9498 hr^{-1}	v_2	0.0952 hr^{-1}
K_{G2MG1}	0.1 hr^{-1}	Rb_0	0.1409 C
k_1	0.0395 hr^{-1}	$E2f_0$	0.1689 C
k_3	0.0893 hr^{-1}	Prb_0	2 C
c_2	0.0698 hr^{-1}	Rb_T	1.9 C
j_2	0.0006 C^{-1}	j_3	5 C^{-1}

Tab 7.9 Optimised Parameter Set for the Physiological Model with Michaelis-Menten Kinetics.

7.11.4 Results and Discussions

Figures 7.14 and 7.15 present the results of the simulation of the physiological model using Michaelis-Menten kinetics to describe the phosphorylation-dephosphorylation reactions associated with G1-S transition. The profiles of chemical species controlling G1-S transition could not be successfully fitted as the concentration of simulated PRb became negative shortly after the start of the simulation. Comparatively speaking, the incorporation of the Michaelis-Menten phosphorylation-dephosphorylation rates does not appear to have improved the situation, not only in terms of the chemical species controlling the G1-S transition, but also in relation to the simulated cell cycle profiles, which are shown to be almost identical to that of the physiological model with first order kinetics. This could be interpreted as either that the proposed mechanism is inadequate or

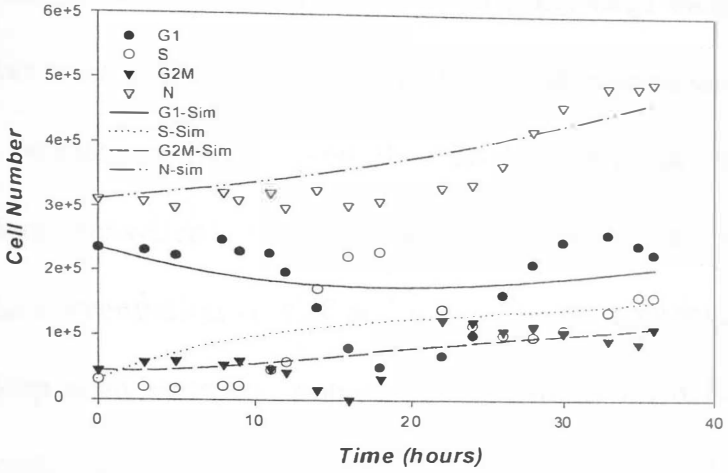

Fig 7.14 **Estimated Results of the Physiological Model after Incorporation of Michaelis-Menten Based Phosphorylation-Dephosphorylation Rates**

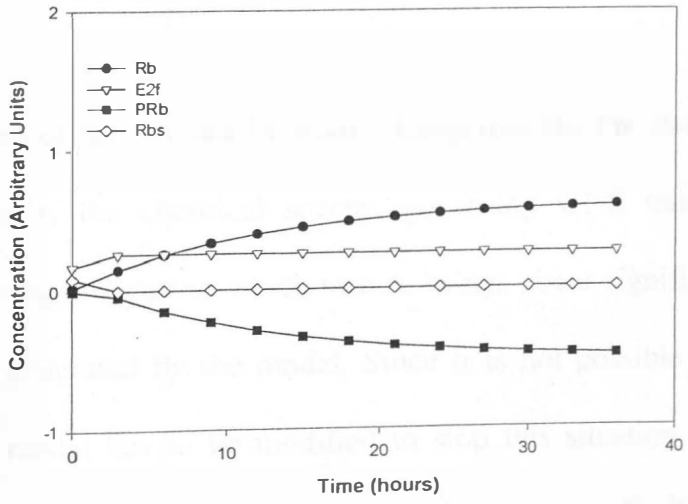

Fig 7.15 **Concentration Profiles of Chemical Agents for G1-S Control.**

that the right set of parameters has not been achieved due to discontinuity in the system. Discontinuity occurs when, during optimisation, unusually large numbers are produced which in turn makes error minimisation slow, difficult and in some cases impossible. To address the first problem it can be said that, so far, only one positive feed back mechanism has been considered which promotes dephosphorylation of Rb at a rate proportional to the concentration of E2f and it now seems appropriate to introduce a second feedback loop as an attempt to stop the concentrations of Rb, E2f and PRb falling below zero. Complications associated with the determination of parameters were somewhat anticipated, since the intracellular concentrations of these chemical species were not measurable and, therefore, assigning the right initial conditions for these species can prove to be very difficult even despite globalisation of the estimated initial conditions along with the rest of the parameters. In the next section a new differential equation describing the changes in concentration of the sequestered Rb (Rbs) will also be introduced to replace the expression Rb_T - PRb - Rb which was previously used to simplify the optimisation process.

7.12 Introduction of the Second Feedback Loop into the Physiological Model

As shown previously, the chemical species governing G1-S transition can assume negative values during simulation which in turn brings about significant changes to the cell cycle profiles generated by the model. Since it is not possible to have a negative concentration, the model has to be modified to stop this situation from recurring. As mentioned above, one possible remedy is to introduce another feedback loop to further regulate the phosphorylation-dephosphorylation steps and stop the chemical species

concentration from depleting during the simulation. More improvement could be made by incorporating a differential expression for the sequestered Rb concentration in order to evaluate its concentration independently of the other species as previously carried out as a possible preventive measure for the occurrence of negative PRb concentration.

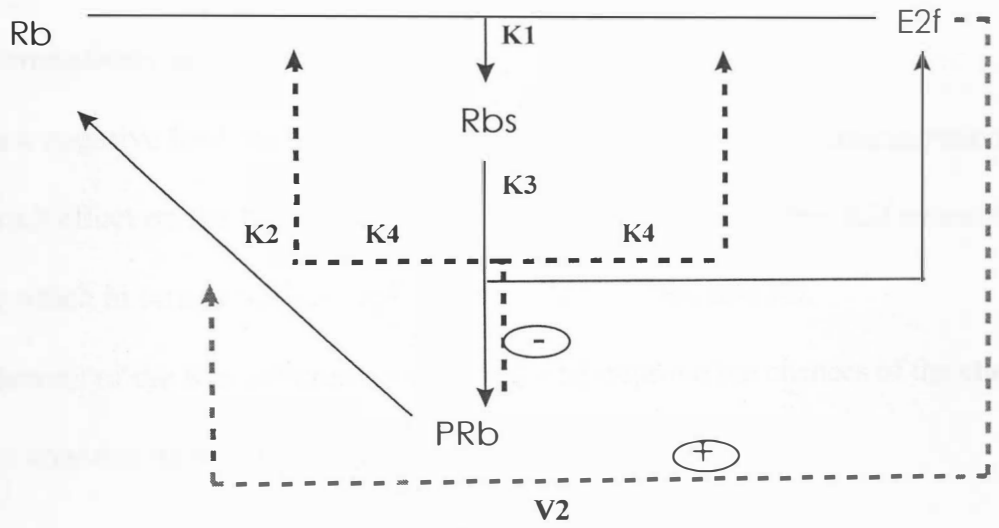

Fig 7.16 **Schematic Diagram of Proposed G1-S Transition with Two Feed Back Loops.**

7.12.1 Development of Model Equations

All the modified equations along with the new differential equation for the Rbs are shown below.

$$\frac{dRb}{dt} = \frac{k_2 \quad [PRb]}{j_2 + [PRb]} + V_2\,[E2f] - k_1[Rb]\,[E2f] + k_4[PRb] \qquad (7.12.1)$$

$$\frac{dE2f}{dt} = \frac{k_3 \quad [Rbs]}{j_3 + [Rbs]} - k_1\,[Rb][E2f] + k_4[PRb] \qquad (7.12.2)$$

$$\frac{dPRb}{dt} = \frac{k_3\ [Rbs]}{j_3 + [Rbs]} - \frac{k_2\ [PRb]}{j_2 + [PRb]} - V_2\,[E2f] \qquad (7.12.3)$$

$$\frac{dRbs}{dt} = k_1[Rb][E2f] + k_4[PRb] - k_3[Rbs] \qquad (7.12.4)$$

7.12.2 Assumptions and General Remarks

- The new negative feed back loop assumes that an increase in PRb concentration has a hindering effect on the formation of Rbs and hence allows the free E2f concentration to rise which in turn promotes dephosphorylation of PRb into Rb.
- Introduction of the Rbs differential equation will improve the chances of the chemical species concentration remaining positive.

7.12.3 Optimisation of Parameters

Optimisation results for physiological model with two feed back loops are shown in Table 7.10.

Optimised Parameters		Optimised Parameters	
K_{SG2M}	0.0585 hr^{-1}	v_2	0.44 hr^{-1}
K_{G2MG1}	0.0551 hr^{-1}	Rb_0	3.1 C
k_1	0 hr^{-1}	$E2f_0$	1.4327 C
k_3	0.1232 hr^{-1}	Prb_0	0.86 C
c_2	0.5 hr^{-1}	Rb_T	1.9 C
j_2	0.0006 C^{-1}	j_3	5 C^{-1}
k_4	0.011 hr^{-1}	Rbs_0	0.0745 C

Tab 7.10 Optimised Parameter for the Physiological Model with Two Feedback Loops.

7.12.4 Results and Discussions

Figures 7.17 and 7.18 present the simulation results of the physiological model after introduction of the second feedback loop and a separate differential expression for the Rbs concentration. Despite the introduction of the second negative feed back loop and extensive search for a suitable set of the parameters, the Rbs and PRb concentration profiles achieved negative values and therefore the optimisation of this model was not possible. It was thought that by allowing the dephosphorylation step to occur more quickly (increase in free E2f) and assigning a high value for the rate coefficient of Rbs complex formation (k_1) the problem would be resolved. During the development of this model it was also assumed that the rate of transition from G1 to S phase was the limiting step and hence no further assumption about other rate coefficients needed to be made. However, it is now believed that other rate coefficients need to be brought in to the equation but under this situation it is very likely that by modelling other phases the system would become "stiff" or overspecified and more difficult to analyse. After examination of past simulation results of the physiological models, their modifications and assumptions, it seems to be an appropriate place to stop but, before that, a number of further experiments need to be carried out to cast away any existing doubts about the suitability or unsuitability of pursuing the current modelling strategies. In the next sections we will look first at the effect of removal of the lag or recuperative period on the model performance, and at the use of the model of Obeyesekere *et al* (1995) in its entirety to see whether it could produce the desired outcome.

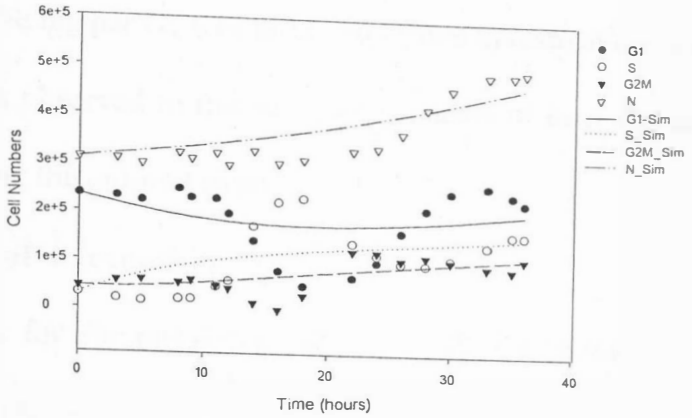

Fig 7.17

Cell Cycle Profiles after Incorporation of the Second Feedback Loop in the Physiological Model

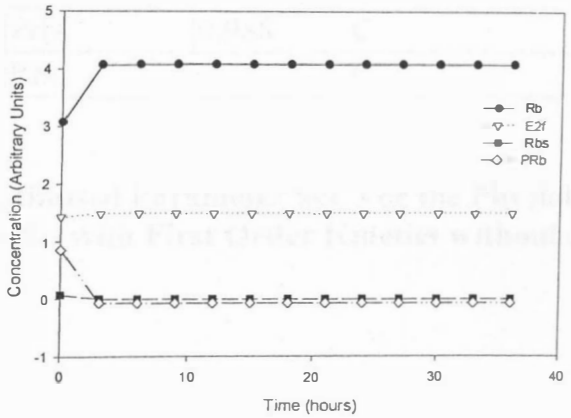

Fig 7.18

Simulated Concentration Profiles of the Chemicals Controlling G1-S Transition in Physiological Model with Two Feedback Loops

7.13 Performance of the Physiological Model Without the Lag Period

As described above, the lag period was removed in this investigation to establish whether any improvement was observed in the simulation results or how big an obstacle the lag period was in achieving the optimal results.

7.13.1 Optimisation of Parameters

Optimised parameters for the physiological model after removal of the lag period is shown in Table 7.11.These parameters were determined by fitting using a least squares routine.

Optimised Parameters		
K_{SG2M}	0.0602	hr^{-1}
K_{G2MG1}	0.0752	hr^{-1}
k_1	0.0735	hr^{-1}
k_3	0.0001	hr^{-1}
c_2	1.37	hr^{-1}
v_2	0.0675	hr^{-1}
Rb_0	2.81	C
$E2f_0$	4.11	C
Prb_0	0.988	C
Rb_T	9	C

Tabe 7.11 **Optimised Parameter Set For the Physiological Model with First Order Kinetics without a Lag Phase**

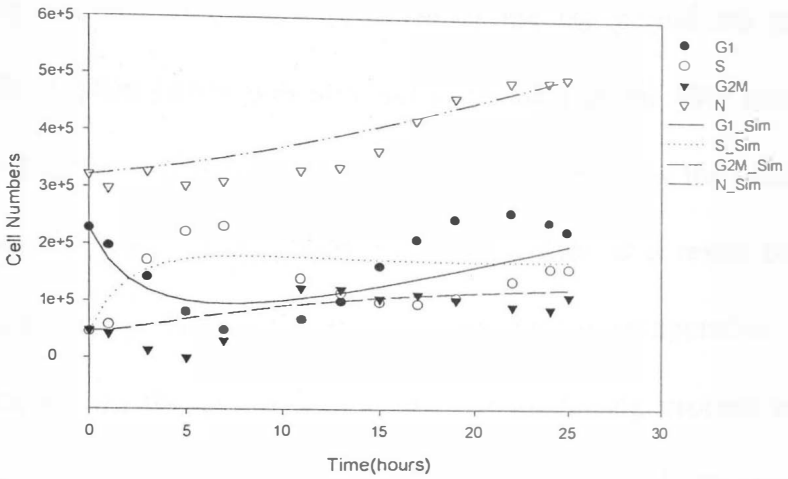

Fig 7.19 **Demonstrating the Improvement in Fit Between the Measured and Predicted Data after Omission of the Lag Period.**

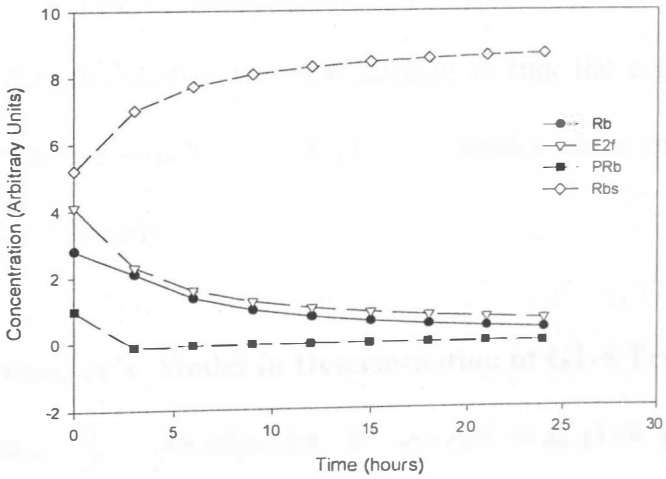

Fig 7.20 **Changes in Concentration of Chemicals in G1-S Transition after Removal of the Lag Period**

7.13.2 Results and Discussions

Simulation and optimisation results after removal of the lag period are presented in Figures 7.19 and 7.20. Optimisation was still not successful as the PRb concentrations still assume negative numbers. However, G1 and S phase cells show the most and G2M and total cell number the least improvement in their profiles as a result of the above modification, which further points to the fact that the lag or recuperative period still remains a major problem in the curve fitting and the modelling process and, despite developing a physiological approach, it has not yet been possible to overcome this difficulty. The optimisation routine has also not been very successful in arriving at a satisfactory condition. One notable problem encountered in the optimisation process was the degree of variation between the optimised profiles of chemical species controlling G1-S transition each time a small change in the initial concentration of these chemicals was made. Up to now, in order to simplify the optimisation process and facilitate parameter determination, an exfoliated version of the experimentally established mechanism for G1-S transition has been considered, but in the wake of this rather cumbersome effort, it is decided in the next section to link the cell cycle model with another physiological model which, although more complex, does simulate the profiles of the chemical species correctly.

7.14 Use of Obeyesekere's Model in Determination of G1-S Transition

The physiological model, first published by Obeyesekere *et al* (1997), is mainly focused on the regulation of progression through the G1 phase of the mammalian cell cycle and involves, in addition to the above species, cyclins D and E and their respective kinases.

In this model a hypothetical stage is introduced where a chemical species known as the maturation promoting factor (MPF) acts as a regulator of the S and G2M phases whose rate of production is autocatalytic. In addition, this model will allow for the phosphorylation kinetics to change in response to varying amounts of growth factor present in the medium. Major differences between the models are that Obeyesekere *et al* do not include a separate component balance for E2f and they assume that the total amount of E2f is constant and hence the amount of free E2f is calculated by the expression ($E2f_T$ -Rb).

7.14.1 Results and Discussion

Figure 7.21 illustrates the simulation results for the Obeyesekere *et al* model prior to its connection to the cell cycle model. In this model PRb and Rbs profiles act as mirror images of each other. PRb is shown to increase while Rbs decreases throughout the simulation time. The Rb curve, however, remains constant throughout and shows very little change in comparison to the other two species. After its connection to the cell cycle model and an attempt to optimise the now combined cell cycle and physiological model it was discovered that due to discontinuities in the system it was not possible to continue and hence this optimisation process was halted. These discontinuities are likely to have been brought about by the autocatalytic term associated with E2f production. In short, changes had to be made to the original Obeyesekere model in order to allow for optimisation of its parameters.The latter, when taken into consideration along with the degree of complexity of the model and the lack of experimental data, serve to demonstrate the unsuitability of combining the cell cycle model with the Obeyesekere

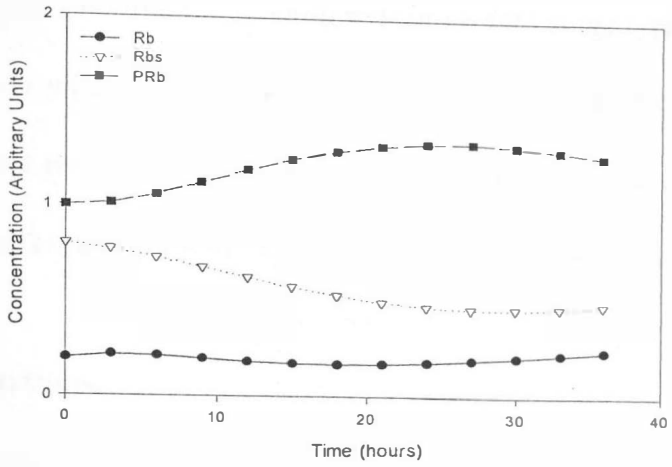

Fig 7.21 **Obeyesekere Model Prior to Its Connection to the Cell Cycle Model**

model. This argument could also be extended to previous physiological models. Apart from the difficulties associated with parameter estimation it was also not possible to incorporate physiological mechanisms for transition of cells between phases of the cell cycle other than G1-S due to the sheer complexity of the resulting model. The above problems may be overcome by simplifying the mechanism even further into a simple predator-prey type of relationship and reducing the cell cycle phases into two where mechanisms for transition of cells could be applied to the entire cycle. In the next section some time will be spent looking at the possibilities that such assumptions can bring about to overcome this problem.

7.15 Cell Cycle Transition Based on the Lotka-Volterra Model

In this section, we are concerned with a simple model for prediction of inter-stage cell cycle transition consisting of two chemical species whose profiles resemble those of

predator and prey, denoted by pd and pr respectively. Our aim here is to simplify the multistage mechanism previously encountered into a two-stage type of interaction where parameter estimation will be easier and overall cell cycle transition could be accounted for. The model used in the physiological part of the model is a replica of the original Lotka-Volterra predator and prey model which is discussed in the next section.

7.15.1 Model Equations

The use of the Lotka-Volterra model for cell cycle transition is interesting in that it produces oscillating behaviour similar to that of a synchronised population. The system's complete indifference to external disturbances makes it even more suitable for use with isolated systems such as this one. The Lotka-Volterra model cannot by itself be considered realistic without making a number of assumptions, which are discussed later in this section. The proposed equations for change in concentration of species with time are shown below:

$$\frac{d[pr]}{dt} = a\,[pr] - g\,[pr][pd] \qquad \textbf{(7.15.1)}$$

$$\frac{d[pd]}{dt} = -b\,[pd] + g\,[pr][pd] \qquad \textbf{(7.15.2)}$$

where a is the net rate of increase in the prey chemical including terms for degradation and inter-conversion reactions. For the predator chemical on the other hand, b represents degradative processes only and its rate of production is dependent on the second term in the equation. The second term in both equations is taken to be exactly the same, unlike the Lotka-Volterra model, where two different coefficients were used, one representing the predation rate and the other the rate of predator increase.

7.15.2 Assumptions and General Remarks

- Population is partially synchronised
- Cell cycle is made up of two stages: G1 and G2MS
- Rate of G1-G2MS transition is proportional to Prey, and the rate of G2MS-G1 to predator concentration

7.15.3 Optimisation of Parameters

Parameters chosen for the optimisation are presented in Table 7.12. These parameters were determined by fitting the simulated data to the experimental data.

Optimised Parameters		
a	0.0602	hr^{-1}
b	0.0752	hr^{-1}
g	0.0735	hr^{-1}
u	0.0001	hr^{-1}
l	1.37	hr^{-1}
pd_0	0.0675	hr^{-1}
Pr_0	2.81	C

Tab 7.12 **Optimised Parameter Set for the Physiological Model with First Order Kinetics without a Lag Phase.**

7.15.4 Results and Discussions

Figures 7.22 and 7.23 demonstrate the effect of combining a physiological predator-prey and a cell cycle model after optimisation of their parameters. As can be seen, the improvement in the match of simulation to experimental results is truly remarkable when compared with those of previous physiological models. The lag period, as is shown in

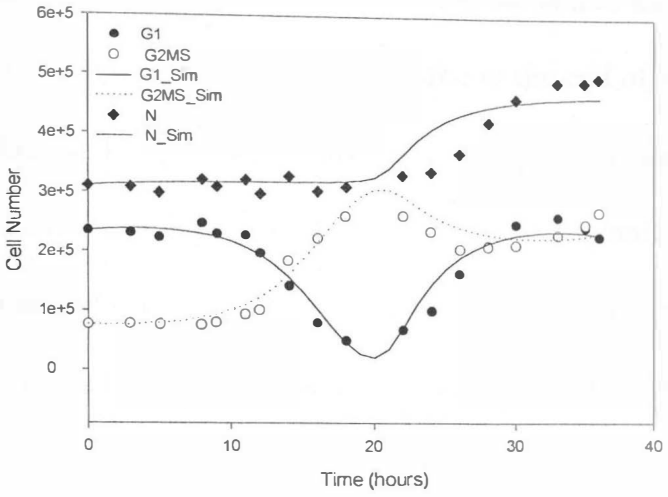

Fig 7.22 **Shows the Measured and Simulated Results after Introduction of a Predator-Prey Model for Prediction of the Cell Cycle Transition**

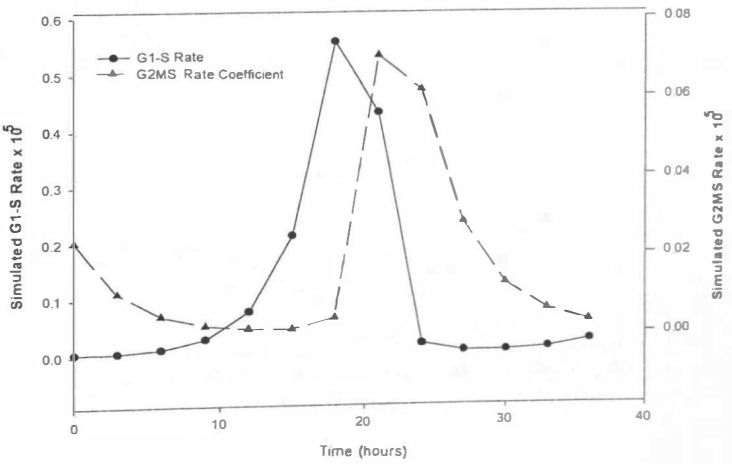

Fig 7.23 **Simulated G1-S and G2MS-G1 Rates for the Predator-Prey Type Model**

Figure 7.22, is predicted very well and so are the oscillatory profiles of G1 and G2M$_S$ phase cells. However, the onset of cell proliferation at the end of the lag period is shown to occur prematurely and the total cell number profile at the end of the simulation period is slightly underestimated. The premature onset of cell proliferation could be attributed to the G2MS-G1 rate coefficient having higher values at the beginning of the culture time than expected and the underestimation of the total cell number towards the end of the simulation period is considered to be due to the more gradual decline in G2MS phase cells as is shown in Figure 7.22. The patterns of change in G1-S and G2MS transitions are as expected, with the exception of the K_{G2MS} values at the beginning of the simulation period and the relative degree of overlap between the two curves being slightly higher than anticipated. At this stage we will accept these results and explore whether the model could produce a similar profile using a different set of data from a different batch of CHO cells The results are shown in Figure 7.24.

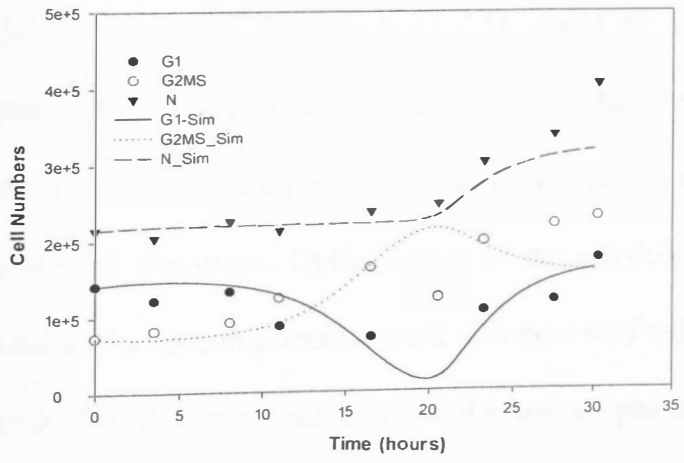

Fig 7.24 **Validation Results of the Combined Cell Cycle and Predator-Prey Physiological Model**

The model validation results are only slightly different in that the lag period is shorter and hence the G1 and G2MS profiles have become out of phase with the measured data as a result. The shorter lag period appears to have a beneficial effect on the total cell number profile and, as it is shown, a better fit to the total cell number data is obtained between 20-30 hours of culture time.

7.16 Summary

With the exception of the predator and prey model, all measures taken to produce the desired profiles for the chemical species governing G1-S transition have been shown to be not successful. The corresponding cell cycle profiles of these physiological models have not shown great improvement either. It is now believed that the use of physiological models to control G1-S transition only is inadequate. Physiological models which can bring great improvements to the cell cycle model are likely to be those that control all the phases and not concentrate on one phase alone. On the other hand simulated results of the predator-prey model as shown in Figures 7.22-7.24 could be successfully used to estimate the cell cycle profile of CHO cells. Its ability to produce better results is due to its simplicity and the extension of the physiological mechanism to control not only G1-G2MS but also G2MS-G1 transition. Optimisation of the physiological models in the absence of measured data for its components could also be a very tedious and often futile exercise. Having looked at the pros and cons of the use of physiological models for estimation of cell cycle parameters it is perhaps a good time to look at the models which interact with their environment and to explore whether this interaction will enhance their predictive ability.

CHAPTER 8

USE OF DYNAMIC OPEN SYSTEMS IN CELL CYCLE MODELLING OF CHO320 CELLS

8.1 Introduction

In this chapter the study is extended to dynamic open systems where the environment within which the system is functioning is also taken into consideration in the estimation of CHO320 growth, based on its cell cycle profile. Environmental conditions in open systems are normally expressed in terms of the presence or absence of a particular, or more correctly a limiting, substrate. In our study this principal was used to construct models for controlling cell cycle phase transition and hence proliferation and death processes in CHO320 Cells. This study was commenced by looking at the long term model previously examined in chapter seven, where the simulated profiles of total cell number and G1 Phase cells overshot the measured data because the model was based on unlimited continuous traverse of cells between the phases of the cell cycle. The long term model was chosen, as the short term model does not exhibit G1 enrichment and is not likely to benefit from this modification.

8.2 Longer Term Model

The model developed in Sections 7.3-7.4, designed to reproduce progress through the cell cycle, was not able to represent the sigmoidal nature of the cell growth curve over the longer term because it allowed unlimited progress through successive cycles. There are two ways to limit such progress: one is by death of the cells, the other is by a substrate (or other) limitation of the rate of progress through the cell cycle. The former is

simpler, if rather crude, and should be attempted before further investment of time. Of course, in practice, both mechanisms may operate.

In Section 7.4, although the death rate parameters were optimised along with other rate constants etc., no attempt was actually made to fit the dead cell profile produced by the simulation to the data set available since we were there concerned only with the distributions of viable cell populations. As a first step it was therefore sought to include this optimisation and dead cell data fit in the model.

8.2.1 Optimisation of Parameters

Optimised parameters for the long term model are shown in Table 8.1.They were obtained by fitting the simulated values by the model to the experimental data.

Rate Constants	hr^{-1}
K_{G1S}	0.1923
K_{SG2M}	0.4182
K_{G2MG1}	0.3054
K_{DG1}	0
K_{DS}	0.1333
K_{DG2M}	0.0993

Table 8.1 **The Optimised Parameter Sets for the Long Term Model with Non-Viable Cell Population Included in the Fitting of Data.**

8.2.2 Results and Discussion

Figures 8.1A-C show the profiles of viable and nonviable cell numbers and the cell cycle populations obtained when parameter fits to the CHO320 dead cell population accumulation are optimised. The cell cycle simulation is difficult to visualise because the G2M phase cell numbers overlie those for S. More particularly, the total cell number profile still fails to achieve its sigmoidal shape with no sign of decline of the growth rate towards the end of the batch culture, even though the accumulating dead cell population has been taken into account in the curve fitting routine. The degree of overshoot for the viable cell population is completely unacceptable and this approach must be set aside. Optimisation of the long term model has caused the simulated S phase cells to decline and overlie the G2M phase cell profile. Profiles of simulated G2M and G1 phase cells closely resemble that of Figure 7.4 and G1, and total cell number profiles retain their exponential rather than sigmoid profiles with no sign of decline towards the end of the batch culture. The degree of overshoot for the total cell number remains the same despite inclusion of the dead cell population in the curve fitting routine. To initiate the treatment of the problems encountered above a substrate dependent G1-S transition rate is implemented as discussed in the next section.

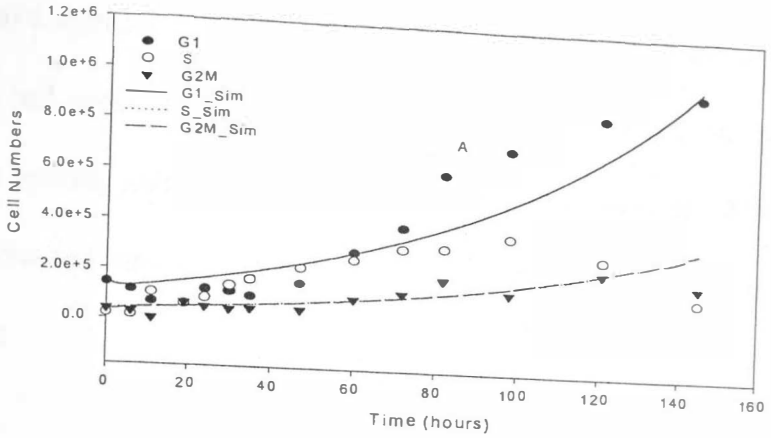

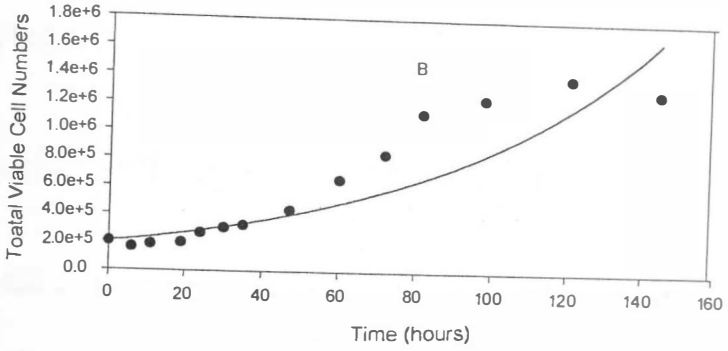

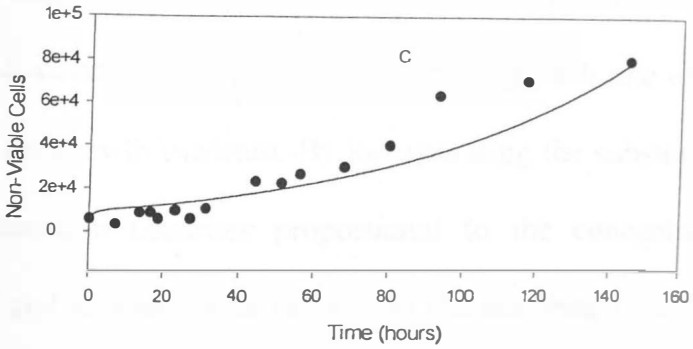

Figure 8.1 **Simulated and Measured Data of the Model for the Long Term Prediction of CHO Cell Population. A: Cell Cycle Profile B: Total Viable Cell Number C: Non-Viable Cell Population.**

8.3 Longer Term Model Based on Substrate Dependent G1-S transition

The alternative approach is therefore to look for a modification of the rates of progress through the cell cycle that is characterised by a dependence on the concentration(s) of one or more limiting substrates, using a model analogous to the Monod saturation model of substrate-limited microbial cell growth but applied to the transition between phases of the cell cycle.

8.3.1 Model Development

The new equation will replace the original Equation 7.4.1 describing the balance on G1 cells as shown below:

$$\frac{dG1}{dt} = 2.K_{G2MG1}\,[G2M] - \left(\frac{\vartheta_{max}\,[\Gamma]}{\varphi + [\Gamma]} + K_{DG1}\right)[G1] \qquad \textbf{(8.3.1)}$$

where ϑ_{max}, φ and Γ are maximum G1-S transition rate constant, saturation constant and limiting substrate concentration respectively. ϑ_{max} and φ values were assumed to have the same magnitude as μ_{max} and K_s in the Monod expression. Initial estimates for these parameters were taken from the Leelavatcharamas PhD thesis (1996), who obtained these values via a Lineweaver-Burk type plot of specific growth rate of CHO cells vs. serum concentration in the growth medium. By incorporating the substrate dependent term, the rate of G1-S transition becomes proportional to the concentration of the limiting substrate present and its magnitude reduces as the substrate is consumed. In addition to Equation 8.3.1, a maintenance model represented by Equation 8.3.2, is introduced to account for the changes in substrate concentration throughout the cultivation period.

$$d[\Gamma] = -1/\gamma_{N\Gamma} .\mu.N - m_e .N \quad (8.3.2)$$

where $\gamma_{N\Gamma}$ is the yield of cell number on substrate, m_e is the cell maintenance coefficient, N is the total viable cell number and μ is the instantaneous specific growth rate based on cell number whose value was obtained by the following expression:

$$\mu = 1/N \, dN/dt \quad (8.3.3)$$

To avoid algebraic loops presented by equations 8.3.2 and 8.3.3 during simulation, the glutamine consumption profile was obtained using a look up table and hence the results presented in figures 8.4(A-C) were obtained using that method.

8.3.2 Assumptions and General Remarks

- Rate of G1-S transition decreases continuously and gradually in proportion to substrate depletion rate.

8.3.3 Optimisation of Parameters

Optimised parameters for the long term model with substrate dependent G1-S transition are shown in Table 8.2. They were obtained by fitting using a least squares routine .

Rate Constants	
K_{SG2M}	0.1503 hr^{-1}
K_{G2MG1}	0.2050 hr^{-1}
K_{DG1}	0.0219 hr^{-1}
K_{DS}	0 hr^{-1}
K_{DG2M}	0.0424 hr^{-1}
φ	0.5316 mmol
ϑ_{max}	0.3084 hr^{-1}

Table 8.2 The Optimised Values of Parameters for the Cell Cycle Model Based On Substrate Dependent G1-S Transition.

8.3.4 Results and Discussions

Figures 8.2A, 8.2B and 8.2C show simulations and results of cell cycle sub populations, total viable cell number and the dead cell numbers, produced by the model with a substrate dependent G1-S transition rate. In comparison to the previous attempt in Section 7.4, improvements in the simulated G1 and S profiles were observed. However, G2M profiles show less conformity and in fact, along with S phase, assume negative values towards the end of simulation time, which in turn leads to the underestimation of the total viable cells in Figure 8.2B. The simulated dead cell profile remains constant throughout the simulation time and demonstrates the greatest deviation from the measured data in comparison to the other states. The priority is now to improve on the death cell profile by assuming a substrate dependent death rate expression to bring the simulated death profile more in line with the experimental data. S-G2M and G2M-G1 transition rate coefficients could also be manipulated with the objective of improving the simulated total cell profile.

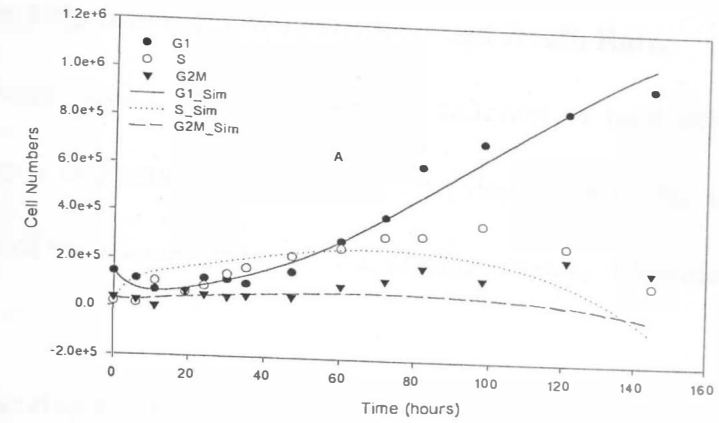

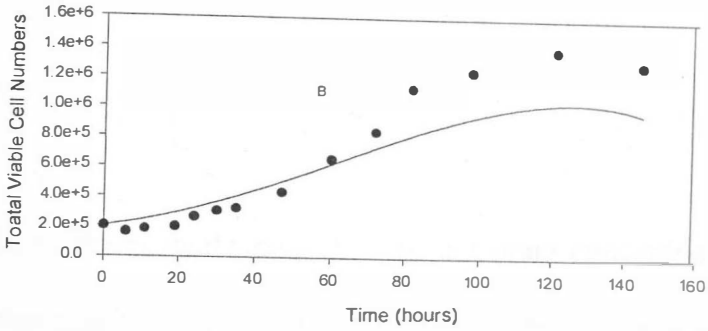

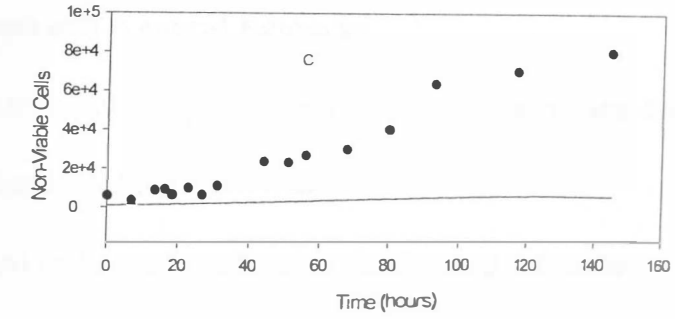

Figure 8.2 **Cell Cycle (A), Total Viable Cell Number (B) and Non-Viable Cell (C) Profiles by Substrate Dependent G1-S Transition Model**

8.4 Substrate Dependent G1-S Transition and Death Rate.

The death rate term, which was previously a function of total cell density only, was replaced with a new expression which is not only dependent on the total cell density but is also a function of the concentration of a depleting limiting substrate.

8.4.1 Model Development

The new death rate expressions takes the form:

$$K_d = \frac{K_{d0} \cdot K_D}{K_D + [\Gamma]} \qquad (8.4.1)$$

Where K_{d0} is the maximum death rate (at zero substrate concentration) and K_D is the death saturation constant respectively and are taken to be the same for all the cell cycle phases and therefore a function of total cell number.

8.4.2 Assumptions and General Remarks

- Cell death occurs in all the phases and is not specific to any one phase and hence is taken to be a function of total cell number.
- Death rate is also reciprocally related to the limiting substrate

8.4.3 Optimisation of Parameters

Optimised parameters for the long term model with substrate dependent G1-S transition and death rate are shown in Table 8.3. They were obtained by fitting the simulated values generated by the model to the experimental data.

Rate Constants	
K_{SG2M}	0.1 hr^{-1}
K_{G2MG1}	0.5599 hr^{-1}
K_{d0G1}	0.0053 hr^{-1}
K_{d0S}	0 hr^{-1}
K_{d0G2M}	0.4279 hr^{-1}
K_D	1.1099 mmol
φ	0.5316 mmol
ϑ_{max}	0.3084 hr^{-1}

Table 8.3 The Optimised Parameters for the Cell Cycle Model Based On Substrate Dependent G1-S Transition and Death Rate.

8.4.4 Results and Discussion

Figure 8.3 presents the simulated and experimental data for the substrate dependent G1-S and death rate model. As is shown, the results are very similar to the case in Section 8.3, where only G1-S transition was assumed to be substrate dependent. In other words, the substrate dependent death term does not appear to have made any noticeable change in the profiles of the model states. G2M and S still assume negative values towards the end of the simulation period in more or less the same manner as in section 8.3, and consequently the total cell number data are underestimated. There is a slight increase in the number of dead cells towards the end of the culture time which may have contributed to a slightly better fit, observed in the G1 profile. Although G1-S transition is affected by substrate, a Monod type relationship is not believed to describe this situation very well. Experimentally the G1-S appears to stop abruptly after the concentration of the limiting

substrate reaches a critical level. This abrupt cessation of G1-S transition, as experimentally suggested, cannot be mathematically described well. Substrate dependent cell cycle transition greatly improved the simulated profile of the cell cycle states, but its effect on the simulated dead cell population, however, was disappointingly poor. As mentioned previously, the assumption that the rate of G1-S transition decreases in a continuous and steady manner in proportion to the depleting substrate concentration may not be a reasonable one and, as can be seen in Figure 8.3, this assumption does limit the cell proliferation excessively and as a result leaves no space for the exponential increase of the dead cell population during the optimisation process. To overcome the problem, associated with underestimation of dead cell population, age as a regulatory parameter of cell cycle transition is to be introduced. Age is a good choice as both birth and death in all but the very simplest organisms are age dependent, and it is usually necessary to take account of a population age structure in order to have a reliable description of their dynamics. In the next section an analysis of the age dependent phase transition model under a number of different assumptions will be made.

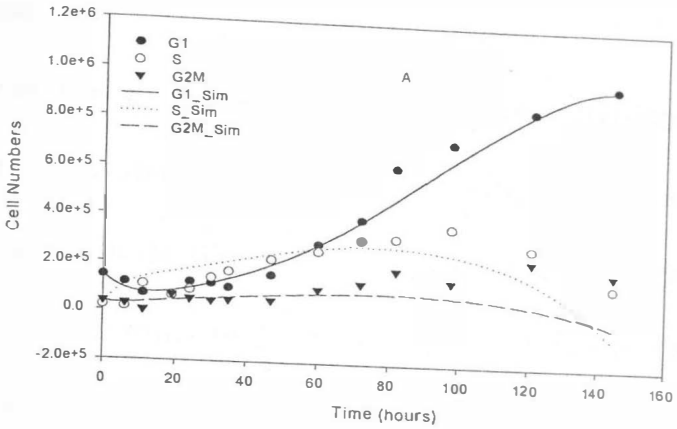

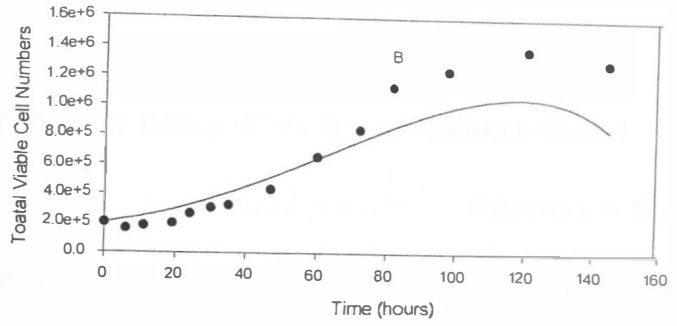

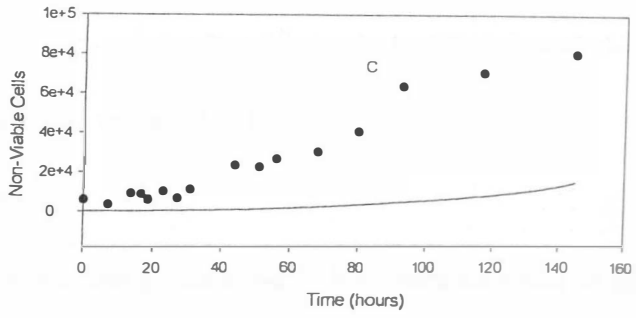

Figure 8.3

Measured and Predicted Cell Cycle (A),Total Cell Number (B) and Dead Cell Population (C) Results after Introduction of Substrate Dependent G1-S and Death Rates

8.5 Age Dependent Cell Cycle Transition

8.5.1 Introduction

Synchronous growth studies have shown that between division cycles, the enzyme content, and hence the metabolic activity of CHO cells, varies. For this reason, together with what was discussed in the previous section, it may prove to be fruitful to describe CHO cell populations in terms of their cell age distribution. One of the means of controlling or predicting the traverse of cell numbers is to base their rate of immigration or emigration to or from a phase in the cell cycle on their age. In the following sections an age dependent model to describe cell cycle transition will be studied and comparison with the substrate dependent cell cycle transition will be made in order to establish their suitability.

8.5.2 Overview of the Age Based Population Balance Model

One of the first publications on age based population dynamics is that of Foerster (1959). He argued that if a small increment Δt of time passes by nothing would happen to the age elements of the population except that the elements would grow older by a small age increment Δa; That is to say that the age distribution $N_a (t + \Delta t, a)$ at time $t + \Delta t$ would be the same as it was at time t, if every cell in that element was Δa younger, and this is presented symbolically in Equation 8.5.1.

$$N_a (t + \Delta t, a) = N_a (t, a-\Delta a) \qquad (8.5.1)$$

According to Foester, while the population N has been exposed to time, two factors have acted on them:

1- Loss of elements in each group

2- Loss in each group from environmental interaction

So the new equation will be:

$$N_a(t + \Delta t, a) = N_a(t, a-\Delta a) - N_a\theta\,\Delta a \qquad (8.5.2)$$

Where θ is a compound loss factor. By expansion of N_a around t and a we obtain

$$N_a(t + \Delta t, a) = N_a(t, a) + \partial N_a/\partial t\,.\Delta t + \ldots. \qquad (8.5.3)$$

$$N_a(t, a-\Delta a) = N_a(t, a) - \partial N_a/\partial a\,.\Delta a + \ldots. \qquad (8.5.4)$$

Inserting these two equations into equation 6.1.2 and neglecting higher powers he arrived at :

$$\boxed{\partial N_a/\partial t + \partial N_a/\partial a = -N_a.\theta} \qquad (8.5.5)$$

Equation 8.5.5 forms the basis upon which the age based cell cycle model will be constructed. One of the problems associated with Equation 8.5.5 is that it is a partial differential and hence its solution and simulation is far more complex. In the following sections the development of the model equations for the cell cycle components and the particular approach by which the solution of these partial differentials was obtained will be discussed.

8.5.3 Assumptions and General Remarks

This study was initiated by analysing cell cycle transitions of cells based on the chronological age of the culture. Although chronological as opposed to physiological age is a less plausible option theoretically, it is, however, a preferred choice when simplicity is also a criterion in model development. One of the interesting steady state models to have been based on chronological age is that of Martens *et al* (1995). This is a

combined cell cycle and metabolic model for determination of proliferation and substrate consumption and product formation rates of hybridoma cells in chemostat culture, comprising four states: A or indeterminate, B or determinate, O or apoptotic and D or dead cells state. For the purposes of this study a number of improvements were made to the model. To begin with, the metabolic component of the model was dispensed with as it was not of direct relevance to our investigation and also complicated simulation and optimisation of the model for its large number of parameters. An apoptotic stage was not considered at this stage and hence was omitted from the balance equations. In solving the population balance model the assumptions made were the same as those of Martens's.

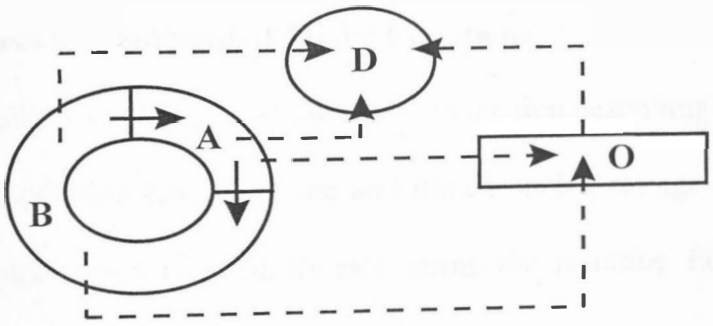

Figure 8.4 **Schematic representation of Martens Model: A, Indeterminate state; B, Determinate state; O, Apoptotic state; D, Dead cell population.**

- The transition from state B to state A occurs at a constant age t_B of the state B cells. Therefore the rate of transition from state B to state A can be replaced by the boundary condition $n_{A(0)} = 2n_{B(tB)}$.
- The transition of cells from state A to state B occurs at age t_A of the state A cells. Thus, the rate of transition from state A to state B can be replaced by the boundary condition $n_{A(tA)} = n_{B(0)}$.
- Loss of cells due to necrosis is equal for both A and B states and assumed to be independent of age .
- The apoptotic stage is merged with the necrotic stage to form stage D or dead cells in the adapted model.

8.5.4 Development and Solution of Model Equations

By analogy to Equation 8.5.5, a partial differential equation describing the rate of change of the CHO cell population based on time and the chronological age of the culture was developed, and after substitution of its rate terms the resulting Equation 8.5.6 was developed as shown.

$$\partial N(t,a)/\partial t + \partial N(t,a)/\partial a = -N(t,a).kd \qquad (8.5.6)$$

The above equation had to be somehow modified into a simpler expression in order to make simulation possible. In our approach a general solution to the equation 8.5.6. was obtained using the Change of Dependent Variable method. The solution steps are shown overleaf.

8.5.5 Solution of Partial Differential Equation for the Total Cell Population

The Change of Dependent Variable method was used to obtain the solution to Equation 8.5.6. N(a,t) was represented as A(a).T(t), substituted into Equation 8.5.6 and the A(a) and T(t) terms were separated so that all the A(a) terms are on one side and the T(t) terms on the other.

$$\partial[A(a).T(t)]/\partial t + \partial[A(a).T(t)]/\partial a = [A(a).T(t)](-kd) \quad (8.5.7)$$

Equation 8.5.7 is divided through by A(a) and T(t).

$$\{A(a). (\partial[T(t)]/\partial t) + (\partial[A(a)]/\partial a) .T(t) \}/ [A(a).T(t)] = -kd \quad (8.5.8)$$

Equation 8.5.8 is expanded and a $(\partial[A(a)]/\partial a)$ term is subtracted from both sides of the equation.

$$(\partial[T(t)]/\partial t)/T(t) = -(\partial[A(a)]/\partial a)/A(a) -kd \quad (8.5.9)$$

Since the left hand side of the Equation 8.5.9 is only dependent on t, it must be a constant.

$$(\partial[T(t)]/\partial t)/T(t) = Z \quad (8.5.10)$$

Where Z is a constant. Now Equation 8.5.10 was solved for T(t).

$$T(t) = C_1 e^{(Zt)} \quad (8.5.11)$$

where C1 is the constant of integration. The right-hand side of the equation 8.5.9 must of course be equal to the same constant.

$$-(\partial[A(a)]/\partial a)/A(a) -kd = Z \quad (8.5.12)$$

Solving for the A(a) we have :

$$A(a) = C_1 e^{|(\int -kd - Z) da|} \quad (8.5.13)$$

Now we multiply the A(a) solution with the T(t) solution.

$$N(a, t) = C_1^2 \, e^{\left|\int (-kd - Z)\, da\right|} \cdot e^{(Zt)} \qquad (8.5.14)$$

Equation 8.5.14 on simplification will give the solution to the population balance partial differential equation. Equation 8.5.14 is the age density function for the cell number. In order to evaluate the total number of cells between 0 and tc, Equation 8.5.14 needs to be integrated between those two limits. The final results are shown below. Before integration, the constant C_1^2 was obtained by introducing the initial conditions as follows:

(at t= 0, $a_0 = 0$, N = N(0, 0))

Following integration and substitution of limits we have:

$$N_T = N(0, a_0)\, e^{(Zt)} / (kd+Z)\, [1-e^{(kd+Z)-tc}] \qquad (8.5.15)$$

8.5.6 Determination of Generation time t_C

To determine t_C, boundary conditions were applied to the age distribution function of the cycling cells (8.5.14) and the following expression in terms of t_C was obtained.

$$t_C = (\ln 2 + Zt)/(kd + Z) \qquad (8.5.16)$$

It is now possible to simulate the population balance model to see how the total cycling and dead cell populations will change when subject to time and age constraints. In our approach two different cases were considered:

- Case A deals with a situation where death processes are taken to be first order with respect to total cell population.
- Case B assumes death processes to be substrate dependent.

8.5.7 Optimisation of Parameters

The optimised parameter sets for the model based on chronological age is shown in Table 8.4. These parameters were obtained by fitting the simulated values to the experimental data.

Parameters	First Order Death Rate (Case A)	Parameters	Substrate Dependent Death Rate (Case B)
kd	0.0033 hr^{-1}	kd0	0.0049 Cells hr^{-1}
Z	0.0049 -	K_D	0.0407 mmol
N(0,0)	$5.90e^3$ Cells	Z	0.0109
		N(0,0)	$6.35e^3$ Cells

Table 8.4 The Optimised Parameter Sets for the Cell Cycle Model with Age Dependent Phase Transition with First Order and Substrate Dependent Death Rate.

8.5.8 Results, Discussions and Validation

The simulation results of the adapted model of Martens *et al* (1995) for both cases are shown in Figure 8.5A-B. As is illustrated, the simulated cycling and necrotic cell population profiles in Figure 8.5A increase exponentially but both are overestimated. The greatest deviation is observed at the beginning of the culture time where the optimised value for the initial cycling cell population of age zero caused the overestimation of the cycling cell curve. The decrease in the cycling cell population profile towards the end of the culture time does not occur. In Case B, however (Figure 8.5B), the simulated results show marked improvement in the general fit of simulated cycling and dead cell profiles. The decline phase associated with substrate exhaustion which was previously absent

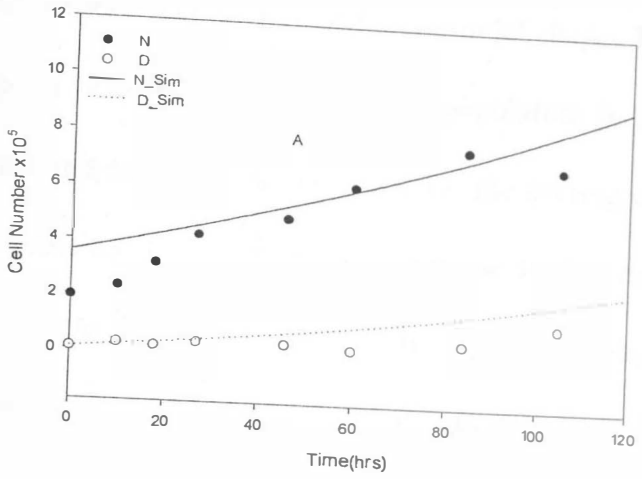

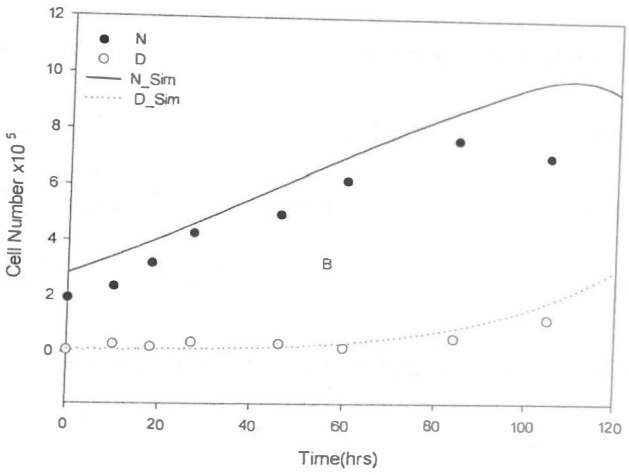

Figure 8.5A-B **Simulated and Experimental Results of the Adapted Martens Model Showing Cycling and Dead Cell Populations Over the Batch Culture. A: First Order Death Rate B: Substrate Dependent Death Rate**

(Case A) is now clearly visible and the cycling cell profile is shown to have changed from being previously exponential to a slightly sigmoidal shape. The simulated dead cell population gives a good fit whilst the cycling cell population is still overestimated. The gap between the actual and estimated initial value for the cycling cells of age zero is also shown to have been reduced. It was decided to analyse further the predictive ability of this model (with substrate dependent death rate) by attempting to fit the simulated profiles of cycling and dead cells to another set of data with very different starting initial conditions in terms of their cell cycle sub-populations. The data comes from the extended experiment described in Chapter 6 to determine how cell cycle components affect the overall growth of the cells in batch culture. Out of the five batches batch three was chosen, as it is highly enriched in S phase cells at the start of the batch and hence demonstrates the greatest contrast to the previous scenario where the sample was highly enriched in G1 phase cells. The results are presented in Figure 8.6. As can be seen, the degree of overestimation of cycling cells has been reduced and generally the fit to the data has improved. The reason for this improvement is attributed to the behaviour of the S phase cells. Since the lag period is absent in batch three cells, the proliferation of cells starts immediately after the inoculation and continues in a rather steady manner until the critical concentration of the substrate is reached. This is more acceptable in relation to the concept of chronological age where the aging process is assumed to be uniform throughout the culture period. In order to account for the lag period and periods during which aging or maturation do not occur, age models should be based on physiological rather than chronological age. Although development of physiological models may be

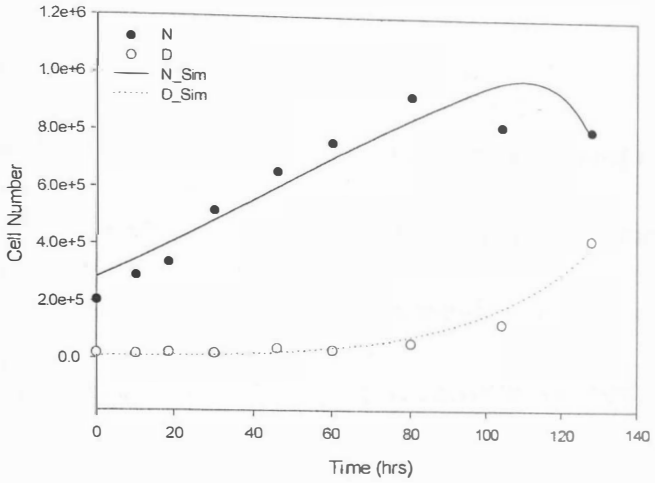

Figure 8.6 **Validation of the Adapted Martens Model Using a Sample with High S Rather than G1 Phase Cells at the Start of the Cultivation Period**

possible their solution is harder. However, if time permits models based on physiological age would be another interesting turning in our search for the ideal model.

CHAPTER 9

GENERAL DISCUSSION, CONCLUSIONS AND FURTHER WORK

The work described in this thesis has contributed towards development, construction and hence selection of better approaches to dynamic modelling of chinese hamster ovary cell growth and laid the foundation for subsequent expansion and broader application of the selected models to cover other aspects such as productivity in these cell lines with a view to better control strategies.

9.1 Conclusions

This work commenced by exploring the existing published literature on the growth of CHO320 cells as well as the various approaches to modelling of their growth. Having surveyed the relevant literature, a number of biological experiments were designed to establish the nature of and relationship between the changes in cell cycle of CHO320 cells and parameters such as cell volume and cell mass and substrate consumption of cells under those conditions using flow cytometery as the main analytical tool. With respect to substrate effects, it can be said that lower glutamine concentrations (1mmol, 0.5mmol) led to lower growth in CHO320 cells. Hayter et al (1991) has also observed a decrease in viable cell concentration at medium glutamine concentration of 1mmol in comparison to medium containing 2mmol of glutamine in the same cell line. Glutamine is not believed to have a direct effect on the cell cycle of CHO320 cells as previously thought and the discrepancies between the partially synchronised batches particularly 1mmol and 0.5mmol are likely to have been due to error in data processing as a result of

the accidental change in flow cytometer settings during the acquisition of data in the above samples. Changes in glucose concentrations were found not to have a major effect on cell cycle, growth, or other parts of the cellular machinery. Residual glucose concentration in synchronous cultures was found to be higher than that of asynchronous ones. There appears to be a correlation between the consumption of glutamine and glucose. Glucose consumption was found to be higher in the partially synchronous batch where glutamine concentration was 2mmol. The biological experiments were extended to gain further insight into the way the relative proportions of cell cycle sub-populations at the start of the batch, contribute towards their kinetics of growth by initiating a succession of inoculate states at different starting points in terms of the relative proportions of the cell cycle sub populations. Variations in the measured parameters among batches could be accounted for simply by reference to their cell cycle profiles. Some difficulty was however observed when attempting to explain the mean relative mass changes in CHO320 cell populations. Generally a small decline in the total viable cell number was observed as the inoculation gap with respect to the reference culture increased. In most cases this decline was not significantly large and could be partly due to error in measurement. Another notable difference was the period within which Glucose was exhausted. Depletion of glucose in the batch with cells rich in S phase cells at the time of inoculation was found to be the least, it being exhausting shortly after 105 hours of the cultivation period. The batch of cells inoculated 46 hour after the reference culture, comprised of relatively speaking higher G1 cells exhibit the highest consumption of glucose whose exhaustion took place at around 55 hour of the cultivation period reflecting the variations in demand for metabolites within the cell cycle sub population.

Glutamine concentrations had been measured but due to an error during the analysis, they were not reliable enough to be included in the discussion.

In parallel with these experiments mathematical approaches to early state estimation of CHO320 cells were initiated, starting from simple, dynamic, closed systems described by first order differential equations. Models in this category were shown to be inadequate as far as long term prediction of batch data is concerned and of little use when estimating the changes in the first doubling time of the batch culture of the partially synchronised cells where lag and oscillatory periods are to be estimated.

Following the problems encountered in simple models, a model based on delayed regulation was considered and this brought about improvement to the predicted profile of cells during the lag period but its prediction of the ensuing oscillatory period was not satisfactory and the transition of cells from lag into oscillatory period was too rigid to be desired within a biological context. Another step was that based on models with changing rate coefficients which were developed for short term prediction of partially synchronised cells in batch cultivation. They were shown to give a great improvement to the previous models in predicting the oscillatory patterns of batch data. The latter was however a purely pragmatic approach and hence a more plausible model based on experimentally proven mechanisms was proposed. Optimisation of these models proved to be a futile exercise as determination of the appropriate parameter sets in the absence of experimental data corresponding to the profiles of species involved in the molecular

mechanism proved to be difficult and hence the profiles of sub-populations were not predicted satisfactorily.

Models with a molecular mechanism for G1-S transition which had been discussed previously however paved the way for the model whose cell cycle transition rates are based on the Lotka-Volterra predator and prey relationship. Improvement on model with predator-prey differentials was shown to be remarkable and this model can be used for short term prediction of the profiles of the cell cycle population and total cell number in a partially synchronised culture.

The next stage in model development was that of systems which interacted with their surrounding environment. Between the two major categories of partial differential models based on age and simpler first order ordinary differential models the models which were based on age as a regulatory parameter for transition and substrate dependent death rate exhibited better simulated viable and dead cell profiles despite difficulties in estimation of the initial number of viable cells at the start of the batch culture. Unlike the models based on ordinary differentials where cell cycle data were used directly in estimation of viable and non-viable cells, the age models made use of the cell cycle sub populations implicitly. The simulated cell cycle population produced by models with ordinary differentials is a good fit but the underestimation of the non-viable cells is partly believed to be related to the optimisation process and partly to the assumptions made in constructing the model. In summary, models with first order ordinary differential equation with substrate dependent G1-S transition are believed to be a better choice for

prediction of long term data as their solution and simulation are easier, they make use of the cell cycle data directly and produce reasonably good results. The age based partial differential models however have complex solutions and the assumptions in constructing them are also generally more involved. As far as the short term data is concerned models with changing rate coefficients and particularly those which are based on a predator-prey type of relationship produce the best results.

9.2 Future Work

Having evaluated and selected the more plausible mathematical models for prediction of CHO320 cell growth profiles using their cell cycle sub populations, further elaboration of these models should follow but as time did not permit their implementation, these propositions for further improvement are given instead:

9.2.1 Convergence of the Mathematical Models

Initially, in this thesis, due to difficulty in developing a model which could predict the earlier part of the batch profiles (lag and oscillatory periods) as well as the mid-terminal part of the batch cultures where cell cycle sub-population profiles exhibited a radically different behaviour, the batch data was divided into short and long term sets. It is now suggested that an attempt be made to combine these two models, starting with those models with variable rate coefficients where fit to cell cycle sub-populations within the first doubling time was found to be good and then incorporating terms, possibly substrate dependent ones, to control the onset and switching off mechanisms of $G1\text{-}^{S}$ transition and hence help producing the G1 accumulation phase.

9.2.2 Broadening of Application of the Model

Emphasis could also be placed on expanding the selected model to cover other aspects such as productivity particularly in relation to the mode of cultivation. Productivity can be improved by many fold in fed batch cultivation and control strategies can be implemented to maximise production. Proliferation of CHO320 cells could be further characterised not only by introduction of apoptotic and quiescent stages into the model but also by developing correlations to link the growth rate with those states. Models based on physiological age could be constructed to take into account the non-uniformity of the aging process particularly in non balanced growth. Comparison between age dependent and substrate dependent death processes could be made and the concept of mean age could be used to simplify the calculations, development and implementation of analogies based on age and specific growth rate.

Appendix I

Matlab Optimisation Routines

This is a list of programs used to run a Matlab optimisation routine for a selected model.

double.m - is a script file containing the fermentation data.

obinit.m - is a script file containing initial values of model parameters.

Comptune.m-is a script file to run least square optimisation routine.

Comptarg.m- is a function file which is used as an objective function for least square optimisation.

Script file to tune parameters for a selected model by least squares optimisation.

```
% Load in fermentation data
% The data is stored in a .m file

load  double

%Specify the size of the fermentation data to be
%considered in optimisation.

cl = cl(1:18,:);
cl(:,1) = cl(:,1)-cl(1,1);

% Set up initial fermentation conditions.

obinit

% Load in previously saved result

load tmp

% Globalising parameters being tuned, so that optimisation routine
% can change their values!
global   z K pd qd pm qm d0 e0 m0 rbs0 rb0
global   ad gf a1 b1 h ae a2 b2 de g am f dm
global   ps pe qe dd

% Create initial vector for tuning parameters

x0 =[ z K pd qd pm qm ad gf a1 b1 h ae a2 b2 de g am f dm ps pe qe dd d0 e0 rbs0 rb0
m0];

% Create a control options vector

options = foptions; options(1) = 1;
options(16) = sqrt(eps);options(17) = sqrt(eps);
options(14)=5e3;

% Call the  least square optimisation routine

xnew = leastsq('comtarg',x0,options,[],cl);
```

Function File

```
function [errors] = comtarg(x, cl)
% This is the objective function to calculate the errors
% needed for tuning the parameters of the model "comply".

%  parameters being tuned are declared global, otherwise
% SIMULINK won't know that the optimisation routine has
% attempted to change their values!

global   z K  pm qm pd qd d0 e0 rbs0 rb0 m0
global ad gf al b1 h ae a2 b2 de g am f dm ps pe qe dd

% Only positive parameter values are considered

x = abs(x);

% creating parameter values from the input x vector
rbs0    =x(1);
z       =x(2);
K       =x(3);
pm      =x(4);
qm      =x(5);
ps      =x(6);
qd      =x(7);
pe      =x(8);
qe      =x(9);
ad      =x(10);
gf      =x(11);
a1      =x(12);
b1      =x(13);
h       =x(14);
ae      =x(15);
a2      =x(16);
b2      =x(17);
de      =x(18);
g       =x(19);
am      =x(20);
f       =x(21);
dm      =x(22);
pd      =x(23);
dd      =x(24);
d0      =x(25);
e0      =x(26);
m0      =x(27);
```

```
rb0     =x(28);

% Unpack the reference data
t_ref   = cl(:,1);
G1_ref  = cl(:,2);
G2MS_ref = cl(:,3);
L_ref   = cl(:,5);
W_ref   = cl(:,6);
% Run the simulation

[arb] = rk45('comply',[0 max(t_ref)],[],[1e-10 1e-10 1e-1]);

Aquiring the simulated results at the measured fermentation times

G1_sim = G1((t_ref)+1);
G2MS_sim = G2MS((t_ref)+1);
L_Sim = L((t_ref)+1);
W_Sim = W((t_ref)+1);


% Calculating the error values
G1_error = G1_sim - G1_ref;
G2MS_error = G2MS_sim - G2MS_ref;
L_error = L_Sim - L_ref;
W_error = W_Sim - W_ref;

% Concatenating the errors for return

errors =[G1_error; G2MS_error; L_error; W_error];


% Plotting the results
subplot(2,1,1), plot(cl(:,1),cl(:,2:3),'o',t,[G1 G2MS])
subplot(2,1,2), plot(cl(:,1),cl(:,5:6),'o',t,[L W])

drawnow
```

References

Adams, R.L.P. (1980). Cell Synchronisation. In: *Cell Culture for Biochemists.* Elsevier/North – Holland, p. 162. Biomedical Press, New York.

Al-Rubeai, M., Chalder, S., Bird, R., Emery, A.N.(1991).Cell cycle, cell size and mitochondrial activity of hybridoma cells during batch cultivation. *Cytotechnology*, 7:179-186

Al-Rubeai, M., Emery, A.N., Chalder, S. (1991). Flow cytometric study of mammalian cells. *Journal of Biotechnology*, 19:67-82.

Bailey *et al* (1959). The carbohydrate nutrition and metabolism of a strain of mammalian cells growing *in vitro*. *J. Biological Chemistry*. 234: 1042-1047.

Barnes, D.W., Sirbasku, D.A., Sato, G.H. (Eds.) (1984). *Methods for preparation of media, supplements and substrates for serum-free animal cell culture.* Alan R. Liss, New York.

Baserga, R. and Surmacz, E. (1987). Oncogenes, cell cycle genes and the control of cell proliferation. *Biotechnology*, 5: 355.

Burns, F.J. and Tannock, I.F. (1970). On the existence of a G0 phase in the cell cycle. *Cell Tiss. Kinet.* 3(4): 321-344.

Cazzador, L., Mariani, L. (1993). Growth and production modeling in Hybridoma continuous cultures. *Biotechnology and Bioengineering*, 42:1322-1330.

Chau, P.C., Cain, S.C. (1997). Transition probability cell cycle model-I. balanced growth. *Journal of Theoretical Biology*, 185:55-67.

Chau, P.C., Cain, S.C. (1997). Transition probability cell cycle model-II. Non-balanced growth. *Journal of Theoretical Biology*, 185:69-79.

Cook, J.R. and Cook, B. (1962). Effect of nutrients on the variation of individual generation times. *Exp. Cell Res.* 28: 524-530.

Cooper, S. (1988). *Journal of Theoretical Biology.* 135: 393-400.

Dalili, M. and Ollis, D.F. (1989). Transient kinetics of hybridoma growth and monoclonal antibody production in serum-limited cultures. *Biot. Bioeng.* 33: 984-990.

Dulic, V., Lees, E. and Reed, S.I. (1992). *Association of human cyclin E with a periodic G_1-S phase protein kinose.*

Eagle, H. (1958). Amino acid metabolism in mammalian cell cultures. *Science*, 130: 432-437.

Edwards, D., Hanson, M. (1994). *Guide to Mathematical Modelling*, 3. Macmillan Press Ltd.

Foerster, H.V. (1959). Some remarks on changing populations. *The Kinetics of Cellular Proliferation*. pp 382-407. Grune-Stratton, New York.

Fredrickson, A.G. (1976). Formulation of structured growth models, *Biotechnology and Bioengineering*, 18: 1481-1486.

Glacken, M.W., Adema, E., Sinskey, A.J. (1988). Mathematical description of hybridoma culture kinetics: I. Initial metabolic rates. *Biotechnol. Bioeng.* 32: 491-506.

Glassy, M.C., Tharakan, J.P. and Chau, P.C. (1988). Serum-free media in hybridoma culture and monoclonal antibody production. *Biot. Bioeng.* 32: 1015-1028.

Goergen, J.L., Marc, A., Engasser, J.M. (1994). Influence of lactate and ammonia on the death rate of hybridoma. In: Spier, R.E., Griffiths, J.B., Berthold, W. (Eds.) *Animal cell technology; products of today, prospects for tomorrow*. pp 161-163. Butterworth Heinemann, Oxford.

Gold, H.J. (1977). *Mathematical Modeling of Biological Systems.* Wiley-Interscience publication, 1st edition.

Goldstein, S. (1990). Replicative senescence: the human fibroblast comes of age. *Science*, 249: 1129-1133.

Griffiths, B. (1986). Can cell culture medium costs be reduced? Strategies and possibilities. *Trends Biot.* 4: 268-272.

Häggström, L. (1990). Energetics of glutaminolysis: a theoretical evaluation. In: Spier, R.E., Griffiths, J.B., Meignier, B. (Eds.). *Production of biologicals from animal cells in culture*. pp 79-81. Butterworth Heinemann, Oxford.

Hartwell, L.H., Weinert, T.A. (1989). Checkpoints: Controls that ensure the order of cell cycle events. *Science*, 246: 629-634.

Hatzimanikatis, V., Lee, K.H., Bailey, J.E. (1999). A mathematical description of regulation of the G1-S transition of the mammalian cell cycle. *Biotechnology and Bioengineering*, Vol. 65, 6:631-637.

Hayter, P.M., Curling, E.M.A., Baines, A.J. (1991). Chinese hamster ovary cells growth and interferon production kinetics in stirred batch culture. *Applied Microbiology and Biotechnology,* 34:559-564.

Hayter, P.M., Curling, E.M.A., Gould, M. L., Baines, A. J., Jenkins, N., Salmon, I., Strange, P.G., Tong, J.M., Bull, A.T.(1992). Glucose-limited chemostat culture of chinese hamster ovary cells producing recombinant human interferon-γ. *Biotechnology and Bioengineering*, 39, 327-335.

Howard, A. and Pelc, S.R. (1953). Synthesis of desoxyribon ucleic acid in normal and irradiated cells and its relation to chromosome breakage. *Heredity*. London (supplement), 6: 261-273.

Hu, W.S., Frame, K.K. (1989). Cell volume measurement as an estimation of mammalian cell biomass. *Biotechnology and Bioengineering*.Vol. 36, pp 191-197.

Hughes, A. (1952). *The Mitotic Cycle.* Butterworths, London.

Jäger, V. (1992). A novel perfusion system for the large scale cultivation of animal cells based on a continuous flow centrifuge. In: Spier, R.E., Griffiths, J.B., Macdonald, C. (Eds.). *Animal cells technology; developments, processes and products*. pp 397-402. Butterworth-Heinemann, Oxford.

Kitano, K. (1991). Serum-free media. In: Ho, C.S., Wang, D.I.C. (Eds.). *Animal cell bioreactors.* pp 73-106. Butterworth-Heinemann, London.

Kromenaker, S.J., Srienc, F. (1991). Cell cycle dependent protein accumulation by producer and non-producer Murine Hybridoma cell lines. *Biotechnology and Bioengineering*, Vol.38, pp 665-677.

Kurano, N., Leist, C., Messi, F., Kurano, S. and Fiechter, A. (1990b). *J. Biotechnol.* 15: 113-128.

Lajtha, L.G. (1963). Differential sensitivity of the cell life cycle. *J. Cell. Comp. Physiol.* 62: (Suppl. 1), 141-156.

Leelavatcharamas, V., Emery, A.N., Al-Rubeai, M. (1994). Growth and interferon-γ production in batch culture of CHO cells. *Cytotechnology*, 15: 65-71.

Leelavatcharamas, V.(1996).Growth. interferon-γ production and the cell cycle in batch, continuous and perfusion culture of CHO cells. *Ph.D. thesis, University of Birmingham*

Lew, D.J. and Reed, S.I. (1992). A proliferation of cyclins. *Trends in Cell Biology*, 2: 77-81.

Linardos. T.I., Kalogerakis, N., Behie, L.A. (1992). Cell cycle model for growth rate and death rate in continuous suspension Hybridoma cultures. *Biotechnology and Bioengineering*, Vol. 40, pp 359-368.

Mayerson, M., Enders, G.H., Wu, C., Su, L., Gorken, C., Nelson, C., Harlow, E. and Tsai, L. (1992). A family of human cdc2-related kinases. *EMBO J.* 11: 2909-2917.

Martens, D. E., de Gooijer, C.D., van der Velden-de Groot, C. A. M., Beuvery, E. C., Tramper, J. (1993). Effect of dilution rate on growth, productivity, cell cycle and cell size, and shear sensitivity of hybridoma cell in a continuous culture. *Biotechnology and Bioengineering*, 41: 429-439

Martens, D. E., Sipkema, E.M., de Gooijer, C.D., Beuvery, E. C., Tramper, J. (1995). A combined cell cycle and metabolic model for the growth of hybridoma cells in steady state continuous culture. *Biotechnology and Bioengineering*, Vol.48, pp 49-65.

McKeehan, W.L. (1986). Glutominolysis in animal cells. In: M.J. Morgan (Ed.) *Carbohydrate metabolism in cultural cells.* 111-150. Plenum Press, New York.

Meijer, J. J., Dijken, J.P. (1995).Effects of glucose supply on myeloma growth and metabolism in chemostat culture. *Journal of Cellular Physiology*,162:191-198.

Miller, W.M., Blanch, H.W., Wilke, C.R. (1987). A kinetic analysis of Hybridoma growth and metabolism in batch and continuous suspension culture. *Biotechnology and Bioengineering*, Vol.32, 947-965.

Miller, W.M., Wilke, C.R., Blanch, H.W. (1988). Transient responses of hybridoma metabolism to lactate and ammonia pulse and step changes in continuous culture. *Bioprocess Engineering,* 3:113-122.

Miller, W.M., Wilke, C.R., Blanch, H.W. (1989). Transient responses of hybridoma cells to nutrient additions in continuous culture: I. Glucose pulse and step changes. *Biotechnology and Bioengineering.* 33: 477-486.

Morgan *et al* (1986). Carbohydrate metabolism in cultured cells. In: *The utilisation of carbohydrates by animal cells.* pp 29-33.

Morgan, D.O. (1995). Principles of CDK regulations. *Nature*, 374: 131-134.

Nielsen, L.K., Reid, S., Greenfield, P.F. (1997). Cell cycle model to describe animal cell size variation and lag between cell number and biomass dynamics. *Biotechnology and Bioengineering.* Vol.56, 4: 372-379.

Novak, B., Nagy, C., Cyorffy, B., Chen, K., Tyson, J.J. (1998). Mathematical model of the fission yeast cell cycle with checkpoint controls at the G1-S and G2-M and Mataphase-Anaphase transitions. *Journal of Biophysical Chemistry*, 72: 185-200.

Nurse, P. (1980). Cell cycle control – both deterministic and probabilistic. *Nature*, 286: 9-10.

Obeyesekere, M.N., Knudsen, E.S., Wang, J.Y.J., Zimmerman, S.O. (1997). A mathematical model of the regulation of the G1 phase of Rb +/+ and Rb -/- mouse embryonic fibroblasts and an osteosarcoma cell line. *Cell Proliferation*.30: 171-194.

Ormerod, M.G. (Ed.). (1994). Flow cytometry: a practical approach. *ISBN* 0-19963461-0. 91-97. IRL Press, Oxford.

Ozturk, S.S., Palsson, B.O. (1990). Effects of dissolved oxygen on hybridoma cell growth, metabolism and antibody production kinetics in continuous culture. *Biotechnol.* Prog. 6: 437-446.

Ozturk, S.S., Riley, M.R., Palsson, B.O. (1992). Effects of ammonia and lactate on hybridoma growth, metabolism and antibody production. *Biotechnology and Bioengineering*. 39: 418-431.

Pardee, A.B. (1974). A restriction point for the control of normal animal cell proliferation. *Proc. Natl. Acad. Sci. USA.* 71(4): 1286-1290.

Pardee, A.B., Dubrow, R., Hamlin, J.L. and Kletzien, R.F. (1978). Animal cell cycle. *Ann. Rev. Biochem.* 47: 715-750.

Reed, S.I., Bailey, E., Dulic, V., Hengst, L., Resenitzky, D. (1994). G1 control in mammalian cells. *Journal of Cell Science,* 18: 69-73.

Reitzer, L.J., Wice, B.M., Kennell, D. (1979). Evidence that glutamine, not sugar, is the major energy source for cultured HeLa cells. *J. Biol. Chem.* 254: 2669-2676.

Reuveny, S., Velez, D., Macmillan, J.D., Miller, L. (1987). Factors effecting monoclonal antibody production in culture. *Develop. Biol. Stand.* 66: 169-174.

Sato, G.H. (1975). The role of serum in cell culture. In: Litwack, G. (Ed.) *Biochemical actions of hormones*, Vol. 3, pp. 391-396. Academic Press, New York.

Shapiro, H.M. (1988). *Practical Flow Cytometry* (2nd edition), pp 87-99. Alan R. Liss Inc.

Shields, R. (1977). Transition probability and the origin of variation in the cell cycle. *Nature*, 273: 704-707.

Shields, R. (1978). Further evidence for random transition in the cell cycle. *Nature*, 273: 755-758.

Shioya, S., Uchiyama, K. (1999). Modeling and optimisation of α- amylase production in a recombinant yeast-fed batch culture taking account of the cell cycle population distribution. *Journal of Biotechnology,* 71: 133-141.

Smith, J.A., Martin, L. (1973). Do cells cycle? *Proceedings from National Academy of Science*, 70: 1263-1267.

Suzuki, E., Ollis, D.F. (1989). Cell cycle model for antibody production kinetics. *Biotechnology and Bioengineering.* 34: 1398-1402.

Toby, R.A. and Ley, K.D. (1970). Regulation of initial DNA synthesis in chinese hamster cells: 1. Production of stable, reversible G_1 arrested population in suspension culture. *Journal of Cell Biology,* 46:151-157.

Tsuchiya, H.M., Fredrickson, A.G. and Aris, R. (1966). Dynamics of microbial cell populations. *Ann. Rev. Micro.* 6: 125-146.

Vriezen, N., Romein, B., Luyben, K.Ch.A.M., van Dijken, J.P. (1996). Effects of glutamine supply on growth and metabolism of mammalian cells in suspension culture. *Biotechnology and Bioengineering.* 54: 272-286.

Vriezen, N., Romein, B., Leiderman, L., Hsu, Y., Karkare, S., Lu, H.S., Lin, F. (1997). Effects of glutamine supply on growth and metabolism of mammalian cells in suspension culture. *Biotechnology and Bioengineering,* 54: 272-286.

Watson, J.V. (1992). Flowcytometry data analysis. *Basic Concepts and Statistics.* Cambridge University Press.

Weinberg, R.A. (1995). The retinoblastoma protein and cell cycle control. *Cell*, 81: 323-330.

Wilson, M.R. (1998). Apoptotic signal transduction. *Biochemical Cell Biology*, Vol.76, pp 573-581.

Xiong, Y. and Beach, D. (1991). Population explosion in the cyclin family. *Curr. Biol.* 1: 362-364

Zeng, A-P. (1995). Mathematical modelling and analysis of glucose and glutamine utilization and regulation in cultures of continuous mammalian cells. *Biotechnology and Bioengineering. 47*: 334-346

Zeng, A-P. (1995). Mathematical modelling and analysis of monoclonal antibody production by hybridoma cells. *Biotechnology and Bioengineering.* 50: 238-247.

Zetterberg, A. and Engstrom, W. (1981). Glutamine and the regulation of the DNA replication and cell multiplication in fibroblasts. *J. cell. Physiol.* 108:365-373

Zielke, H.R., Ozand, P. T., Tildon, J. T., Sevdalian, D. A., Cornblath, M. (1978). Reciprocal regulation of glucose and glutamine utilisation by cultured human diploid fibroblasts. *J. Cell. Physiol.* 95: 41-48.

Zielke, H.R., Zielke, C. L., Ozand, P. T. (1984). Glutamine: a major energy source for cultured mammalian cells. *Fed. Proc.* 43: 121-125.